

Top-Quark Physics: Status and Prospects

Ulrich Husemann

*Institut für Experimentelle Kernphysik
Karlsruhe Institute of Technology, Germany*

Abstract

After the discovery of the top quark more than 20 years ago, its properties have been studied in great detail both in production and in decay. Increasingly sophisticated experimental results from the Fermilab Tevatron and from Run 1 and Run 2 of the LHC at CERN are complemented by very precise theoretical predictions in the framework of the standard model of particle physics and beyond. In this article the current status of top-quark physics is reviewed, focusing on experimental results, and a perspective of top-quark physics at the LHC and at future colliders is given.

Contents

1	Introduction	4
1.1	Overview	4
1.2	Historical Remarks	5
1.2.1	The Road to the Top	5
1.2.2	Tevatron Run I: Discovery and First Measurements	8
1.2.3	Tevatron Run II: Is the Top Really the Sixth Quark of the Standard Model?	9
1.2.4	LHC Run 1: From Re-Discovery to a Top Factory	10
1.2.5	LHC Run 2: Towards Ultimate Precision	11
1.3	Working Groups Across Experiments and Combination of Results .	11
2	Top-Quark Physics at Hadron Colliders	12
2.1	Hadron Collider Kinematics	12
2.2	High- p_T Physics at Hadron Colliders	14

Email address: `ulrich.husemann@kit.edu` (Ulrich Husemann)

2.3	Monte-Carlo Simulation Tools for Top-Quark Physics	15
2.4	The Top Quark in the Standard Model	16
2.4.1	Quantum Numbers and Decays	16
2.4.2	Mass	19
2.5	Top Quark-Antiquark Pair Production	20
2.6	Single-Top Quark Production	22
2.7	Summary	24
3	Experimental Techniques in Top-Quark Physics	24
3.1	Analysis Objects	25
3.1.1	Leptons	25
3.1.2	Jets, Missing Transverse Momentum, and Particle Flow	26
3.2	Data Selection	28
3.2.1	Preselection	28
3.2.2	Event Selection and Major Backgrounds	29
3.2.3	Background Estimation Techniques	30
3.3	Top-Quark Reconstruction	32
3.3.1	Neutrino Reconstruction	32
3.3.2	Jet-Parton Assignment and Kinematic Fitting	32
3.3.3	Boosted Top-Quark Reconstruction	34
3.4	Statistical Methods	35
3.4.1	Maximum-Likelihood Method	35
3.4.2	Multivariate Classification	37
3.4.3	Matrix-Element Method	37
3.4.4	Unfolding Techniques	38
3.4.5	Statistical Combination of Measurements	40
4	Top-Quark Production	40
4.1	Observables and Measurement Techniques	41
4.2	Inclusive $t\bar{t}$ Production	43
4.3	Differential $t\bar{t}$ Production Cross Section	46
4.4	$t\bar{t} + X$ Production	49
4.5	Single Top-Quark Production	52
4.5.1	CKM Matrix Element V_{tb}	54
4.5.2	Single Top + X Production	55
4.6	Summary	57
5	Top-Quark Mass	57
5.1	Kinematic Reconstruction	58
5.2	Alternative Methods to Extract The Top-Quark Mass	60
5.2.1	Kinematic Methods	60

5.2.2	Top-Quark Mass from Single-Top Quark Events	62
5.2.3	Cross-Section Methods	62
5.3	Combinations of Top-Quark Mass Results	63
5.4	Top Quark-Antiquark Mass Difference	64
5.5	Summary	65
6	Top Quark Properties	65
6.1	Basic Top-Quark Properties	66
6.1.1	Top-Quark Electric Charge	66
6.1.2	Top-Quark Width and Lifetime	67
6.2	$t\bar{t}$ Production Asymmetries	68
6.2.1	Forward-Backward Asymmetries at the Tevatron	69
6.2.2	Charge Asymmetries at the LHC	70
6.3	Spin Observables in Events with Top-Quarks	71
6.3.1	W -Boson Polarization in Top-Quark Decays	73
6.3.2	Top Quark Polarization and $t\bar{t}$ Spin Correlations	74
6.4	Anomalous Top-Quark Couplings	77
6.4.1	Anomalous Wtb Couplings and CP Violation	78
6.4.2	Flavor-Changing Neutral Currents	79
6.4.3	Heavy-Particle Decays to Top Quarks	81
6.4.4	Top Quarks and Dark Matter	86
6.4.5	Top Couplings in an Effective Field Theory Approach	87
6.5	Top Quarks as a Tool	88
7	Future Top-Quark Physics	90
7.1	Towards the High-Luminosity LHC	90
7.2	Top-Quark Physics at Future Lepton and Hadron Colliders	92
8	Conclusions	93

1. Introduction

1.1. Overview

Particle physics has recently celebrated the 20th anniversary of the discovery of the top quark. Over the last two decades the most massive particle of the standard model (SM) of particle physics has been studied in great detail, both at the Tevatron collider at Fermi National Accelerator Laboratory (FNAL) and at the Large Hadron Collider (LHC) at the European Organization for Nuclear Research (CERN). The results are documented in more than 200 publications by the Tevatron and LHC experiments as well as in many preliminary results, presentations at conferences and workshops, etc.

The goal of this review is two-fold: it is intended as an introduction to the field, and at the same time it aims to convey the current state of the art in top-quark physics. While the focus of the review is on experimental results, a glimpse of the many achievements in related developments in particle physics phenomenology is also given. The introductory part is based on master-level lectures on top-quark physics given at Karlsruhe Institute of Technology (KIT) and assumes some previous knowledge usually taught in introductory lectures on experimental and theoretical particle physics. In the later parts of the review, a variety of recent results on top-quark physics will be introduced. The focus is on the basic physics and measurement ideas, leaving out many of the details which experimental physicists have spent most of their time on. For a given physics question, the analysis methods, as well as the sensitivities, of the different experiments are often very similar. Therefore the numbers and figures quoted in the review should be taken as illustrative examples.

There has been a substantial number of review articles on top-quark physics published in recent years. The review articles [1, 2, 3, 4, 5, 6, 7, 8, 9, 10] are general overviews of top-quark physics from an experimental point of view, sometimes restricted to just Tevatron or LHC results. In [11, 12] the theoretical and phenomenological aspects of top-quark physics are discussed. Further review articles deal with more specialized topics, for example single top-quark production [13, 14, 15], the top-quark mass [16], $t\bar{t}$ production asymmetries [17], or top-quark physics at the HERA ep collider [18].

This review is structured as follows: The remainder of this chapter is dedicated to a brief historical introduction to top-quark physics. In Section 2 the basic concepts of top-quark physics are introduced. The most important experimental techniques employed to study top quarks are discussed in

Section 3. Some readers may want to skip these introductory chapters and jump directly to the discussion of recent top-quark physics results starting in Section 4. In this chapter measurements of top-quark production in various production and decay channels are introduced. One of the most important measurements in top-quark physics is the determination of the top-quark mass, which will be discussed in Section 5. Further production and decay properties of the top quark, including those expected in beyond standard model (BSM) physics scenarios, have been studied in great detail, as shown in Section 6. The review is completed with a look at the prospects for top-quark physics at future collider experiments in Section 7.

1.2. Historical Remarks

The discovery of the top quark by the CDF and D0 collaborations at the Tevatron in 1995 [19, 20] marks the end of a long quest for the sixth and last quark of the SM and at the same time the beginning of a long quest to understand the top quark’s properties and its role in the SM and beyond.

1.2.1. The Road to the Top

In the original quark model by Gell-Mann [21] and Zweig [22], based on the approximate $SU(3)$ symmetry of the mass spectrum of light mesons and baryons [23, 24], hadrons consist of the three lightest quarks: up, down, and strange. It was realized by Cabibbo in 1963 that electroweak currents that change the strangeness quantum number of a hadron by one unit ($\Delta S = 1$) show a different coupling strength than currents with $\Delta S = 0$ [25]. In modern particle physics language this means that the physical quarks (mass eigenstates) and the quarks that participate in the electroweak interaction (flavor eigenstates) are not aligned, a phenomenon called flavor mixing. A fourth quark, the charm quark, was postulated by Glashow, Iliopoulos, and Maiani in 1970 to explain the strong suppression of flavor-changing neutral current (FCNC) processes such as $K^0 \rightarrow \mu^+ \mu^-$ by the destructive interference of scattering amplitudes with up and charm quarks (“GIM mechanism”) [26]. The charm quark was discovered by interpreting the J/ψ resonance observed in experiments at Brookhaven National Laboratory (BNL) [27] and Stanford Linear Accelerator Center (SLAC) [28] as a $c\bar{c}$ bound state. This discovery completed the second generation of quarks. In both quark generations a quark with a third component of the weak isospin of $I_3 = +1/2$ and a charge of $Q = +2/3$ in units of the elementary charge e (“up-type quark”) and a

quark with $I_3 = -1/2$ and charge $Q = -1/3$ (“down-type quark”) form a weak isospin doublet.

The 1964 experiment by Christenson, Cronin, Fitch, and Turlay used neutral kaon decays to show that the weak interaction is not invariant under the combined discrete symmetry operation of charge conjugation C and parity P (“CP violation”) [29]. Kobayashi and Maskawa realized in 1973 that what is known now as the electroweak sector of the SM provides a mechanism for CP violation through flavor mixing only if there are at least three generations of quarks [30]. The charged lepton of the third generation, the tau lepton, was discovered at SLAC in 1975 [31], shortly followed by the discovery of the Υ resonances at FNAL in 1977 [32], interpreted as bound states of a third-generation quark, the bottom quark, and its antiparticle ($b\bar{b}$).

The open question at the time was if the bottom quark is a weak isospin singlet or is part of another doublet. To shed light on this question, the quantum numbers of the bottom quark were determined in e^+e^- collision experiments at Deutsches Elektronen-Synchrotron (DESY). The cross section for the production and hadronic decay of the $\Upsilon(1S)$ resonance in e^+e^- collisions is proportional to the partial width of the $\Upsilon(1S)$ for decays to electrons, Γ_{ee} , which can be related to the bottom-quark charge. The experimental results of the PLUTO collaboration from 1978 favored a charge of $Q = -1/3$ [33]. Measurements of the angular distribution of b hadrons produced in e^+e^- collision supported the quantum numbers $I_3 = -1/2$ and $Q = -1/3$ for the bottom quark [34], strongly suggesting that the bottom quark is the down-type quark of the third generation whose $I_3 = +1/2$ isospin partner was yet to be discovered.

An isospin partner for the bottom quark is also well-motivated theoretically by the chiral anomaly. In quantum field theories, anomalies are symmetries of the Lagrangian that are absent in the full theory including quantum corrections. For a four-dimensional chiral gauge theory to be renormalizable, the chiral anomaly, generated by the non-conservation of gauge currents e.g. in triangle diagrams, must be absent. In the SM the chiral anomaly is “accidentally” canceled because there is the same number of quark and lepton flavors, and the number of color charges is three. Hence, to avoid chiral anomalies the third generation of quarks should be a weak isospin doublet, consisting of the bottom quark and its isospin partner, the top quark.

In the early 1980s it seemed natural to search for top quarks with masses

similar to the bottom quark mass, of the order of 10 GeV¹. Direct searches for the process $e^+e^- \rightarrow t\bar{t}$ were conducted at the e^+e^- colliders PEP (SLAC, center-of-mass energy $\sqrt{s} \lesssim 30$ GeV), PETRA (DESY, $\sqrt{s} \lesssim 45$ GeV), TRISTAN (High Energy Accelerator Research Organization (KEK), $\sqrt{s} \lesssim 64$ GeV), SLC (SLAC, $\sqrt{s} \approx 91$ GeV), and LEP 1 (CERN, $\sqrt{s} \approx 91$ GeV). In absence of a signal, lower limits on the top-quark mass of up to $m_t > 45$ GeV at 95% confidence level (CL) were placed, see e.g. [2] for references and further details.

At the Sp̄S proton-antiproton collider at CERN with $\sqrt{s} = 540$ GeV, top quarks could manifest themselves in decays of real W bosons, $W^+ \rightarrow t\bar{b}$,² if their mass is below 70 GeV. In 1984, the UA1 experiment claimed a “clear signal” compatible with a W boson decaying into a 40-GeV top quark [35]. From today’s perspective, the “signal” was most likely caused by an underestimation of the background from W -boson production in association with jets, for which no adequate simulation tools existed at the time. At the end of their data-taking the Sp̄S experiments UA1 and UA2 were only able to provide lower limits on the top-quark mass up to approximately $m_t > 70$ GeV at 95% CL, see e.g. [2] for references.

In parallel, indirect hints of a large top-quark mass came from the observation of $B_d^0\bar{B}_d^0$ flavor oscillations with the ARGUS experiment at DESY [36], in the process $e^+e^- \rightarrow \Upsilon(4S) \rightarrow B_d^0\bar{B}_d^0$. The CERN UA1 experiment had reported a three-standard deviation excess of same-sign muon pairs in $p\bar{p}$ collisions earlier [37] that can be interpreted as evidence for $B_d^0\bar{B}_d^0$ oscillations. The oscillation frequency depends on the mass difference Δm_d between the two B_d^0 -meson mass eigenstates, which in turn is a function of the top-quark mass m_t . The large oscillation frequency observed by ARGUS pointed to top-quark masses well above 50 GeV. Additional indirect constraints on m_t were derived from the combined analysis of electroweak precision data obtained at the “ Z boson factories” LEP 1 and SLC. Some of the radiative corrections to the masses of the W and Z bosons are proportional to m_t^2 and further electroweak observables are sensitive to m_t as well. From the LEP experiments alone, a value of $m_t = 173^{+12}_{-13}{}^{+18}_{-20}$ GeV was quoted before the

¹In this article, natural units with $\hbar = c = 1$ are used throughout. Hence energy, momentum, and mass are measured in units of GeV, and the units for time and length are GeV^{-1} .

²Charge-conjugated decays are implied, unless stated otherwise.

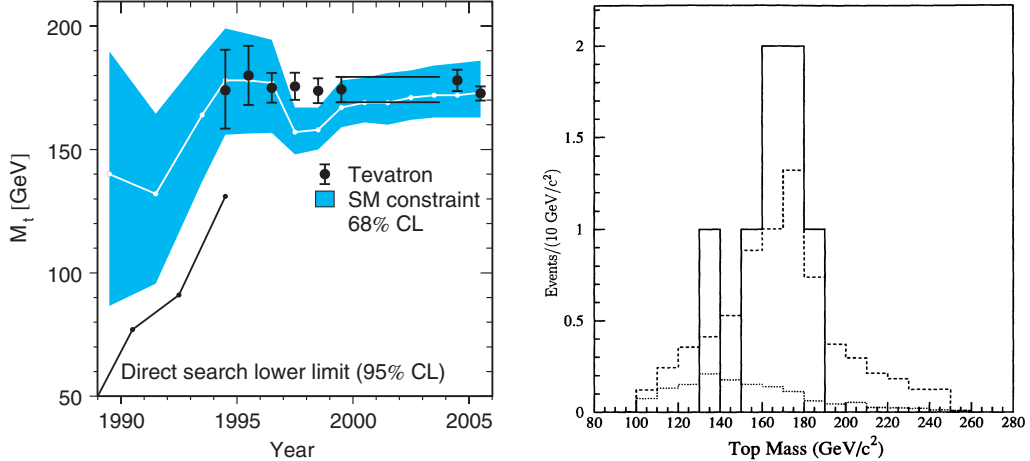


Figure 1: Comparison of direct and indirect determinations of the top-quark mass as a function of time [39] (left). Reconstructed top-quark mass distribution in data (solid histogram) and MC simulation (dashed histograms) based on seven candidate events recorded by the CDF experiment between August of 1992 and May of 1993 [40] (right).

discovery of the top quark [38], where the first uncertainty interval comes from the experimental uncertainties propagated through the combined analysis and the second uncertainty interval corresponds to the lack of knowledge of the Higgs boson mass in the 1990s. The limits on m_t as a function of time are compared to direct measurements at the Tevatron in Fig. 1 (left).

1.2.2. Tevatron Run I: Discovery and First Measurements

At the Tevatron $p\bar{p}$ collider at FNAL, the center-of-mass energy of 1.8 TeV marked a significant increase compared to the SpS, such that the top quark became directly accessible in collider experiments for the first time. The first Tevatron collisions were recorded by the CDF experiment in 1985. In subsequent years, CDF improved the lower limit on the top-quark mass to $m_t > 91$ GeV at 95% CL [41]. Starting in 1992, the Tevatron commenced its Run I with the two experiments CDF and D0 taking data with improved detectors. For “heavy” top quark masses above approximately 85 GeV the decay $t \rightarrow W^+ b$ is allowed kinematically, which was reflected in modified search strategies at the Tevatron. First indications of an excess of collision events above the background expectation compatible with $t\bar{t}$ production showed up in the following years [40, 42], see Fig. 1 (right). The discovery of the top quark was announced publicly in a joint seminar of the CDF and

D0 collaborations at FNAL on March 2, 1995, and published in the journal Physical Review Letters the following day [19, 20]. A popular account of the top-quark discovery can be found in [43].

Typical Tevatron Run-I top physics analyses used between 100 pb^{-1} and 125 pb^{-1} of integrated luminosity³, equivalent to tens to hundreds of $t\bar{t}$ pairs available for analysis, depending on the decay channel. Top-quark physics highlights of Run I included measurements of the $t\bar{t}$ production cross section [44, 45], the top-quark mass [46] and various other properties, such as the W -boson polarization in the decay $t \rightarrow W^+ b$ [47, 48] and first searches for physics beyond the SM with top quarks, e. g. for decays of a hypothetical heavy resonance $Z' \rightarrow t\bar{t}$ [49] or top-quark decays into charged Higgs bosons, $t \rightarrow H^+ b$, which occur in models with an extended Higgs sector compared to the SM [50, 51]. Top-quark physics at Tevatron Run I also pioneered various novel data analysis techniques, such as the matrix-element method (MEM) to determine the top-quark mass [52, 53].

1.2.3. Tevatron Run II: Is the Top Really the Sixth Quark of the Standard Model?

Tevatron Run II started in 2001 with an increased center-of-mass energy of 1.96 TeV and significant upgrades to the CDF and D0 detectors. Until the end of Tevatron data-taking on September 30, 2011, the Tevatron delivered a total of 12 fb^{-1} of integrated luminosity each to CDF and D0. Typical top-quark analyses were thus performed on data samples of several hundreds to thousands of events containing top quarks. Using the Run-II datasets, the Tevatron experiments have addressed a broad range of questions in top-quark physics, from inclusive production cross sections and precise measurements of the top-quark mass and couplings to a variety of searches for BSM physics with top quarks. At the time of writing this review, many “legacy” publications using the full Run-II datasets have already been published, others are being finalized. Three highlights of the Run-II top-quark physics program are briefly sketched in the following.

The precision achievable in measurements of the top-quark mass at the Tevatron was limited both by the dataset size and by uncertainties in the reconstruction of jet energies. Further refinements to the MEM and novel concepts to constrain uncertainties in the jet-energy scale from the data itself

³In the following, luminosity figures are given per experiment, unless noted otherwise.

(“in-situ calibration”) during Tevatron Run II lead to a significant reduction of the uncertainty on the top-quark mass, culminating in the current single most precise Tevatron measurement of the top-quark mass, performed by the D0 collaboration, which has a relative uncertainty of only 0.43% [54, 55].

The SM predicts the electroweak production of single top quarks in addition to the dominant $t\bar{t}$ pair production, which is a quantum chromodynamics (QCD) process. Single top-quark production was observed for the first time by CDF and D0 in 2009 [56, 57]. Sophisticated multivariate analysis methods were necessary to separate the small signal from an overwhelming background. The development and validation of these methods also paved the way for Higgs-boson searches at the Tevatron and similar methods are being employed in top-quark and Higgs-boson physics as well as in searches for BSM physics at the LHC.

In $t\bar{t}$ production a small forward-backward asymmetry between the top quark and antiquark is expected [58]. The Tevatron Run II results on the $t\bar{t}$ production asymmetry gained considerable interest. The first results already indicated asymmetry values larger than expected from QCD [59, 60]. By 2011, with about half of the Run II datasets analyzed, the CDF experiment observed discrepancies between the data and next-to-leading order (NLO) QCD expectations at the level of three standard deviations for $t\bar{t}$ invariant masses above 450 GeV [61]. These observations triggered a plethora of publications from the theory community as well as an extensive measurement program. However, after a full suite of measurements and improved SM predictions including next-to-next-to-leading order (NNLO) QCD corrections, no strong hints of BSM physics in $t\bar{t}$ production asymmetries remain.

1.2.4. *LHC Run 1: From Re-Discovery to a Top Factory*

The start of LHC data taking at $\sqrt{s} = 7$ TeV in 2010 was also the beginning of a new era in top-quark physics. With approximately 3.5 times higher center-of-mass energy compared to the Tevatron, cross sections for top-quark production are expected to be more than 20 times higher than at the Tevatron. Already after the first three years of data-taking, the datasets recorded by the ATLAS and CMS experiments contained about a million top-quark events, rendering the LHC the first “top-quark factory.”

The goal for the first months at the LHC was to “rediscover the SM,” i.e. to identify and measure the basic properties of all known SM particles, including the top quark. First measurements of the $t\bar{t}$ production cross section by the CMS and ATLAS collaborations became available in the second

half of 2010 [62, 63] using the first 3 pb^{-1} of pp collisions data. With the full 2010 dataset of about 35 pb^{-1} the precision on the $t\bar{t}$ production cross section already approached the precision achieved at the Tevatron. Data-taking at the LHC commenced in 2011, with another 5 fb^{-1} of data recorded at $\sqrt{s} = 7\text{ TeV}$. For the 2012 data-taking run of the ATLAS and CMS experiments, the center-of-mass energy of the LHC was increased to 8 TeV and a dataset of 20 fb^{-1} was recorded. With these LHC Run-1 datasets, a wide variety of precision measurements of top-quark properties and searches for BSM physics with top quarks were performed. Some of the analyses of the Run 1 datasets are still being finalized at the time of writing this review. Results on top-quark production have also been obtained using data taken with the LHCb experiment during LHC Run 1.

1.2.5. LHC Run 2: Towards Ultimate Precision

After a two-year shutdown for maintenance of the LHC machine and experiments (“Long Shutdown 1”), the LHC was restarted in early 2015 (“Run 2”). The center-of-mass energy was further increased to 13 TeV , which boosted typical top-quark cross sections by a factor of about three compared to Run 1. ATLAS and CMS have recorded pp collision data equivalent to a luminosity of about 3.5 fb^{-1} in 2015 and approximately 40 fb^{-1} in 2016. At this integrated luminosity, the Run-2 top-quark datasets are already about five times as large as the Run-1 datasets. The LHC design instantaneous luminosity of $1 \times 10^{34}\text{ cm}^{-2}\text{s}^{-1}$ was reached and exceeded by 50% in 2016. Again, cross section measurements were the first top-physics results based on the LHC Run-2 datasets that were published. Many further results on top-quark properties and searches for BSM physics keep appearing while this review is being written.

1.3. Working Groups Across Experiments and Combination of Results

While first and foremost, the Tevatron and LHC experiments publish experimental results based on their own datasets and methods, there are also collaborative efforts across the experiments. The statistical combination of measurements aims at reducing the statistical and systematic uncertainty of a result. This requires good understanding of how systematic uncertainties are defined in each experiment and how they are correlated across the experiments.

Both at the Tevatron and at the LHC working groups have formed to define guidelines for the combination of physics measurements. The guidelines

may include recommendations on the treatment of systematic uncertainties and their correlations, “reference cross sections” for signal and background processes considered in top-quark physics, and agreements on how to present the results of measurements.

At the Tevatron, the Top Subgroup of the Tevatron Electroweak Working Group [64] has provided combinations of CDF and D0 measurements on the top-quark mass and the $t\bar{t}$ production cross section. Similarly, the LHC Top Physics Working Group (LHCtopWG) [65] has developed recommendations on systematic uncertainties, as well as compilations, comparisons, and combinations of ATLAS and CMS measurements.

2. Top-Quark Physics at Hadron Colliders

The basic tool for top-quark physics is a high-energy particle collider. The dominant $t\bar{t}$ production process is accessible both at lepton and at hadron colliders, provided the center-of-mass energy of the collisions is above the production threshold of twice the top-quark mass and the luminosity is large enough to acquire datasets with a sufficient number of $t\bar{t}$ pairs. Until now only hadron colliders have provided sufficient center-of-mass energy and luminosity for top quarks to be produced. Therefore the discussion of top-quark physics in this chapter is focused on hadron colliders. A brief account of the top-quark physics prospects at future lepton colliders will be given in Section 7.2.

This chapter starts with brief overviews of hadron collider kinematics and physics at large momentum transfer, often called “high- p_T physics,” as well as simulation tools for hadron collider physics. The discussion of basic hadron collider physics is followed by a brief account of the production mechanisms and decay channels of top quarks as well as the most important properties of the top quark expected in the SM.

2.1. Hadron Collider Kinematics

Most experiments at circular colliders utilize a right-handed coordinate system with the z axis pointing along the counterclockwise beam direction, the y axis pointing upwards, and the x axis pointing towards the center of the collider ring. The coordinates are often expressed in a cylindrical coordinate system that reflects the symmetry of the detector, with the distance to the beam axis ρ , the angle θ from the z axis (“polar angle”) and the angle ϕ from

the x axis in the xy plane (“azimuthal angle”), perpendicular to the beam axis.

In hadron colliders the particles participating in the fundamental collision processes are the partons within the hadrons. The z components of the colliding partons’ momenta, p_z , are unknown in a given collision event, only their probability distribution is known. This is accounted for by choosing kinematic variables which are insensitive to the lack of knowledge about p_z . The velocity of a particle along the z direction, $\beta_z = p_z/E$, is often expressed in terms of the rapidity y :

$$y \equiv \tanh^{-1} \beta_z = \tanh^{-1} \left(\frac{p_z}{E} \right) = \frac{1}{2} \ln \left(\frac{E + p_z}{E - p_z} \right). \quad (1)$$

It can be shown that rapidity distributions, e.g. the number of particles per unit rapidity, dN/dy , are invariant under Lorentz boosts along the z direction. In the limit of momenta much larger than the mass of a particle, the rapidity converges to pseudorapidity:

$$\lim_{|\vec{p}| \gg m} y \equiv \eta = -\ln \tan \left(\frac{\theta}{2} \right). \quad (2)$$

The pseudorapidity of a particle is a purely geometrical quantity, it only depends on the polar angle θ , but not on the particle’s mass. Another class of kinematic variables often used at hadron colliders are transverse quantities, such as the transverse momentum $p_T \equiv \sqrt{p_x^2 + p_y^2}$, with p_x and p_y being the x and y components of the particle momentum. Transverse quantities are invariant under Lorentz boosts along the beam direction by construction.

The initial-state particles of a hadron-hadron collision are collinear to the z axis to very good approximation. Momentum conservation in the xy plane requires that the vectorial sum of the transverse momenta of all final-state particles is (approximately) zero as well. This constraint can be used to indirectly detect weakly interacting particle that do not leave a signal in a hadron collider detector, such as neutrinos. The corresponding observable is the missing transverse momentum \vec{p}_T^{miss} , defined as the negative vectorial sum of all reconstructed particle momenta in a collision event. Its absolute value E_T^{miss} is often called missing transverse energy (MET). For a single undetected particle, E_T^{miss} is equivalent to the p_T of that particle; however, the particle’s p_z remains undetermined. Experimentally MET reconstruction is challenging, because the observable depends on all other particles in the detector and their calibration and is prone to misreconstruction.

2.2. High- p_T Physics at Hadron Colliders

For many QCD processes at hadron colliders, the physics effects at short distances—or equivalently at high energies—and at large distances, i. e. small energies, can be factorized. The cross section for such a process can be expressed as a cross section for the high-energy (“hard”) parton-parton scattering process weighted by parton distribution functions (PDFs) of the partons participating in the scattering processes, integrated over all parton momenta and summed over all parton types. The hard scattering cross section is process-specific and can be computed in perturbative QCD, while the PDFs are universal and can be measured independently of the hard process. The factorization formula for the cross section reads

$$\sigma = \sum_{jk}^{\text{partons}} \int_0^1 dx_j dx_k f_j(x_j, \mu_F^2) f_k(x_k, \mu_F^2) \hat{\sigma}(x_j x_k s, \mu_F, \alpha_S(\mu_R)). \quad (3)$$

The PDFs $f_i(x_i, \mu_F^2)$ are universal functions that describe the probability to find a parton i with a given longitudinal momentum fraction x_i when the hadron is probed at a momentum transfer of μ_F . This introduces a new energy scale μ_F to the process, called the factorization scale, which can be viewed as the energy scale that separates physics processes at short distances from those at long distances. The PDF absorbs all long-distance effects in the initial state that would lead to infrared and/or collinear divergences⁴ in collider observables if treated in perturbative QCD. The hard scattering cross section $\hat{\sigma}$ is a function of the partonic center-of-mass energy squared $\hat{s} = x_j x_k s$ (s being the pp center-of-mass energy squared), the factorization scale and the strong coupling constant α_S . As $\hat{\sigma}$ is computed in perturbation theory, the renormalization procedure to treat ultraviolet divergences⁵ results in an additional energy scale, the renormalization scale μ_R . The default choice of energy scale to compute $t\bar{t}$ pair production is the top-quark mass: $\mu_R = \mu_F = m_t$.

In the above discussion, only the partonic final state has been considered. However, QCD color confinement requires the final state particles to

⁴Infrared divergences occur if massless particles with vanishing momenta are radiated from other particles. Massless particles radiated at very small angles lead to collinear divergences.

⁵In perturbation theory, ultraviolet divergences occur if particle momenta in virtual (“loop”) corrections approach infinity.

be color-neutral. The process of converting colored partons into hadrons, called hadronization, cannot be computed in QCD perturbation theory. Instead phenomenological models are employed, as implemented in Monte Carlo (MC) event generators, see Section 2.3. As the hadronization probability is unity, the cross section σ remains unchanged.

2.3. Monte-Carlo Simulation Tools for Top-Quark Physics

To compare calculations of hadron-hadron collisions to experimental data software tools based on the Monte Carlo (MC) method are employed. The output of these tools is simulated collision events that resemble experimental data both with respect to the physics processes involved in the hadron-hadron scattering and the interactions of the final state particles with the particle detector. The following discussion is restricted to the simulation of the physics processes in MC event generators.

MC event generators follow the factorization approach discussed in Section 2.2. The PDFs, which are required to describe the structure of the colliding hadrons, have been derived from a set of measurements sensitive to the hadron structure, e.g. deep inelastic ep scattering and jet production. Recent PDF sets are available from several research groups; examples include NNPDF3.0 [66], CT14 [67], MMHT2014 [68], HERAPDF2.0 [69], and ABMP2016 [70]. Technically PDFs can be accessed conveniently via a common interface provided by the LHAPDF [71] program library. The hard scattering cross section may be implemented at different orders in QCD perturbation theory. General-purpose MC event generators of the first generation typically included only $2 \rightarrow 1$ and $2 \rightarrow 2$ processes at leading order (LO). Starting in the early 2000s, also $2 \rightarrow n$ processes (with $n \lesssim 6$) and NLO event generators became available. This increased the precision of MC predictions significantly, as e.g. the emission of additional partons or real and virtual NLO corrections were included in simulated $t\bar{t}$ events. In parallel automated MC event generators were introduced, first at LO, then also at NLO. These generators are able to automatically compute the full set of contributions to the hard process given the Feynman rules of the underlying theory (both SM and BSM).

The process of turning partons into hadrons cannot be treated perturbatively and relies on models. The process can be separated into two steps, parton shower and hadronization, both of which are implemented in general-purpose MC event generator packages. The parton shower is a probabilistic method to model the fragmentation of partons that effectively resums soft

and collinear radiation off the partons, typically to leading logarithmic (LL) order precision in the corresponding observables, see also Section 2.5. Various specialized matching and merging techniques are available to consistently interface NLO and $2 \rightarrow n$ event generators to the parton shower without double-counting parton emissions due to higher order processes and the parton shower. Hadronization is described with models, the most popular being based on the Lund string model [72] and the cluster model [73].

Current MC event generators used in top-quark physics at the LHC include the NLO generator POWHEG v2 [74, 75, 76, 77] and the automated LO and NLO generator MADGRAPH5_AMC@NLO [78, 79]. Both are typically interfaced to PYTHIA8 [80, 81] or HERWIG7 [82] for the parton shower. Other popular MC generator choices include the LO generator for $2 \rightarrow n$ processes ALPGEN [83] and SHERPA [84, 85], which includes LO and NLO matrix elements as well as its own parton shower.

Oftentimes calculations of the inclusive production cross section for signal and background processes include higher-order corrections and are thus more precise than current MC event generators. As will be discussed in Sections 2.5 and 2.6, cross sections for $t\bar{t}$ and single top-quark production are available up to NNLO accuracy [86, 87, 88]. For such processes the normalization of the MC sample is corrected with a scale factor to match the more precise calculation, ignoring the effect that higher-order corrections may have on the shapes of kinematic observables.

2.4. The Top Quark in the Standard Model

2.4.1. Quantum Numbers and Decays

In the SM the top quark has the following properties: The top quark is a fundamental fermion with spin $s = 1/2$. It carries an electric charge of $Q = 2/3$ and is a color triplet. It forms a weak isospin doublet together with the bottom quark, where the top quark is the up-type quark with the third component of the weak isospin $I_3 = +1/2$.

Decays. The top quark decays via the electroweak charged-current process $t \rightarrow W^+ q$, where q is a down-type quark. The part of the SM Lagrangian density describing this interaction reads

$$\mathcal{L}_{Wtb} = -\frac{g}{\sqrt{2}} V_{tb} \bar{q} \gamma^\mu \frac{1}{2} (1 - \gamma_5) t W_\mu^- + \text{h.c.}, \quad (4)$$

where g is the electroweak coupling constant, V_{tq} is the element of the Cabibbo-Kobayashi-Maskawa (CKM) matrix responsible for $t \rightarrow q$ transitions, \bar{q} is the adjoint spinor of the down-type quark, and t is the spinor of the top quark. The $V-A$ Dirac structure of the Wtb vertex, $\gamma^\mu(1 - \gamma_5)/2$, reflects the experimental fact that W bosons only couple to left-handed quarks and right-handed antiquarks. At LO the total decay width of the top quark is given by

$$\Gamma_t^{\text{LO}} = \frac{G_F}{8\pi\sqrt{2}} m_t^3 \left(1 - \frac{m_W^2}{m_t^2}\right)^2 \left(1 + 2 \frac{m_W^2}{m_t^2}\right) \approx 1.5 \text{ GeV}, \quad (5)$$

where m_t is the top-quark mass, m_W is the W -boson mass, and $G_F = \sqrt{2} g^2/(8 m_W^2)$ is the Fermi constant. The comparatively small mass of the bottom quark has been neglected in Eq. (5). The decay width has been computed in a fully differential way including NNLO QCD corrections and NLO electroweak corrections, which reduce the top-quark decay width by approximately 10% compared to the LO prediction [89, 90]. The partial decay width for the decay channel $t \rightarrow W^+ q$, $\Gamma(t \rightarrow Wq)$, is proportional to the CKM matrix element $|V_{tq}|^2$. Experimentally, the relation $|V_{tb}| \gg |V_{ts}| > |V_{td}|$ holds, such that the “CKM-allowed” decay $t \rightarrow W^+ b$ is by far the dominant decay mode, with a branching fraction $\mathcal{B}(t \rightarrow Wb) \equiv \Gamma(t \rightarrow Wb) / \sum_{q=d,s,b} \Gamma(t \rightarrow Wq) = 0.998$ expected for a unitary CKM matrix for three quark generations [91]. The inverse of the total decay width, the top-quark mean lifetime, is $\tau_t = 5 \times 10^{-25} \text{ s}$. This value is shorter than the typical time scale of hadronization, which can be estimated from the inverse of the energy scale Λ_{QCD} at which QCD becomes non-perturbative: $1/\Lambda_{\text{QCD}} \approx 1/(200 \text{ MeV}) \approx 3 \times 10^{-24} \text{ s}$. This leads to two important consequences: Top quarks decay before hadronization and do not form bound states such as top mesons ($t\bar{q}$) or toponium ($t\bar{t}$). The top-quark spin polarization and the correlation between spins are largely preserved and can therefore be computed and observed more easily than for other quarks. The fraction of polarization transferred to the decay products, often called the “spin analyzing power” κ , is different for the different decay products. The value for the W^+ boson is $\kappa = 0.39$ and for the b quark $\kappa = -0.39$, and the value for the neutrino or the up-type quark of the W^+ -boson decay is $\kappa = -0.3$. The charged lepton or the down-type quark from the W^+ -boson decay assume the value $\kappa = 1$. In an ensemble of 100% polarized top quarks the charged lepton will be emitted parallel to the top-quark spin with the highest probability [12], making charged leptons the most attractive top-quark decay products to study polarization effects.

W-Boson Polarization. The SM top-quark decay is governed by an electroweak $V-A$ interaction; therefore the W boson in the final state is polarized. This renders top quarks the only SM source of polarized W bosons. At LO the SM predicts the following fractions of left-handed polarization (F_L), longitudinal polarization (F_0), and right-handed polarization (F_R):

$$F_L = \frac{2m_W^2}{m_t^2 + 2m_W^2} \approx 0.3, \quad F_0 = \frac{m_t^2}{m_t^2 + 2m_W^2} \approx 0.7, \quad (6)$$

$$F_R = \frac{m_b^2}{m_t^2} \frac{2m_W^2}{(1 - m_t^2/m_W^2)^2(m_t^2 + 2m_W^2)} \approx 0,$$

where $F_L + F_0 + F_R = 1$. The most precise SM prediction of the polarization fractions includes NNLO QCD corrections [92].

The large value of $F_0 \approx 0.7$ is related to the Brout-Englert-Higgs mechanism [93, 94, 95, 96, 97], which is responsible for the W boson's longitudinal degree of freedom and hence its mass. To conserve momentum and angular momentum, a right-handed W boson can only be produced together with a positive-helicity bottom quark. Due to the comparatively low bottom quark mass m_b , the left-handed bottom quarks produced in top-quark decays dominantly carry negative helicity, hence the fraction F_R of right-handed W bosons is close to zero.

Classification of Decays. Experimentally collision events containing $t\bar{t}$ pairs are classified by the decay of the W^+ and the W^- boson from the $t\bar{t}$ decay. W^+ (W^-) bosons decay into hadronic final states $q\bar{q}'$ with a branching fraction of approximately 2/3 and into a charged lepton ℓ^+ (ℓ^-) and its corresponding (anti)neutrino ν_ℓ ($\bar{\nu}_\ell$) with a branching fraction of approximately 1/9. This results in the following classification scheme for $t\bar{t}$ decay channels:

- Fully hadronic (also: all-hadronic, all-jets) channel:
 $t\bar{t} \rightarrow W^+ b W^- \bar{b} \rightarrow q\bar{q}' b q''\bar{q}''' \bar{b}$,
- Single-lepton (also: lepton+jets, semileptonic) channel:
 $t\bar{t} \rightarrow W^+ b W^- \bar{b} \rightarrow \ell^+ \nu_\ell b q\bar{q}' \bar{b}$ and $t\bar{t} \rightarrow W^+ b W^- \bar{b} \rightarrow q\bar{q}' b \ell^- \bar{\nu}_\ell \bar{b}$,
- Dilepton channel: $t\bar{t} \rightarrow W^+ b W^- \bar{b} \rightarrow \ell^+ \nu_\ell b \ell'^- \bar{\nu}_{\ell'} \bar{b}$.

The fully hadronic channel has the largest branching fraction of $(2/3)^2 \approx 0.45$ but also suffers from the largest background. The single-lepton channel with

its moderate branching fraction of $2 \times 2/3 \times (2 \times 1/9) \approx 0.29$ has moderate backgrounds, while the dilepton channel has the smallest branching fraction of only $(2 \times 1/9)^2 \approx 0.05$, but only very small backgrounds⁶. A more detailed discussion of the background processes most relevant to $t\bar{t}$ production follows in Section 3.2.2.

2.4.2. Mass

In the SM, the mass of fermions is generated by their Yukawa coupling to the Higgs boson, linking the left-handed and right-handed components of their spinors. The corresponding part of the SM Lagrangian for top quarks reads:

$$\mathcal{L}_{\text{Yukawa},t} = -y_t \frac{v}{\sqrt{2}} (\bar{t}_L t_R + \bar{t}_R t_L) = -y_t \frac{v}{\sqrt{2}} t\bar{t} = -m_t t\bar{t}, \quad (7)$$

where y_t is the Yukawa coupling constant of the top quark, v is the vacuum expectation value of the Higgs field, t_L and t_R are the left-handed and the right-handed components of the top-quark spinor t , and m_t is the top-quark mass. It is worth noting that—unlike for any other fundamental fermion—the numerical value of y_t is unity to good approximation. This may just be a numerical coincidence, but is often interpreted as a hint of the special role that the top quark could play in BSM physics.

The mass of the top quark is not a uniquely defined quantity. In QCD perturbation theory quark masses are renormalized and thus become energy-scale dependent. The pole mass (also “on-shell mass”) m_t^{pole} is a seemingly obvious choice to define the top-quark mass. As the top quark does not hadronize it can be considered an unstable “free” fermion and its pole mass is defined as the real part of the (renormalized) top-quark propagator’s pole. However, this definition is only unique in a given fixed order of QCD perturbation theory. Moreover, as quarks cannot be observed as free particles due to QCD confinement, the full quark propagator does not contain a pole. It can also be shown that certain radiative corrections that have to be considered to all orders (“infrared renormalon”) are hard to control and lead to irreducible intrinsic uncertainties of the m_t^{pole} definition. Another open

⁶The factors $2 \times 1/9$ (instead of $3 \times 1/9$) in the single-lepton and dilepton channels are introduced because only electrons and muons are considered charged leptons in the above classification scheme, while tau leptons are treated separately due to their many leptonic and hadronic decay modes and large hadronic backgrounds.

question is if the mass parameter used in MC generators can be identified with m_t^{pole} , as MC generators use an energy cut in the parton shower as well as a hadronisation model, both of which cannot be easily mimicked by a perturbative calculation.

The class of scale-dependent “short-distance masses,” such as the mass definition in the modified minimal subtraction renormalization scheme (“ $\overline{\text{MS}}$ mass”), do not contain non-perturbative ambiguities. Short-distance masses can be converted to pole mass in a given order of perturbation theory in a unique way, which however comes with uncertainties due to the truncation of the perturbative series [98, 99]. The inclusive intrinsic uncertainty of the top-quark pole mass due to renormalon effects has recently been demonstrated to be only 70 MeV [100], much smaller than other uncertainties occurring in measurements of the top-quark mass at hadron colliders. On the other hand, attempts to calibrate the top-quark mass used in MC generators to a short-distance mass for e^+e^- initial states show larger uncertainties of the order of 300 MeV [101]. The debate on the ultimate precision achievable in top-quark mass measurements is ongoing.

2.5. Top Quark-Antiquark Pair Production

The most abundant production process for $t\bar{t}$ pairs at hadron colliders is QCD pair production. At parton level two LO processes with cross sections proportional to α_S^2 contribute that lead to $t\bar{t}$ final states (see Fig. 2): gluon-gluon (gg) fusion in the s -, t -, and u -channel⁷ and quark-antiquark ($q\bar{q}$) annihilation. The relative fractions of gg and $q\bar{q}$ initiated processes depends on the PDFs of the initial-state hadrons and the center-of-mass energy of the collisions. In pp collisions, $q\bar{q}$ annihilation can take place between valence quarks or sea quarks and sea antiquarks, while in $p\bar{p}$ collisions, valence quarks from the proton can annihilate with valence antiquarks from the antiproton. This makes $q\bar{q}$ annihilation more likely in $p\bar{p}$ collisions at the Tevatron compared to pp collisions at the LHC. The center-of-mass energy \sqrt{s} of the collisions determines at which momentum fraction x the partons in the initial state hadrons are probed: to produce a $t\bar{t}$ pair at rest, the partonic center-of-mass energy $\sqrt{x_1 x_2 s}$ must be equal to twice the top-quark mass. For larger \sqrt{s} , smaller x values and larger momentum transfers get relevant,

⁷The Lorentz-invariant kinematic variables s , t , and u are called Mandelstam variables. In scattering processes they denote the “direction” of the momentum transfer by a virtual particle.

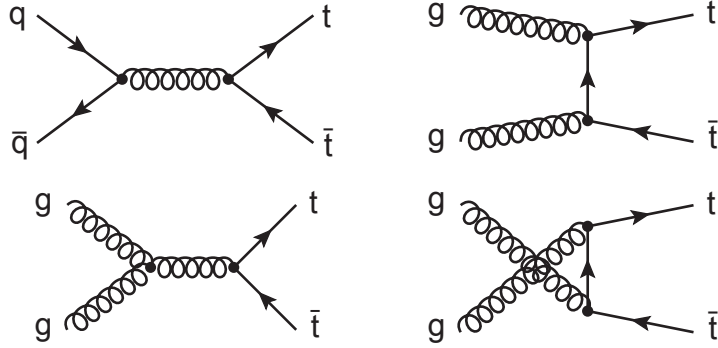


Figure 2: Feynman diagrams for $t\bar{t}$ production in QCD at LO: $q\bar{q}$ annihilation (top left), gg fusion in the s -channel (bottom left), gg fusion in the t -channel (top right), and gg fusion in the u -channel (bottom right). Feynman diagrams created with JAXODRAW [102].

and it becomes increasingly likely to probe a gluon inside the hadrons. At the LHC at $\sqrt{s} = 13$ TeV, $t\bar{t}$ production is dominated by gg fusion (approximately 90%), while only 10% of the $t\bar{t}$ pairs are produced via $q\bar{q}$ annihilation.

At NLO, $t\bar{t}$ production processes with cross sections proportional to α_S^3 become relevant. These processes include higher-order corrections to the LO processes with the real emission of gluons and virtual corrections. In addition new production channels open up: Processes with qg and $\bar{q}g$ initial states contribute for the first time at NLO. The ultraviolet divergences occurring in NLO calculations are systematically canceled by renormalization. This introduces the renormalization scale μ_R into the calculation. Infrared and collinear divergences of the initial state particles are systematically absorbed in the PDFs, introducing the factorization scale μ_F into the calculation, as discussed in Section 2.2. The inclusive $t\bar{t}$ production cross section is known to NLO accuracy since the late 1980s [103, 104]. The first full NNLO calculation of the inclusive $t\bar{t}$ production cross section, i. e. including processes up to α_S^4 , became available in 2013 [86].

The precision of $t\bar{t}$ cross section calculations can be further improved by resumming contributions which may become large in certain areas of phase space to all orders in QCD perturbation theory. These may include e. g. the emission of soft gluons or effects at the kinematic production threshold, where the velocity of the $t\bar{t}$ pair $\beta_{t\bar{t}}$ approaches zero, $\hat{s} \approx 2m_t$. The leading contributions at n -th order are proportional to $\alpha_S^n \ln(\dots)^{2n}$, hence they are often called leading logarithmic (LL) contributions. Contributions at next-to-leading logarithmic (NLL) order are proportional to $\alpha_S^n \ln(\dots)^{2n-1}$, etc.

Logarithmic corrections to the inclusive $t\bar{t}$ production cross section are known to next-to-next-to-leading logarithmic (NNLL) order. The most precise prediction of the inclusive $t\bar{t}$ production cross section to date (NNLO+NNLL) reaches an uncertainty of less than 4% [86]. Prior to the full NNLO result several NLO+NNLL calculations were published, often referred to as “approximate NNLO,” as they already included important parts of the NNLO calculations. Numerical access to the cross section formulae for $t\bar{t}$ production as a function of α_S , μ_R , and μ_F and for a given PDF set is provided by software tools such as TOP++ [105] and HATHOR [106]. Differential cross sections at approximate NNLO can be obtained from the DIFFTOP program [107].

Additional improvements to the SM prediction of the $t\bar{t}$ cross section are obtained by including electroweak corrections proportional to $\alpha_S^2 \alpha$ [108, 109, 110]. Another approach is to consider the full process $pp \rightarrow W^+ b W^- \bar{b} + X$, i.e. both $t\bar{t}$ production and decay, at NLO, including all interference effects and kinematic configurations in which only one or none of the top quarks is on its mass shell [111, 112].

Top quarks and antiquarks produced in $t\bar{t}$ pair production show only very small polarization (approximately 1%, depending on the initial state and the choice of the quantization axes [113]); however, their spins are significantly correlated. The quantum-mechanical observable connected to a spin is its projection to a quantization axis. The magnitude of the $t\bar{t}$ spin correlation effect depends on the choice of the quantization axes (“spin basis”); therefore the spin basis is often chosen to maximize the size of the effect. One typical choice is the beam basis, for which the quantization axis for both the top quark and antiquark is the beam axis in the laboratory frame. One can show that in the beam basis, the spins in $q\bar{q} \rightarrow t\bar{t}$ are 100% correlated close to the kinematic threshold, where $\beta_{t\bar{t}}$ is close to zero. In the helicity basis, the quantization axes are the flight directions of the t and the \bar{t} in the $t\bar{t}$ rest frame and hence the spin projections are equal to the t and \bar{t} helicities. In the helicity basis $q\bar{q} \rightarrow t\bar{t}$ are 100% correlated for $\beta_{t\bar{t}} \rightarrow 1$. The process $gg \rightarrow t\bar{t}$ does not show 100% spin correlation for any choice of quantization axes, as the t and the \bar{t} carry like helicities for $\beta_{t\bar{t}} \rightarrow 0$ and opposite helicities for $\beta_{t\bar{t}} \rightarrow 1$.

2.6. Single-Top Quark Production

Top quarks can also be produced singly in electroweak processes; the inclusive cross section is about two to three times smaller than for strong $t\bar{t}$ production. The production processes are classified by the virtuality of the

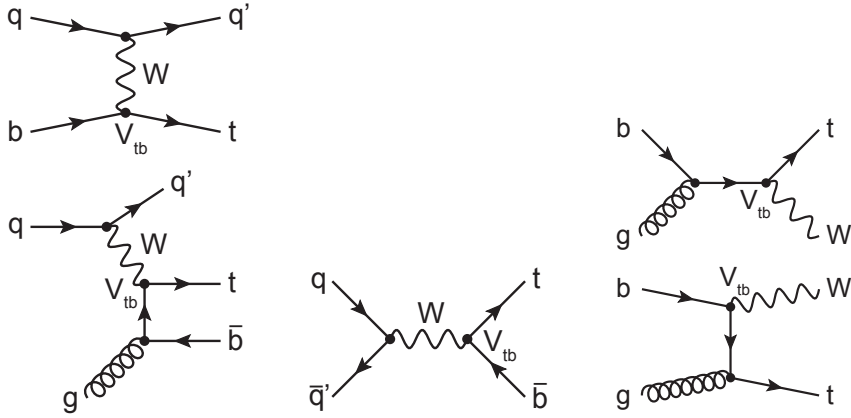


Figure 3: Feynman diagrams for electroweak single top-quark production at LO: t -channel production in the five-flavor scheme and four-flavor scheme (left), s -channel production (center), and associated Wt production (right). Feynman diagrams created with JAXODRAW [102].

W boson exchanged in the process. The most abundant single top-quark production process at the LHC is t -channel production (SM expectation: 70% of the total cross section), followed by the associated production of a top quark and a real W boson (25%), and s -channel production (5%). At the Tevatron, 70% t -channel and 30% s -channel single top-quark production are predicted by the SM, the Wt contribution is negligible. LO Feynman diagrams of these processes are displayed in Fig. 3. The electroweak production vertex contains the CKM matrix element V_{tb} . This offers the opportunity to measure V_{tb} directly in single top-quark production. As the W boson only couples to left-handed quarks and right-handed antiquarks, the top (anti)quarks produced in the above processes are 100% polarized.

Single-top production in the t -channel is mediated by a space-like virtual W boson. The process can be calculated in a scheme in which the initial state b quark originates from flavor excitation in the proton (five-flavor scheme (5FS)). The LO production process in the 5FS is $qb \rightarrow q't$. Alternatively, in the four-flavor scheme (4FS) the LO process is the $2 \rightarrow 3$ process $qg \rightarrow q't\bar{b}$, where the initial-state gluon splits into a $b\bar{b}$ pair and one of the b quarks interacts with the virtual W boson to produce the top quark. The “spectator” quark q' is typically emitted at rather small angles with respect to the beam axis, resulting in one of the most striking signatures of t -channel single top-quark production, a jet at large $|\eta|$.

Theoretically the t -channel process is known differentially to NNLO, first calculated assuming stable top quarks [87], recently also for production and decay [88]. Earlier calculations of the t -channel production cross section were performed at approximate NNLO [114]. The NLO corrections to the LO t -channel cross section are “accidentally” small—of the order of a few percent—and the NNLO corrections are of the same order.

In s -channel single top-quark production a time-like virtual W boson is exchanged. The process is known to approximate NNLO [115]. In associated Wt production the W boson is real. This process is known to approximate NNLO accuracy [116]. NLO corrections to Wt production in which the intermediate top (anti)quark is on its mass shell, called “double resonant” processes, share the same final state with $t\bar{t}$ production. In MC generators this overlap can be consistently removed by either removing all double-resonant contributions (“diagram removal”) or by local cancellation of double-resonant contributions via subtraction terms (“diagram subtraction”). Both methods lead to comparable results. A more comprehensive way of dealing with the overlap between Wt and $t\bar{t}$ production is to consider the full process $pp \rightarrow W^+ b W^- \bar{b} + X$ at NLO, as introduced in Section 2.5. Numerical access to single top-quark production cross sections at fixed-order NLO for all three production channels is provided as part of the parton-level MC generator Monte Carlo for Femtobarn Processes (MCFM) [117] and recent versions of HATHOR [118].

2.7. Summary

In the SM, the properties of the top quark are well defined. The high-precision computations available for top-quark production and many top-quark properties enable tests of the SM as well as searches for BSM physics when confronted with measurements of comparable precision. These measurements will be the subject of the remainder of this review.

3. Experimental Techniques in Top-Quark Physics

A typical hadron collider detector consists of a tracking detector, an electromagnetic and a hadron calorimeter, and a muon detector, grouped around the interaction point like the shells of an onion. Momenta of charged particles are determined by tracking their trajectories in strong magnetic fields. In the calorimeters, particle energies are determined in a destructive measurement from electromagnetic and hadronic showers initiated by the particles. The

raw signals of the various subdetectors are further processed to reconstruct basic analysis objects such as electrons, muons, and jets. The experimental signatures of events with $t\bar{t}$ pairs or single top quarks may contain charged leptons, neutrinos, and jets, initiated from gluons, light (u , d , s , c) quarks, or bottom (b) quarks. As a consequence of this rich mixture of signatures all subdetectors of a hadron collider detector are required in top-quark physics. Collision events are selected according to the signatures expected from events with top quarks such that these events are kept but background processes with similar signatures are suppressed. Based on the event selection higher-level data analysis methods are employed to obtain physics results.

In this chapter some general aspects of the data analysis chain in top-quark physics are reviewed. Note however that many details of the analysis chain have to be tailored specifically to a given measurement. After a sketch of the reconstruction of the basic analysis objects, aspects of data selection and background suppression methods are discussed. Techniques to reconstruct top quarks and methods of statistical data analysis are also presented.

3.1. Analysis Objects

3.1.1. Leptons

Electrons. Electrons from the decay $W^+ \rightarrow e^+\nu_e$ are reconstructed in the tracking detector and electromagnetic calorimeter. The electrons are expected to have large transverse momenta ($\gtrsim 20$ GeV) and be well isolated from other particles in the event. The isolation requirement is fulfilled for events in which the sum of track momenta or the sum of energy deposited in the calorimeter in a cone around the electron (excluding the energy of the electron and of bremsstrahlung photons) is below a threshold. A further selection (“electron identification”) is applied to distinguish electrons from other particles with similar detector signatures, e. g. charged pions. At the LHC the electron identification is typically based on information on the shapes of energy clusters in the calorimeter, assisted by tracking information. To achieve optimal separation, this information is often processed in multivariate methods, which will be introduced in Section 3.4.2. The energy scale of electrons is typically calibrated against the invariant mass of well-known SM particles, such as the quarkonia J/ψ and Υ , and the Z boson.

Muons. Muons are reconstructed in the tracking detector and the muon detector, but leave only little energy in the calorimeters. Similar to the electron selection, the selection of muons from the decay $W^+ \rightarrow \mu^+\nu_\mu$ is based

on their large transverse momenta and isolation, combined with—typically multivariate—muon identification criteria.

Efficiency Determination. The efficiencies for lepton reconstruction and identification can be determined from correlated pairs of leptons in $J/\psi \rightarrow \ell^+\ell^-$ or $Z \rightarrow \ell^+\ell^-$ events using a tag-and-probe method, see e.g. [119]. One lepton (“tag” lepton) is selected with strict criteria, the other lepton (“probe” lepton) is selected with looser criteria. The fraction of selected events in which both the tag and probe lepton pass the reconstruction or identification criteria is a measure of the corresponding efficiency. The tag-and-probe efficiencies, often determined as a function of the lepton kinematics (transverse momentum and pseudorapidity), may differ in data and simulated data. The simulated data are corrected for this effect by applying appropriate scale factors defined as the ratio of tag-and-probe efficiencies in data and simulated data.

3.1.2. Jets, Missing Transverse Momentum, and Particle Flow

Jets are reconstructed combining the information of subdetectors, typically the hadron and electromagnetic calorimeters and the tracking detector.

Jet Algorithms. While at the Tevatron the jet reconstruction in top-quark physics was mainly based on algorithms that define jets based on geometric cones, the LHC experiments use sequential recombination jet algorithms, most prominently the anti- k_t algorithm [120]. The size of a jet in η - ϕ space is characterized by the radius parameter

$$R = \sqrt{\Delta\eta^2 + \Delta\phi^2}, \quad (8)$$

where $\Delta\eta$ ($\Delta\phi$) is the distance from the jet axis in pseudorapidity (azimuthal angle)⁸. In top-quark physics at LHC Run 2 the radius parameter of the anti- k_t algorithm is chosen to be $R = 0.4$. The anti- k_t algorithm fulfills the requirements of infrared and collinear safety: the same set of jets is reconstructed in an event if an additional particle with very low momentum or at very small angle to another particle is added to the event.

⁸Sometimes the rapidity y is used instead of the pseudorapidity η .

Jet Energy Scale and Resolution. Due to the non-linear detector response to jets, the jet-energy scale (JES) must be calibrated carefully, typically with a combination of simulation-based and data-driven methods. The JES calibration performed to correct the jet response in the LHC data of Run 1 is discussed in great detail in [121, 122]. Also data-simulation discrepancies in the jet-energy resolution (JER) are corrected for, usually by smearing the momenta of simulated jets to match the resolution observed for reconstructed jets in the data.

B-Jets and B-Tagging. Top-quark decays in the dominant mode $t \rightarrow W^+ b$ always produce a bottom quark in the final state, which subsequently hadronizes into a b hadron. Jets containing b hadrons (“ b -jets”) can be identified by dedicated b -tagging algorithms. These algorithms are based on the distinctive properties of b hadrons such as their long lifetime of the order of picoseconds, their high mass of the order of 5 GeV, or their semileptonic decays $B \rightarrow \ell\nu X$. Experimental signatures related to the long lifetimes include secondary vertices with large displacement from the primary collision vertex or charged-particle tracks with large impact parameters relative to the primary vertex. The high mass of b hadrons results in “broader” jets compared to jets from light quarks and high relative p_T of the lepton in semileptonic decays. The lepton from $B \rightarrow \ell\nu X$ is typically non-isolated and carries rather low absolute p_T (“soft lepton”). In addition the fragmentation of b quarks is said to be “hard”: the b hadron carries a large fraction of the b -quark energy. Recent b -tagging algorithms at hadron colliders combine the available information on jets with b hadrons in a single multivariate classifier.

The performance of a b -tagging algorithm can be quantified by the probability to correctly identify a jet coming from a b quark as a b -jet and by the probability to wrongly identify a jet from a light-flavor quark or a gluon (“mistag”). A b -tagging classifier can either be used by assigning b -tags to all jets that show classifier values above standardized working points with a fixed mistag probability or by exploiting the full shape of the classifier’s distribution. As the b -tagging and mistag efficiency may be different in data and simulated data, b -tagging algorithms must be calibrated, such that the simulation can be corrected with scale factors. Datasets enriched with $t\bar{t}$ events are well suited for such a calibration, as they contain two jets with b hadrons from the $t\bar{t}$ decay, see also Section 6.5.

Missing Transverse Momentum. The entire detector is required to reconstruct the missing transverse momentum (MET) caused for example by the

undetected neutrino(s) from leptonic W -boson decays. To calibrate the MET reconstruction, the calibration of all other analysis objects must be known.

Particle Flow. In the CMS experiment, the reconstruction of analysis objects follows the particle-flow approach [123]. For each object type the optimal combination of subdetectors is chosen to determine its four-momentum. One benefit of this approach is the improved jet energy and MET resolution: The energies of all charged particles in a jet are inferred from their momenta, which are very precisely measured by the tracking detectors, and only the neutral hadron energies have to be reconstructed in the low-resolution hadron calorimeter.

3.2. Data Selection

The cross sections for top-quark production are about nine orders of magnitude lower than the inelastic pp scattering cross section. Many other SM processes have cross sections larger than the $t\bar{t}$ or single top-quark production cross section. These processes contribute to the background in a given production and decay channel if they have similar experimental signatures. The signal-to-background ratio⁹ for top-quark events in a hadron collider data sample is improved by a multistage online and offline data selection.

3.2.1. Preselection

The online data selection is performed by a multilevel trigger system, where the first step is usually implemented in custom-made electronics and later steps are implemented in software on large computing farms. The main trigger paths¹⁰ used in top-quark physics consist of triggers that select one or more isolated electrons or muons above a threshold in transverse momentum p_T . These trigger paths enable the efficient selection of single-lepton and dilepton $t\bar{t}$ events as well as single top-quark events. Further possible trigger paths include combinations of triggers sensitive to a large number of high- p_T jets and MET. The trigger efficiency is determined both in data and simulated data, for example using a tag-and-probe method, see Section 3.1.1.

⁹The signal-to-background ratio is the ratio of signal and background events in a given data sample. Another way of expressing the separation of signal and background is the signal purity, defined as the fraction of signal events in a sample containing both signal and background events.

¹⁰A trigger path is a combination of triggers at different levels to select a specific set of trigger objects.

Any difference is corrected for with appropriate scale factors applied to the simulation.

The next step in the data selection is the preselection of high-quality collision events with all relevant detector parts operational, a suitable trigger fired and a primary vertex successfully reconstructed. Events containing signals not from beam-beam collisions, such as beam halo, cosmic rays or coherent noise in the detector, are vetoed.

3.2.2. Event Selection and Major Backgrounds

A further selection step is required to separate signal events with top quarks from background events originating from other physics processes. The signatures of signal events and the most important background processes depend on the production and decay channel considered. The event selection criteria may include cuts on the minimum (and/or maximum) number of leptons, jets, and b -jets. The selection may also exploit the specific kinematic properties of these objects or of global observables in top-quark events, such as MET.

In top-quark decay channels containing one or more charged leptons background processes may be separated in those with real isolated charged leptons and those in which other objects are misidentified as charged leptons (“fake leptons”). One prominent example is QCD multijet production: due to the large production cross section even the small fraction of jets misidentified as charged leptons contributes to the background. Therefore the QCD multijet background is often hard to estimate, as will be discussed in 3.2.3.

Dilepton Channel. In the $t\bar{t}$ dilepton decay channel, exactly two isolated high- p_T leptons with opposite charge signs are selected (e^+e^- , $\mu^+\mu^-$, or $e^\pm\mu^\mp$), which strongly suppresses SM backgrounds. Events with a same-flavor lepton pair with an invariant mass around the Z -boson mass, which occur in the associated production of Z bosons and jets (“ Z +jets”), are rejected. One or two b -tagged jets may be required to further suppress background containing light-flavor or gluon jets.

The most important real-lepton backgrounds for $t\bar{t}$ dilepton events with same-flavor lepton pairs are $\gamma^*/Z \rightarrow e^+e^-/\mu^+\mu^- + \text{jets}$ (“Drell-Yan”) and associated Wt production. For leptons with different flavors, also background from $Z \rightarrow \tau^+\tau^- + \text{jets}$ production with leptonic τ decays becomes relevant. Background processes with one or more misidentified leptons include the production of W bosons in association with jets (“ W +jets”) and QCD multijet

production. Overall the dilepton channel has the smallest branching fraction but the most favorable signal-to-background ratio of all $t\bar{t}$ decay channels.

Single-Lepton Channel. The most striking feature of $t\bar{t}$ pairs decaying in the single-lepton channel is a single isolated high- p_T lepton. The event selection requires this lepton and at least three or four high- p_T jets. Further requirements may be a significant amount of MET from the neutrino and one or two b -tagged jets.

The background level in the single-lepton channel is moderate. The background is composed of processes with isolated high- p_T leptons, such as single top-quark production, W +jets and Z +jets production, and production of electroweak boson pairs, WW , WZ , and ZZ . QCD multijet background also contributes to the background in the single-lepton channel if one of the jets is misidentified as a charged lepton.

Fully Hadronic Channel. The signature of $t\bar{t}$ events in the fully hadronic decay channel consists of six jets, two of which originating from b hadrons. Unlike the channels discussed above, a selection of isolated leptons cannot be used to suppress background in this channel. Therefore the fully-hadronic channel suffers from large QCD multijet background, which may be somewhat reduced by requiring two jets to be b -tagged.

Single-Top Production. In all single top-quark production channels, the top-quark decay $t \rightarrow W^+ b \rightarrow \ell^+ \nu_\ell b$ is considered, requiring a high- p_T lepton and large MET as well as a b -tagged jet from the top-quark decay. The additional signature of t -channel single top-quark production is a light jet with large $|\eta|$ (see Section 2.6). In the s -channel an additional b -jet is expected so that a second b -tag is usually required. The additional W boson in the final state of associated Wt production is usually required to decay leptonically. Therefore the characteristic signature of the Wt -channel is two oppositely charged high- p_T leptons—similar to the $t\bar{t}$ dilepton channel but with only one b -jet. In all single top-quark production channels, $t\bar{t}$ production is a major background. Other backgrounds include W +jets, Z +jets, WW , WZ and ZZ processes as well as QCD multijet events in which jets are misidentified as leptons. The relative importance of the backgrounds depends on the channel.

3.2.3. Background Estimation Techniques

The background remaining after the event selection can be controlled with various techniques. While some of the techniques are specific to certain

analyses, there are also some recurring concepts. These will be discussed in this section.

The level of background from processes that are known to be well-modeled in the MC simulation is estimated directly from simulated events. In case the inclusive cross section predicted by the MC simulation does not match the most precise calculations, the simulated events are often scaled such that their integral matches the number of events expected from the calculation for a given integrated luminosity¹¹.

Background processes for which the simulation has known deficiencies or for which it is difficult to populate the relevant parts of phase space with a sufficient number of simulated events are often estimated from the data itself. The data is split into a signal-enriched signal region and one or more signal-depleted control regions. This split can either be based on the event kinematics or on the analysis-object selection in the same kinematic region. The background rate is determined in the control region(s), often by a maximum-likelihood (ML) fit (see Section 3.4.1) to the data in which the signal and the relevant background rates are free parameters. The background rate is then translated to the signal region using the MC simulation. Such data-driven or data-assisted procedures to determine the background result in estimates of the background rate and often also of further properties, e.g. shapes of kinematic distributions.

A background process often estimated from data is QCD multijet production. Due to the large cross section and the small misidentification probability of jets as charged leptons, simulations of multijet events often do not provide a reliable estimate of the background in events with top quarks. Instead a model of misidentified jets is built from electron or muon candidates in the data for which one or more of the lepton identification criteria failed. Events with such lepton candidates form a disjoint set of events with kinematic properties that closely resemble those of the QCD background events passing the event selection. The normalization of the QCD background is obtained from an ML fit to control regions, while the shapes of kinematic distributions are taken from the model in the signal region.

¹¹This procedure changes the production rates of processes but neglects potential differences in the shapes of kinematic distributions due to higher-order corrections.

3.3. Top-Quark Reconstruction

In many top-quark physics analyses it is desirable to reconstruct the four-momenta of the top (anti)quarks from the leptons, jets, and MET observed in an event. However, a one-to-one correspondence between parton-level objects such as the top quarks and their decay products and reconstruction-level objects such as leptons and jets only exists in a crude LO picture of hadronic collisions. Beyond LO this picture is complicated e.g. due to additional jets from gluon radiation with large p_T and/or at large angles with respect to the original parton. Apart from this conceptual question, the top-quark reconstruction faces problems such as underdetermined kinematics due to neutrinos, and the combinatorics of assigning jets to partons from the top-quark decay (usually the bottom quarks from top decays and the light-flavor quarks from hadronic W decays).

3.3.1. Neutrino Reconstruction

In single-lepton and dilepton final states, one or two neutrinos from W -boson decays escape the detector undetected. The only kinematic observable available is \vec{p}_T^{miss} , a two-vector in the transverse plane. In single-lepton $t\bar{t}$ events, a single neutrino is the only (real) source of MET, however, $p_{z,\nu}$, the z component of its momentum, remains unknown. Using the W -boson mass as a constraint and neglecting the lepton and neutrino masses, two solutions for p_z can be obtained by solving the quadratic equation

$$(p_\ell + p_\nu)^2 = p_W^2 = m_W^2, \quad (9)$$

where p_ℓ , p_ν , and p_W are the four-momenta of the charged lepton, the neutrino, and their parent W boson. For the two neutrinos in dilepton final states the kinematic system is underdetermined and additional assumptions have to be made, see e.g. [124].

3.3.2. Jet-Parton Assignment and Kinematic Fitting

In an LO picture each jet can be assigned uniquely to one parton from the top-quark decay. However, the correct assignment is unknown. For example, in a single-lepton $t\bar{t}$ decay with two bottom quarks and two light quarks from the hadronic W boson decay, there are $4! = 24$ possible permutations of jet-parton assignments. This number is reduced to 12 permutations because exchanging the assignment of the light quarks from the hadronic W -boson

decay does not change the event kinematics. The combinatorics can be further reduced if b-tagged jets are always assigned to the bottom quark or antiquark.

There are various ways to pick the “best” permutation of jet-parton assignments in an event. A popular method is to construct a figure of merit based on a χ^2 -like variable that compares the invariant top-quark and W -boson masses with their nominal values. The mass of the semileptonically decaying top quark is reconstructed from the invariant mass of a charged lepton, a neutrino and a b -jet, $m_{\ell\nu b}$. The mass of the hadronically decaying W boson is inferred from the invariant mass of two jets, m_{jj} , and the mass of the hadronically decaying top quark from the three-jet mass m_{jjj} ¹². The individual terms are usually weighted with factors $1/\sigma^2$, which contain the widths of the invariant mass distributions, for the semileptonic top-quark decay ($\sigma_{m_t, \text{lep}}$), the W -boson decay ($\sigma_{m_W, \text{had}}$) and the hadronic top-quark decay ($\sigma_{m_t, \text{had}}$), determined from the correct jet-parton assignment in MC-simulated events:

$$\chi^2 = \frac{(m_{\ell\nu b}^2 - m_t)^2}{\sigma_{m_t, \text{lep}}^2} + \frac{(m_{jj}^2 - m_W)^2}{\sigma_{m_W, \text{had}}^2} + \frac{(m_{jjj}^2 - m_t)^2}{\sigma_{m_t, \text{had}}^2}. \quad (10)$$

The jet-parton assignment can also be performed using machine-learning techniques that are trained on simulated data to pick the “best” permutation according to a more sophisticated figure of merit. As an alternative to picking the “best” permutation of jet-parton assignments, also all permutations can be considered, weighted by their probability to be the “best” permutation, determined from MC simulations.

A more precise method to reconstruct the kinematics of $t\bar{t}$ events is based on the observation that the resolution of certain kinematic observables is limited and the observables may hence be slightly mismeasured. In a kinematic fit, the figure of merit for the “best” jet-parton permutation is parameterized as a function of those kinematic observables that can only be reconstructed with limited resolution. Examples of such observables include the jet energies and directions and \vec{p}_T^{miss} . Each of these observables is allowed to be varied within its resolution in the kinematic fit. This way, the kinematic fit adjusts the event kinematics to find the optimum figure of merit for a

¹²Note that the correlation between m_{jj} and m_{jjj} is ignored by considering the two observables separately.

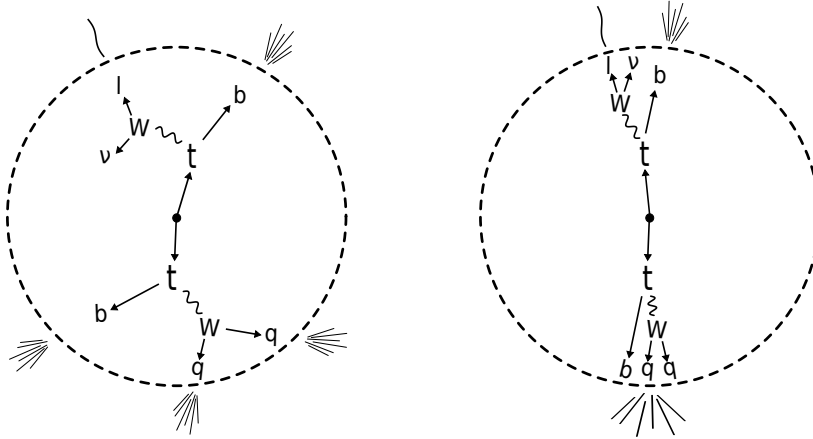


Figure 4: Illustration of resolved (left) and boosted (right) event topologies in single-lepton $t\bar{t}$ decays. Picture courtesy of Shawn Williamson.

given permutation, before selecting the “best” permutation, or weighting all permutations.

3.3.3. Boosted Top-Quark Reconstruction

Top quarks produced in high-energy collisions, e.g. at the current LHC Run 2, may receive large momenta, either in regular SM processes or by hypothetical high-mass particles decaying to top quarks. For top quarks with $p_T \gtrsim 200$ GeV the decay products (jets and leptons) start becoming collimated, such that they begin to overlap in $\eta\phi$ space. This is illustrated in Fig. 4. Such topologies require specialized “boosted-jet” reconstruction algorithms. The boosted-jet reconstruction comes with the additional benefit that the combinatorial problem of jet-parton assignment is mitigated, as events with boosted analysis objects contain fewer (but more complicated) reconstructed objects than events in which all jets can be resolved.

In the last decade a large number of algorithms was conceived to analyze boosted-jet topologies. In these algorithms, jets are first reconstructed with large radius parameters (“fat jets”), $R = 0.8 - 1.5$. As a second step, the substructure of the fat jets is examined. The main classes of jet-substructure algorithms are jet-declustering algorithms and jet-shape algorithms. The key idea of declustering algorithms is to undo the last steps of the jet clustering algorithm to identify those structures in the jet related to the decay of the mother particle. Grooming techniques such as pruning or trimming remove

soft radiation uncorrelated to the decay particles. This results in better resolution for the jet mass and reduced pile-up¹³ dependence. Jet shape algorithms such as n -subjettiness [125] assign a probability to a fat jet to stem from n overlapping jets. Combinations of several techniques can also be used. The exact choice of algorithm depends on the expected event topologies and typical momentum range of the boosted objects. Reviews of jet-substructure algorithms can be found e.g. in [126, 127, 128].

3.4. Statistical Methods

Analysis of top-quark events often relies on advanced statistical methods, many of which are based on the maximum-likelihood (ML) principle. Sophisticated statistical methods are employed in several analysis steps, in order to maximize the precision of measurements or the sensitivity of searches for BSM physics. Examples include the selection of physics objects and entire events (see Section 3.2), the classification of the selected events as either signal or background, and the extraction of physics information such as model parameters from the data.

The methods relevant for top-quark physics are often made available in the C++-based data analysis framework ROOT [129], which is very widely used in particle physics. It is beyond the scope of this review to explain the methods and tools in detail. The interested reader is referred to text books such as [130].

3.4.1. Maximum-Likelihood Method

A typical task in physics data analysis is to extract model parameters from data. The ML method solves this task by first constructing the likelihood function $\mathcal{L}(\vec{\mu})$ as the product of probability densities $P(\vec{x}_i|\vec{\mu})$ for single measurements \vec{x}_i given the true parameter vector $\vec{\mu}$:

$$\mathcal{L}(\vec{\mu}) = \prod_i P(\vec{x}_i|\vec{\mu}). \quad (11)$$

The ML estimator of $\vec{\mu}$ is the maximum of the likelihood function, usually determined by minimizing $-\ln \mathcal{L}(\vec{\mu})$. For discretized (“binned”) data distributions, P is the Poisson distribution of the number of events in each bin

¹³At high-luminosity hadron colliders, the hadron-hadron collision of interest is overlaid by other collisions in the same bunch crossing as well as the “afterglow” of collisions from previous bunch crossings in the detector. These are jointly referred to as pile-up.

given the number of events expected from the model. The model expectation is usually obtained from simulated data and represented as bins of a template histogram. The model parameters $\vec{\mu}$ estimated with the ML method are the normalizations of the histograms, which are in turn proportional to the total number of events expected from the model. Unbinned data distributions can be fitted with continuous probability density distributions, e.g. constructed by kernel-density estimates [131].

In more sophisticated ML models used with binned data further parameters are added that describe the influence of systematic uncertainties on the normalizations and shapes of the template histograms. The model parameters are then split into the “parameter(s) of interest” $\vec{\beta}$ and additional “nuisance parameters” $\vec{\delta}$. In a Bayesian approach, *a-priori* knowledge, for example from auxiliary measurements, is used to constrain $\vec{\delta}$. To obtain an estimate of the parameters of interest and their uncertainties, the nuisance parameters can be either profiled or marginalized. Profiling means that the profile likelihood ratio

$$\lambda(\vec{\beta}) = \frac{\mathcal{L}(\vec{\beta}, \hat{\vec{\delta}})}{\mathcal{L}(\hat{\vec{\beta}}, \hat{\vec{\delta}})} \quad (12)$$

is minimized instead of the original likelihood. The numerator of the profile likelihood ratio is the minimum of the likelihood function at a fixed value of $\vec{\beta}$, where the nuisance parameters assume the values $\hat{\vec{\delta}}$, the denominator is the global minimum of the likelihood function, with parameter values $\hat{\vec{\beta}}$ and $\hat{\vec{\delta}}$. In the marginalization approach the likelihood function is integrated numerically, typically with MC methods. The parameters of interest are then extracted from the projections of the likelihood function on these parameters (“marginal distributions”).

A frequentist method to deal with systematic uncertainties is to perform ensemble tests by drawing pseudo-experiments (also: “toy experiments”, “MC experiments”). Many random variations of distributions are generated and the entire analysis chain is performed on each variation. The variance of the results is a measure of the uncertainty. Examples of software tools used in top-quark physics that include the above sophisticated ML methods are RooFit/RooStats [132, 133] shipped with ROOT, and THETA [134].

One way of interpreting measurements of top-quark properties is to compare the BSM physics prediction for an observable with the corresponding SM prediction. The statistical method applied in the comparison is called

hypothesis test. First the null hypothesis H_0 (e.g. SM) and the alternative hypothesis H_1 (e.g. BSM) are formulated and a test statistic is constructed that is able to discriminate between H_0 and H_1 . A popular choice of the test statistic is the ratio of likelihoods for the vector of measurements \vec{x} given H_0 or H_1 :

$$r(\vec{x}) = \frac{L(\vec{x}|H_0)}{L(\vec{x}|H_1)}. \quad (13)$$

From the observed value of the likelihood ratio r_{obs} , the significance for the hypotheses is obtained.

3.4.2. Multivariate Classification

The selection of analysis objects and the classification of events as signal-like or background-like is often performed using methods from (supervised) machine learning. Such methods use simulated data to teach (“train”) an algorithm how to distinguish signal from background processes based on a non-linear combination of several input variables. It is important for these methods not to generalize peculiar features of the simulated data used for the training to the entire sample (“overtraining”). Among the many methods available in the statistics literature (see e.g. [135]), the most popular in top-quark physics are artificial neural networks (ANNs) and boosted decision trees (BDTs). Currently the main tool employed in the top-quark physics community is the Toolkit for Multivariate Data Analysis (TMVA) [136] which is shipped with ROOT. Alternatives include the PYTHON package SCIKIT-LEARN [137], and the commercial ANN package NEUROBAYES [138].

3.4.3. Matrix-Element Method

The entire parton-level kinematics of a physics process is contained in the squared scattering amplitude of the process, also called the (hard) matrix element. The matrix-element method (MEM) is a method to construct an event-based likelihood discriminant to separate signal from background that fully exploits all information in the event by using the squared matrix element [52]. Currently most MEM implementations use matrix elements at LO QCD perturbation theory; however, concepts to implement NLO corrections into the MEM have emerged recently, see e.g. [139, 140, 141]. The explanation below follows the review article [142].

For an event with a given set of reconstructed kinematic variables \vec{x} a likelihood function $L(\vec{x}|S)$ is constructed under the hypothesis that the event is a signal event. Also for one or more background hypotheses, likelihood

functions $L(\vec{x}|B_i)$ are constructed. These are combined for each event in a likelihood ratio discriminant, e. g. in the form

$$R(\vec{x}) = \frac{L(\vec{x}|S)}{L(\vec{x}|S) + \sum_i c_i L(\vec{x}|B_i)}, \quad (14)$$

where each background likelihood function can be assigned a different weight c_i . For a given signal or background hypothesis the likelihood function is constructed from the sum of cross sections of all sub-processes that lead to the parton-level final state y , with kinematics \vec{y} , that could have lead to the reconstruction-level final state x , with kinematics \vec{x} , using the QCD factorization approach (assuming pp collisions):

$$\sigma(pp \rightarrow y) = \sum_{jk}^{\text{partons}} \int_0^1 dz_j dz_k f_j(z_j) f_k(z_k) \frac{(2\pi)^4}{z_j z_k s} |M(jk \rightarrow y)|^2 d\Phi. \quad (15)$$

In the above equation, the sums are over the partons j and k and the integrals are over their momentum fractions z_j and z_k . The parton distribution functions are denoted $f_i(z_i)$, and the hard matrix element for the process leading to the parton-level final state y is $M(jk \rightarrow y)$. The Lorentz-invariant phase space measure is symbolically written as $d\Phi$. Note that the phase space integral is numerically expensive as all unobserved variables in each event (often of the order of 20) have to be integrated over.

To translate from the parton-level final state y to the reconstruction-level final state x , $\sigma(pp \rightarrow y)$ is folded with a transfer function $W(\vec{x}|\vec{y})$:

$$\sigma(pp \rightarrow x) = \int \sigma(pp \rightarrow y) W(\vec{x}|\vec{y}) d\vec{y} \quad (16)$$

The transfer function accounts for the limited detector resolution and for the combinatorics of assigning reconstruction-level quantities to partons and is determined from MC-simulated data. The final likelihood functions $L(\vec{x}|S)$ and $L(\vec{x}|B_i)$ are obtained by normalizing the cross sections to the (fiducial) cross sections of the processes.

3.4.4. Unfolding Techniques

Physics quantities reconstructed with a collider detector and theoretical calculations of observables cannot be compared directly. This problem can be solved in two ways. Either the theoretical calculations are fed into a detailed

simulation of the detector and hence “forward-folded” into detector-related effects such as limited acceptance and resolution. Alternatively the detector effects can be removed from the reconstructed quantities by unfolding techniques. In top-quark physics unfolding is typically applied in measurements of differential cross sections, see Section 4.3.

Mathematically the relation of reconstructed and “true” quantities can be expressed in a Fredholm integral equation:

$$g(\vec{x}) = \int R(\vec{x}|\vec{y}) f(\vec{y}) d\vec{y} + b(\vec{x}) = \int A(\vec{x}|\vec{y}) \epsilon(\vec{y}) f(\vec{y}) d\vec{y} + b(\vec{x}), \quad (17)$$

where $g(\vec{x})$ is the distribution of the reconstructed quantity as a function of the set of kinematic variables \vec{x} , and $f(\vec{y})$ is the “true” distribution from theory, depending on a different set of kinematic variables \vec{y} . The response function (also: transfer function) $R(\vec{x}|\vec{y})$, which may be written as the product of an acceptance function $\epsilon(\vec{y})$ and a resolution function $A(\vec{x}|\vec{y})$, parameterizes the detector effects. In addition the background distribution $b(\vec{x})$ must be considered. Unfolding means solving Eq. (17) for $f(\vec{y})$, which is an ill-posed mathematical problem. The solution chosen in particle physics analyses starts with discretizing the distributions in bins of histograms:

$$g_i = \sum_{j=1}^m R_{ij} f_j + b_i. \quad (18)$$

A straight-forward matrix inversion to solve for f_j is not useful in a physics analysis, because physics data always contain statistical fluctuations, which cannot be distinguished from real structure in the data without further assumptions. This leads to numerical instabilities in the matrix inversion. Therefore regularization techniques are applied that assume that distributions of physics observables are “smooth.” Various regularization techniques are discussed in the literature. Among the most popular in top-quark physics are Tikhonov regularization, as e. g. implemented in the ROOT class `TUnfold` [143], and regularization by singular-value decomposition as in `TSVDUnfold` [144].

Another approach employed in top-quark physics is called fully Bayesian unfolding [145]. In this approach Bayesian inference is applied to the unfolding problem and the probability density of a true distribution $f(\vec{y})$ given the reconstructed distribution $g(\vec{x})$ is obtained from Bayes’ theorem:

$$p(f|g) \propto \mathcal{L}(g|f) \cdot \pi(f), \quad (19)$$

where $\mathcal{L}(g|f)$ is the likelihood function of the measured values g given the true distribution f and $\pi(f)$ is the prior probability density of f . In this method backgrounds and systematic uncertainties can be included consistently as described in Section 3.4.1.

3.4.5. Statistical Combination of Measurements

Statistical methods can be used to combine sets of measurements from the same or from different experiments with the goal of reducing uncertainties, see Section 1.3. A simple prescription for combining a set of measurements would be the weighted arithmetic mean of the measured values, where the weights are the inverse of the variance of the values. However, in all realistic cases of top-quark physics, not only the statistical and systematic uncertainties of the individual measurements must be considered, but also their correlations.

Information on all uncertainties and their correlations is available if the measurements are interpreted using the same ML model. In such a combination on the level of likelihood functions the model parameters and their uncertainties are estimated from all data in a consistent way. However, such an approach requires a large degree of coordination between the individual measurements and may thus not always be feasible, in particular when combining measurements from different experiments. In this case the combination is often performed on the level of measured values instead of likelihood functions, with a reasonable guess on their covariance matrix. A popular combination method for this purpose is called BLUE (best linear unbiased estimator) [146].

4. Top-Quark Production

The measurement of the production cross section of $t\bar{t}$ pairs and single top quarks constitutes a test of the SM description of heavy quark production. The level of understanding of top-quark production increases with increasingly precise measurements and theoretical calculations of the production processes. In this chapter, recent top-quark production cross section results from the Tevatron and the LHC will be reviewed, illustrating current experimental methods and their precision. The presentation includes inclusive and differential $t\bar{t}$ and single top-quark production cross sections, and cross sections for the associated production of $t\bar{t}$ plus “something else” ($t\bar{t} + X$),

such as jets, missing transverse momentum, photons, W and Z bosons, as well as Higgs bosons.

4.1. Observables and Measurement Techniques

Inclusive Cross Section. The most inclusive observable to measure particle production is the inclusive (also: total) production cross section. The inclusive cross section is a measure of the production probability in the full kinematic phase space of the production processes¹⁴. The first cross section measurements performed in the top-quark sector, both at the Tevatron and the LHC, were inclusive $t\bar{t}$ cross sections $\sigma_{t\bar{t}}$. The observables and techniques discussed in this section apply to other production processes as well.

All cross section measurements start with a basic selection of candidate events to suppress background while retaining a large fraction of signal events in the data sample, see Section 3.2. After the event selection the simplest way to extract $\sigma_{t\bar{t}}$ is to perform a “counting experiment”:

$$\sigma_{t\bar{t}} = \frac{N_{\text{top}} - N_{\text{bkg}}}{\int \mathcal{L} dt \cdot \epsilon}, \quad (20)$$

where N_{top} and N_{bkg} are the number of top-quark events and background events, $\int \mathcal{L} dt$ is the integrated luminosity and ϵ the efficiency to detect top-quark events in the full phase space. While counting experiments are simple and robust, the need for absolute predictions of the signal efficiency and background level limits their precision. More precise cross section results can be obtained by exploiting the kinematic properties of the final state particles. The shapes of kinematic distributions are determined for the signal and all background processes and stored in discretized form in template histograms. The sum of template histograms for the signal and background processes is then fitted to the data using maximum-likelihood (ML) methods as described in Section 3.4.1. Fitting kinematic distributions in signal-enriched and background-enriched regions simultaneously allows for better constraints on the background level, resulting in reduced statistical uncertainty of the result. At the same time additional systematic uncertainties arise due to the limited knowledge of the shapes of kinematic distributions. In more sophisticated fitting procedures, also the shapes of kinematic distributions are

¹⁴In this context, phase space is understood as the space of all possible final state configurations in top-quark events with all possible four-momenta consistent all conservation laws.

allowed to vary within their uncertainties. The top-quark production cross section and its uncertainties may then be determined either from a multi-parameter profile likelihood ratio fit, or the uncertainties are estimated using pseudo-experiments.

Fiducial Cross Section. The need to know the absolute efficiency makes measurements of inclusive cross sections model-dependent. The efficiency ϵ in Eq. (20) may be factorized into the detector acceptance and the detection efficiency of final state particles within the detector acceptance. While the detection efficiency can be calibrated using data to high accuracy (see Section 3.2), a determination of the detector acceptance, i. e. the ratio of detectable events to all events, requires an (often large) extrapolation to the full phase space of the $t\bar{t}$ final state. The extrapolation is usually performed using simulated data samples and hence depends on the MC model on which the simulation is based. This model dependence can be reduced by measuring the cross section in a restricted (“fiducial”) region of the phase space that closely resembles the detector acceptance. Typical phase space requirements include the detector’s pseudorapidity range and a minimum transverse momentum of analysis objects. The fiducial phase space is usually defined in the MC simulation on the particle level, after the particles hadronize but before they decay. The fiducial cross section can then be extrapolated to the full phase space by employing the predictions of different MC models.

Differential Cross Section. Differential cross sections are cross sections as a function of one or more kinematic observables. They allow more detailed insights into the $t\bar{t}$ production mechanism. In recent years, many differential cross section measurements have been performed in a fiducial region of phase space to reduce their model dependence. Measurements of the distribution of kinematic observables can be translated into differential cross sections using the unfolding techniques, such as those described in Section 3.4.4. After all detector-related effects are removed by unfolding, differential cross sections from different experiments, if performed in the same fiducial phase space, can be directly compared among each other. Differential cross sections can also be compared with predictions from MC event generators (for particle-level and parton-level measurements) or from theoretical calculations (only for parton-level measurements). For comparisons at particle level, the software framework RIVET [147] is often used.

4.2. Inclusive $t\bar{t}$ Production

The inclusive $t\bar{t}$ production cross section has been measured for $p\bar{p}$ initial states at the Tevatron and for pp initial states at the LHC as well as for various center-of-mass energies: 1.8 TeV and 1.96 TeV for $p\bar{p}$ collisions, and 5.02 TeV¹⁵, 7 TeV, 8 TeV, and 13 TeV for pp collisions. These measurements test the theoretical understanding of the dependence of the $t\bar{t}$ production cross section on the initial state and the center-of-mass energy. The most precise measurements of the $t\bar{t}$ production cross section so far have been performed in the dilepton and single-lepton decay channels. A summary compiled by the LHCtopWG is displayed in Fig. 5, showing excellent agreement between measurements and the most precise SM predictions to date at NNLO with NNLL resummation [86].

Tevatron Results. At the Tevatron, a combination of inclusive $t\bar{t}$ production cross section measurements from the CDF and D0 experiments has been performed, resulting in a combined value of

$$\sigma_{t\bar{t}} = (7.60 \pm 0.20 \text{ (stat)} \pm 0.36 \text{ (syst)}) \text{ pb}, \quad (21)$$

assuming a top-quark mass of $m_t = 172.5$ GeV [150]¹⁶. The combination achieves a precision of 5.4%, which is dominated by systematic uncertainties due to limitations in signal and detector modeling, as well as the uncertainty of the Tevatron luminosity. The most precise individual measurements at the Tevatron were obtained in the single-lepton channel [151, 152], while the precision in the dilepton channel was limited by the rather small Tevatron dataset [153, 152]. The D0 experiment also pioneered the extraction of the top-quark mass from the $t\bar{t}$ cross section, as will be discussed in Section 5.2.3.

LHC: High-Precision Results. Most recent LHC measurements of the inclusive $t\bar{t}$ cross section are first reported as fiducial cross sections and then extrapolated to the full phase space with several MC models. Given the large

¹⁵In November 2015 the LHC delivered pp collisions at a center-of-mass energy of 5 TeV as part of its heavy-ion program. The inclusive $t\bar{t}$ cross section was measured using a data sample corresponding to an integrated luminosity of 26 pb^{-1} [148].

¹⁶As will be discussed in Section 5.2.3, the $t\bar{t}$ production cross section decreases steeply with increasing m_t . The detection efficiency is a function of m_t as well. Therefore $t\bar{t}$ cross section measurements are quoted at a fixed value of m_t , usually the default value used in the MC simulation. Sometimes the m_t dependence of the cross section is quoted as well.

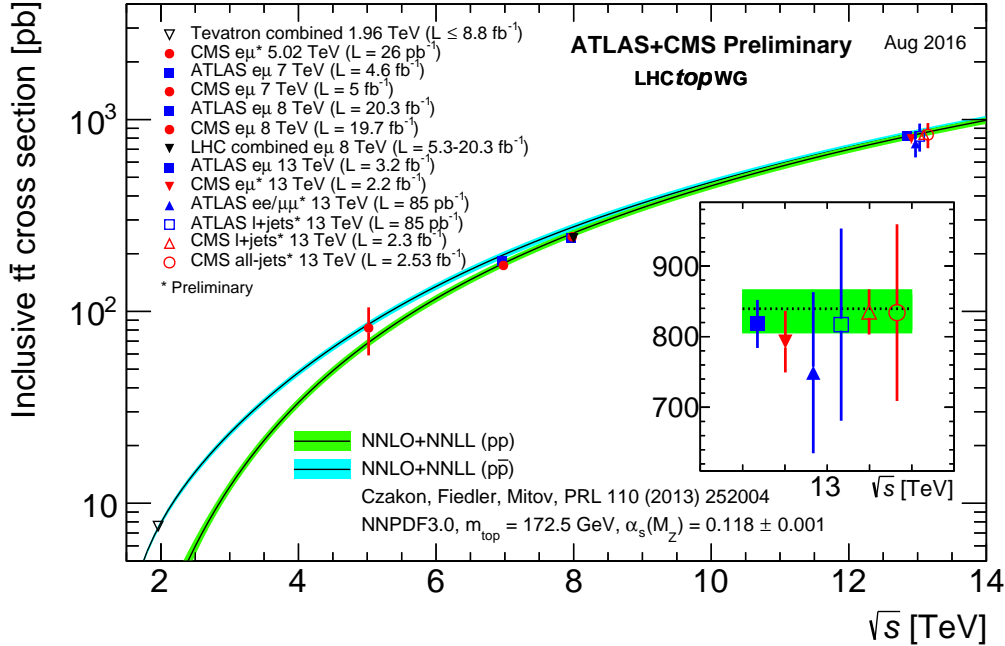


Figure 5: Compilation of measurements and SM predictions of the inclusive $t\bar{t}$ cross section as a function of the center-of-mass energy for $p\bar{p}$ collisions at the Tevatron and pp collisions at the LHC [149].

$t\bar{t}$ data samples recorded at the LHC the precision of these measurements is limited by systematic uncertainties. The most precise LHC measurements to date are summarized in Table 1. The smallest systematic uncertainties in LHC Run 1 have been achieved in the $e\mu$ channel with its low background level and small expected number of jets [154, 155]. For example, the CMS measurement [155] is based on a simultaneous binned profile likelihood ratio fit in 12 different event categories in the $e\mu$ dilepton channel. The categories are defined by the number of b -tagged jets and the number of additional non- b -tagged jets in the events. In the categories with additional jets the fit is applied to the p_T distribution of the non- b -tagged jet with the lowest p_T , while in the categories without additional jets a counting experiment is performed by fitting the total event yield.

Major experimental uncertainties on the ATLAS and CMS high-precision

Table 1: Summary of most precise inclusive $t\bar{t}$ cross section measurements from the ATLAS [154, 157] and CMS [155, 158] experiments together with their relative statistical and systematic uncertainties. The systematic uncertainties are separated into uncertainties originating from experimental and theoretical sources as well as luminosity (and beam energy) uncertainties.

Measurement	$\sigma_{t\bar{t}}$ (pb)	stat (%)	exp (%)	th (%)	lumi (%)	Ref.
ATLAS $e\mu$ 7 TeV	182.9	1.7	2.3	2.0	1.8	[154]
CMS $e\mu$ 7 TeV	173.6	1.2	$^{+2.6}_{-2.3}$		2.2	[155]
ATLAS $e\mu$ 8 TeV	242.4	0.7	2.3	3.1	1.7	[154]
CMS $e\mu$ 8 TeV	244.9	0.6	$^{+2.6}_{-2.2}$		2.6	[155]
ATLAS $e\mu$ 13 TeV	818	1.0		3.3	2.7	[157]
CMS $e/\mu+\text{jets}$ 13 TeV	834.6	0.3		2.7	2.7	[158]

measurements originate from the determination of the luminosity¹⁷, the trigger and lepton identification efficiencies, and the estimation of background from $\gamma^*/Z+\text{jets}$ events. Another class of uncertainties, particularly important when fiducial cross sections are extrapolated to the full phase space, is due to the $t\bar{t}$ modeling in the MC simulation. Adding all uncertainties in quadrature, both ATLAS and CMS arrive at very similar total uncertainties below 4% for LHC Run 1, comparable to the current uncertainty of the most precise SM prediction of less than 4% [86].

In 2014, the ATLAS and CMS inclusive $t\bar{t}$ cross section measurements available at $\sqrt{s} = 8 \text{ TeV}$ at the time were combined, to arrive at an even smaller total uncertainty of 3.5% [156]. The current uncertainty on $t\bar{t}$ cross sections measured with LHC Run 2 data [157, 158] is slightly higher than the uncertainties obtained in Run 1, but is expected to improve with larger data samples and better understanding of systematic uncertainties.

LHC: Further Results. The inclusive $t\bar{t}$ cross section has also been established in other decay channels and found to be consistent with the high-precision channels with electrons and muons. This constitutes a check of the $t\bar{t}$ production mechanism, because the cross section could be influenced by BSM

¹⁷At the level of precision achieved in measurements of the $t\bar{t}$ production cross section at the LHC also the uncertainty on the beam energy becomes relevant. So far, this is only taken into account by ATLAS.

physics differently in different channels. The additional $t\bar{t}$ decay channels in which the $t\bar{t}$ cross section has been determined include final states with one or two tau leptons [159, 160, 161, 162, 163, 164], which are sensitive to charged Higgs boson production, and fully hadronic $t\bar{t}$ decays [165, 166, 167, 168, 169]. Inclusive $t\bar{t}$ cross section measurements have also been pursued for top quarks with large transverse momenta (“boosted top quarks”), together with differential cross section measurements, as will be discussed in Section 4.3.

Top quark-antiquark production has become accessible also in pp collisions at the LHCb experiment, where the process has been established with a significance of 4.9 standard deviations using a dataset of approximately 2 fb^{-1} at $\sqrt{s} = 8\text{ TeV}$ [170]. While classic collider experiments at the Tevatron and the LHC cover the “central” kinematic region of $|\eta| < 2.5$, the forward-spectrometer design of LHCb leads to coverage of the complementary kinematic region of forward pseudorapidities, $2.0 \lesssim \eta \lesssim 4.5$. The fiducial $t\bar{t}$ production cross section in this kinematic region is measured along with the cross sections for associated $W + b\bar{b}$ and $W + c\bar{c}$ production. The signature is a high- p_T electron or muon and two heavy-flavor tagged jets, and $t\bar{t}$, $W + b\bar{b}$, and $W + c\bar{c}$ candidate events are separated using a multivariate discriminant. The measured fiducial cross sections are in agreement with SM predictions at NLO.

4.3. Differential $t\bar{t}$ Production Cross Section

The Tevatron and the LHC experiments have published differential $t\bar{t}$ cross section measurements as a function of various kinematic properties of analysis objects. Kinematic observables may be separated in quantities that can be measured directly and reconstructed quantities that have to be inferred from the quantities measured directly. Some differential cross section results are presented as normalized to the inclusive or fiducial $t\bar{t}$ cross section determined from the same measurement. In this way normalization uncertainties, e.g. the luminosity uncertainty, cancel and the sensitivity of the measurement to the shapes of kinematic distributions is improved.

Kinematic Observables. The directly measured observables, e.g. the kinematic distributions of leptons and jets with b hadrons, are corrected back to the level of stable particles, which are accessible in MC generators, in a fiducial region of phase space. The fiducial region is usually defined by the detector acceptance in p_T and η for leptons and jets. Particle-level charged leptons are taken as the generated leptons and sometimes “dressed” with soft

photons from quantum electrodynamics (QED) radiation. Particle-level jets are jets clustered from stable generated particles except neutrinos with the same anti- k_t algorithm applied to reconstructed particles. On particle-level b -tagging is mimicked by adding “ghost b hadrons” [171] with negligible momenta to the list of final-state particles before the jet algorithm is applied and declaring jets in which one or more ghost b hadrons are found as b -jets. The particle-level observables can be compared to the output of MC event generators, for example using RIVET [147], to test how well a given MC generator models the observables.

The kinematics of the top quarks and antiquarks or of the $t\bar{t}$ system are defined only on the level of partons rather than particles. The partons are considered before decay, but after gluon and photon radiation. Parton-level observables have the advantage that they can be compared with theoretical calculations directly. While it is reasonable to assume a very good correspondence between the particle and the parton level, strictly speaking there is no unambiguous way to translate particle-level results to the parton level. Therefore particle-level pseudo-observables (“pseudo-top”) have been agreed upon in the LHCtopWG, where care has been taken to define the reconstructed quantities in a theoretically safe and unambiguous way, see e.g. [172, 173]. Differential cross sections can also be determined as a function of event-level quantities such as momentum sums which do not require the reconstruction of the top quark and antiquark from their decay products.

At the level of stable top quarks, differential cross section measurements can be compared with SM predictions directly. These predictions are available at various levels of precision that go beyond the precision available in current MC event generators: approximate NNLO with NNLL resummation [174], approximate NNLO [107, 175] and approximate next-to-next-to-next-to-leading order (N^3LO) [176]. Recently also differential distributions at full NNLO precision became available [177, 178].

Tevatron Results. The limited size of the $t\bar{t}$ data samples at the Tevatron only allowed for a small number of differential cross section measurements. CDF published the differential $t\bar{t}$ cross section as a function of the invariant $t\bar{t}$ mass [179], which can also be interpreted as a search for exotic particles decaying into $t\bar{t}$. D0 published a comprehensive set of differential cross sections using the full Tevatron Run II dataset [180], see Fig. 6.

LHC Results. The LHC experiments have published a large number of differential $t\bar{t}$ cross section measurements at $\sqrt{s} = 7 \text{ TeV}$ and 8 TeV [181, 182, 183,

172, 184, 185, 186, 173], and recently also at $\sqrt{s} = 13$ TeV [187, 188, 189, 190]. A small selection of the vast body of results is presented in Figs. 6 and 7, including both particle and parton level observables. After unfolding, these results are compared with the predictions of MC generators at particle and parton level, and SM predictions at parton level. Generally current MC event generators as those introduced in Section 2.3 describe the differential cross sections well over a wide kinematic range. In CMS, the measured p_T spectrum of top quarks was found to be softer than most MC predictions, while ATLAS results are consistent with the predictions. The recent full NNLO calculation of the top-quark p_T spectrum shows improved agreement with the measured spectrum, compared to previous calculations. Recently, due to the large $t\bar{t}$ data samples at the LHC, also the first double differential cross sections were published, for example as a function of p_T and y of the top quark [191]. To study the production of top quarks with large transverse momenta, differential cross section measurements using boosted-top reconstruction techniques (see Section 3.3.3) have been devised [192, 187, 193, 194, 169]. A first differential $t\bar{t}$ cross section measurement as a function of the mass of boosted top quarks has been performed as a proof of principle to measure m_t in boosted-top final states [195].

Differential $t\bar{t}$ production cross sections measured as a function of further event-level quantities provide additional insight into the production mechanisms and are at the same time sensitive probes of BSM physics contributions to $t\bar{t}$ production. Measurement of the jet multiplicity and the number of additional jets, not coming from the decay products of the $t\bar{t}$ pair, in $t\bar{t}$ events from ATLAS [196, 197, 187, 198, 199] and CMS [200, 201, 202, 188, 190] probe the treatment of QCD radiation in MC event generators. Of particular interest for rare SM processes such as associated $t\bar{t}H$ production (with the decay $H \rightarrow b\bar{b}$) as well as for the search for BSM physics is the production of $t\bar{t}$ pairs with additional b -jets. In measurements of these processes, the ratio of cross sections for $t\bar{t}$ production with two additional b -jets and $t\bar{t}jj$ production, where j is a jet of any flavor, has been used as a robust observable sensitive to $t\bar{t}b\bar{b}$ production [203, 204, 205].

Differential cross sections as a function of event-level observables such as the missing transverse momentum (E_T^{miss}), the scalar sum of the jet transverse momenta (H_T), or the scalar sum of the transverse momenta of all physics objects (S_T) are sensitive to rare processes, e.g. the associated production of $t\bar{t}$ and W , Z , or Higgs bosons, as well as to BSM physics processes with lepton+multijet signatures [206, 207].

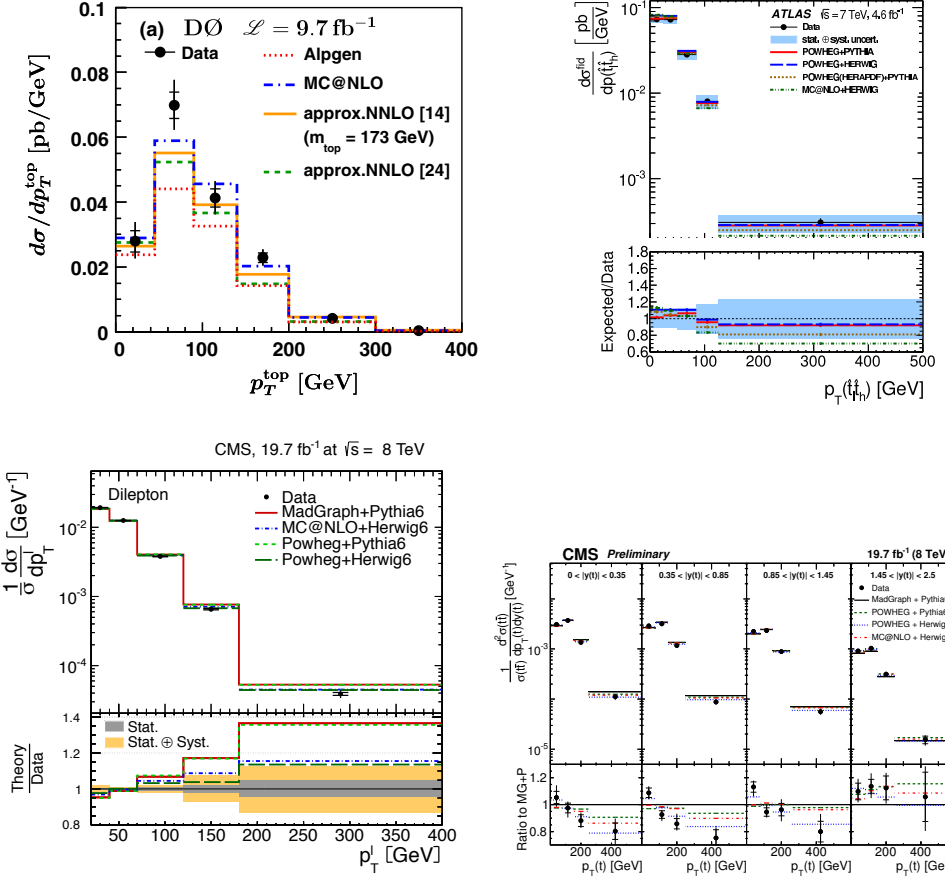


Figure 6: Examples of differential cross section measurements from the Tevatron and the LHC: Top-quark transverse momentum at the Tevatron [180] (top left). Transverse momentum of the pseudo-top-quark pair at $\sqrt{s} = 7 \text{ TeV}$ [172] (top right). Transverse momentum of the lepton from the top-quark decay at $\sqrt{s} = 8 \text{ TeV}$ [186] (bottom left). Transverse momentum of the top-quark for four different intervals of the top-quark rapidity at $\sqrt{s} = 8 \text{ TeV}$ [191] (bottom right). The distributions are unfolded to particle or parton level and compared to predictions using recent MC event generators and/or higher-order QCD calculations.

4.4. $t\bar{t} + X$ Production

The production of $t\bar{t}$ pairs in association with “something else” ($t\bar{t} + X$), where X can be the electroweak gauge bosons γ , W , and Z , or the Higgs boson, is predicted to be rare in the SM, with inclusive production cross sections in pp collisions at $\sqrt{s} = 13 \text{ TeV}$ predicted by NLO QCD below 1 pb. Measuring these processes gives access to the coupling of the top quark to the

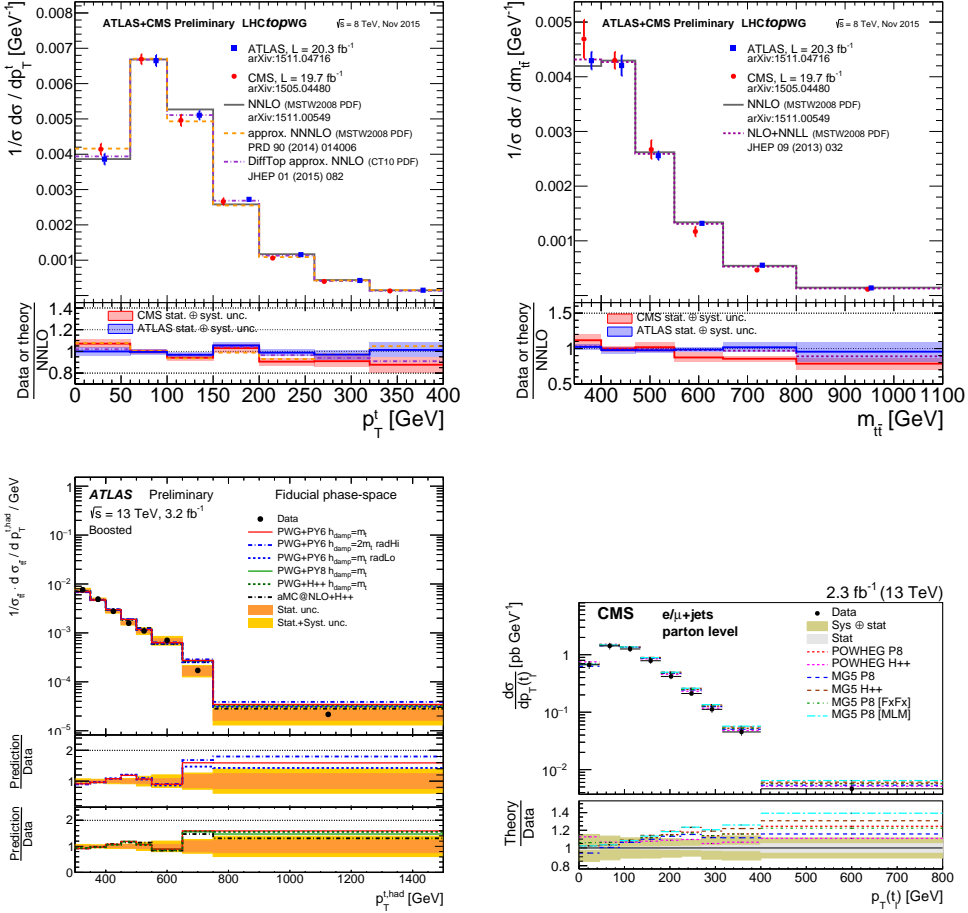


Figure 7: Examples of differential cross section measurements from the LHC: Comparison of ATLAS and CMS measurements of the top-quark transverse momentum (top left) and the $t\bar{t}$ invariant mass (top right) at $\sqrt{s} = 8$ TeV [65]. Transverse momentum of the hadronically decaying top quark at $\sqrt{s} = 13$ TeV using boosted-top reconstruction [187] (bottom left). Transverse momentum of the leptonically decaying top quark at $\sqrt{s} = 13$ TeV [190] (bottom right). The distributions are unfolded to parton level and compared to predictions using recent MC event generators and/or higher-order QCD calculations.

similar final states.

Electroweak Gauge Bosons. Evidence for $t\bar{t}\gamma$ production was first reported by CDF [208]. The process was first observed by ATLAS [209] in the experiment’s full dataset recorded at $\sqrt{s} = 7 \text{ TeV}$ and also measured by CMS in $\sqrt{s} = 8 \text{ TeV}$ data [210]. The production cross section, defined in a fiducial region of phase space, is compatible with the SM prediction at NLO. The challenge of these analyses lies in separating photons from $t\bar{t}\gamma$ production from hadron decays into photon pairs and hadrons and electrons misidentified as photons, which is done by studying the photon isolation.

Measurements of $t\bar{t}W$ and $t\bar{t}Z$ production have only become feasible with the large LHC datasets. The processes feature very massive final states of more than 425 GeV and therefore profit a lot from the increase in production cross sections at LHC Run 2 compared to Run 1. The LHC experiments have seen evidence of these processes in leptonic decays of the W and Z bosons in combination with single-lepton and dilepton decays of the $t\bar{t}$ pair, in events containing multiple jets, b -tagged jets and two to four charged leptons [211, 212, 213, 214, 215]. While the backgrounds in these events are generally low, it is difficult to estimate the number of analysis objects wrongly identified as leptons (“fake leptons”) precisely. The fake lepton background is usually modeled from data events in control regions, as described in Section 3.2.3. The measurements are compatible with SM predictions and are used to constrain BSM physics contributions to the Ztt coupling [212].

Higgs Boson. Higgs-boson production in the associated $t\bar{t}H$ channel is a process that has not yet been established experimentally. The channel is challenging due to the small production cross section, approximately 0.5 pb at $\sqrt{s} = 13 \text{ TeV}$ [216], and large irreducible backgrounds. In particular in the $H \rightarrow b\bar{b}$ decay channel, the background from $t\bar{t} b\bar{b}$ production is large and hard to control. With sophisticated multivariate methods, both physics motivated (matrix-element method, see Section 3.4.3) and from machine learning, and the inclusion of final states with boosted top quarks, so far only upper limits on the production cross section have been determined. Both ATLAS and CMS first conducted three independent analyses in the $H \rightarrow b\bar{b}$, $H \rightarrow \gamma\gamma$ and multilepton¹⁸ decay channels that were statistically combined in a second

¹⁸The multilepton channel summarizes all Higgs-boson decays with multiple leptons from the decay channels $H \rightarrow ZZ$, $H \rightarrow W^+W^-$, and $H \rightarrow \tau^+\tau^-$.

step.

The individual $t\bar{t}H$ searches performed using the LHC Run 1 dataset [217, 218, 219, 220, 221] were combined with other Higgs-physics results from ATLAS and CMS to arrive at a significance of 4.4 standard deviations for $t\bar{t}H$ production, where only 2.0 standard deviations were expected. This unexpected result is driven by a small excess of events in the multilepton channel [222]. With the four-fold increase in $t\bar{t}H$ production cross section at $\sqrt{s} = 13$ TeV, the LHC experiments are expected to finally become sensitive to $t\bar{t}H$ production with 30 fb^{-1} to 50 fb^{-1} of luminosity. First preliminary results using up to 13 fb^{-1} of data have already been presented [223, 224, 225, 226, 227, 228, 229, 230, 231], already with increased sensitivities compared to the Run-1 results.

Invisible Particles. The production of $t\bar{t}$ pairs in association with invisible particles results in a significant amount of MET. Such processes have been studied in the context of searches for BSM physics, in particular in the search for supersymmetric particles or more generically in dark-matter searches. This will be discussed in Section 6.4.4.

4.5. Single Top-Quark Production

Electroweak single top-quark production was first observed at the Tevatron [56, 57]. The expected inclusive cross section in $p\bar{p}$ collisions at $\sqrt{s} = 1.96$ TeV is small, of the order of 3 pb adding all production channels [115, 114]. At the LHC, single top-quark production in the t -channel has a moderately large cross section, of the order of 65 pb at $\sqrt{s} = 7$ TeV [114], so that single top-quark production was established early in LHC Run 1 [232, 233]. In the following the most precise measurements of single top-quark production available from the Tevatron and the LHC are summarized. A more detailed account of single top-quark production at the LHC can be found in two recent reviews [13, 14].

Tevatron Results. At the Tevatron, only t -channel and s -channel production were accessible. The characteristic t -channel signature of a semileptonically decaying top quark and a spectator jet in forward direction is overwhelmed by background mainly from $W + \text{jets}$ production. This requires sophisticated multivariate techniques to separate signal and background and profile likelihood ratio fits to extract the production cross section. Both CDF and D0 have published single top-quark production measurements using the above

techniques with their full Run-II datasets [234, 235] as well as a combination [236], shown in Fig. 8 (left). The s -channel, which has a smaller production cross section and larger backgrounds compared to the t -channel, was only established as a separate single top-quark production channel by combining the full CDF and D0 Run-II datasets [237]. The combined Tevatron results are in good agreement with SM predictions at approximate NNLO [115, 114].

LHC Results. Similar to the Tevatron, the cross section measurements at the LHC are based on multivariate separation of signal and background and profile likelihood ratio fits to extract the cross section. Precise measurements of the t -channel single top-quark production cross section have been performed at $\sqrt{s} = 7\text{ TeV}$ [238, 239], 8 TeV [240, 241], and 13 TeV [242, 243]. As for $t\bar{t}$ production, modeling uncertainties have been reduced by reporting fiducial cross sections in addition to inclusive cross sections [241, 244]. With the large datasets available at the LHC, also the first differential cross sections for t -channel single top-quark production as a function of the t or \bar{t} transverse momentum and rapidity became feasible [245, 246].

An interesting observable in t -channel single top-quark production in pp collisions is the ratio of production rates for top quarks and antiquarks, $R_{t\text{-ch}} = \sigma_t/\sigma_{\bar{t}}$. While the top quark is produced with an up-type quark (or down-type antiquark) in the initial state, the top antiquark is produced with a down-type quark (or up-type antiquark). Hence $R_{t\text{-ch}}$ is sensitive to the ratio of PDFs for up-type and down-type quarks (and down-type and up-type antiquarks), with a naive expectation of $R_{t\text{-ch}} = 2$ for up and down valence quarks only. Also anomalous Wtb couplings as expected from BSM physics would modify $R_{t\text{-ch}}$. Experimentally $R_{t\text{-ch}}$ is a robust observable in which many uncertainties cancel. Measurements of $R_{t\text{-ch}}$ from LHC Run 1 [239, 240] and Run 2 [242] are compatible with the SM prediction, see Fig. 8 (right). Another complementary constraint on PDFs can be obtained from the ratio of t -channel cross sections at $\sqrt{s} = 7\text{ TeV}$ and 8 TeV [240].

The Wt associated production channel, whose cross section was negligible at the Tevatron, was observed for the first time at the LHC [247, 248, 249, 250, 251]. The Wt production cross sections obtained by ATLAS and CMS at $\sqrt{s} = 8\text{ TeV}$ have recently been combined [252]. At the LHC, the smallest single top-quark production cross section is expected in the s -channel. First evidence for this process has been reported in an ATLAS analysis at $\sqrt{s} = 8\text{ TeV}$ using a sophisticated MEM technique (see Section 3.4.3) [253], the corresponding CMS search shows a slightly smaller significance [254].

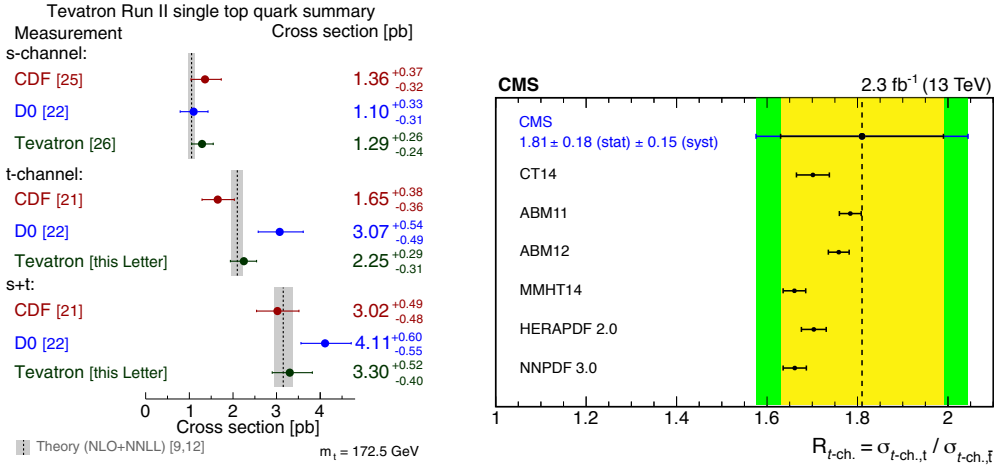


Figure 8: Compilation of Tevatron measurements of the single top-quark cross section in the s -channel and the t -channel as well as for both channels combined [236] and compared to SM predictions at approximate NNLO [115, 114] (left). Ratio of top quark and antiquark production cross sections in the t -channel at the LHC compared to various PDF sets [242] (right).

A summary of inclusive single top-quark cross section measurements at the LHC in all production channels and for different center-of-mass energies is presented in Fig. 9. All measurements are in good agreement with each other and with the SM predictions.

4.5.1. CKM Matrix Element V_{tb}

As the single top-quark production cross section is proportional to $|V_{tb}|^2$, many of the cross section measurements at the Tevatron and the LHC presented above are also interpreted in terms of constraints on $|V_{tb}|$. In such analyses, it is usually assumed that single top-quark production is only mediated by W -boson exchange, that $|V_{tb}|^2$ is much larger than the sum of $|V_{ts}|^2$ and $|V_{td}|^2$, and that the Wtb vertex is a CP-conserving $V-A$ coupling with a coupling strength modifier μ_V^L , with $\mu_V^L = 1$ in the SM, see Section 2.4.1. No assumptions about the unitarity of the CKM matrix are made.

A compilation of V_{tb} results from the LHC is presented in Fig. 10. The current most precise value is obtained from a combination of CMS t -channel cross section measurements at $\sqrt{s} = 7 \text{ TeV}$ and 8 TeV [240]:

$$|\mu_V^L V_{tb}| = 0.998 \pm 0.038 \text{ (exp)} \pm 0.016 \text{ (th)}, \quad (22)$$

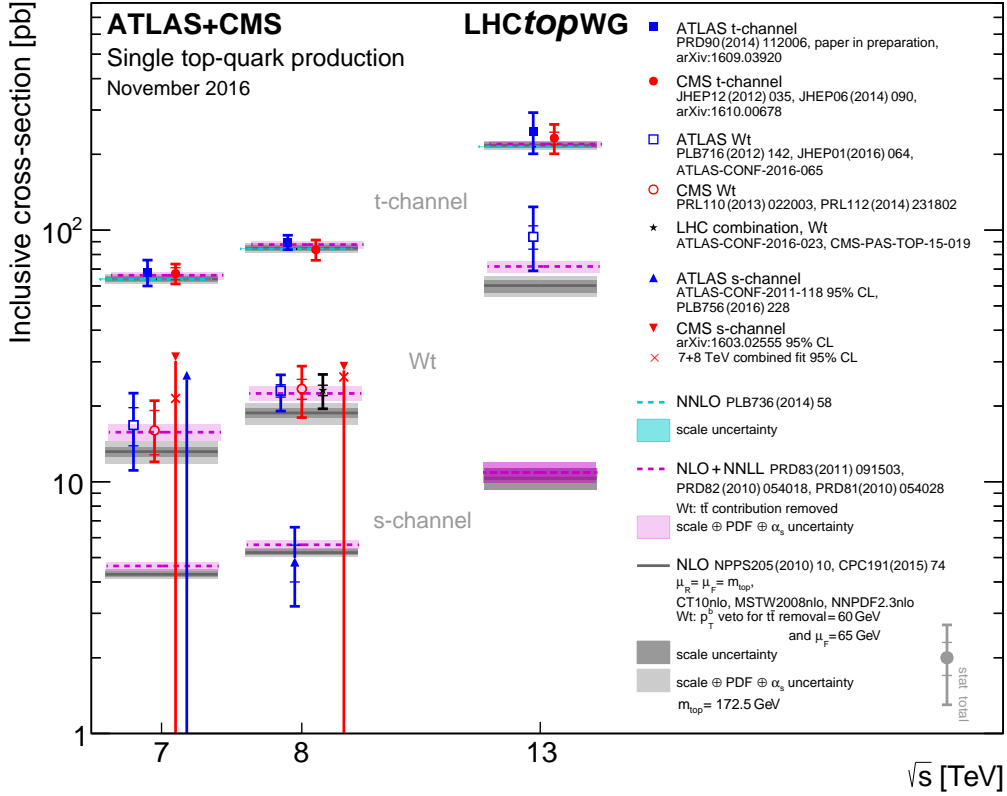


Figure 9: Compilation of measurements and SM predictions of the inclusive single top-quark cross section for different LHC center-of-mass energies [65].

where the first uncertainty originates from experimental and the second from theoretical sources. A value for $|V_{tb}|$ was also extracted from the combination of Wt production measurements: $|\mu_V^L V_{tb}| = 1.02 \pm 0.09$ [252].

4.5.2. Single Top + X Production

The associated production of single top-quarks and additional particles has only received little attention so far. The associated production of a single top-quark with a Higgs boson (tHq and tHW) is sensitive to the sign of the top-quark's Yukawa coupling relative to the Higgs coupling to vector bosons, while in $t\bar{t}H$ production only the absolute value of the Yukawa coupling is probed. The process is extremely rare in the SM due to destructive interference of the scattering amplitudes for the Higgs boson coupling to the W boson and the top quark and would be enhanced significantly by BSM

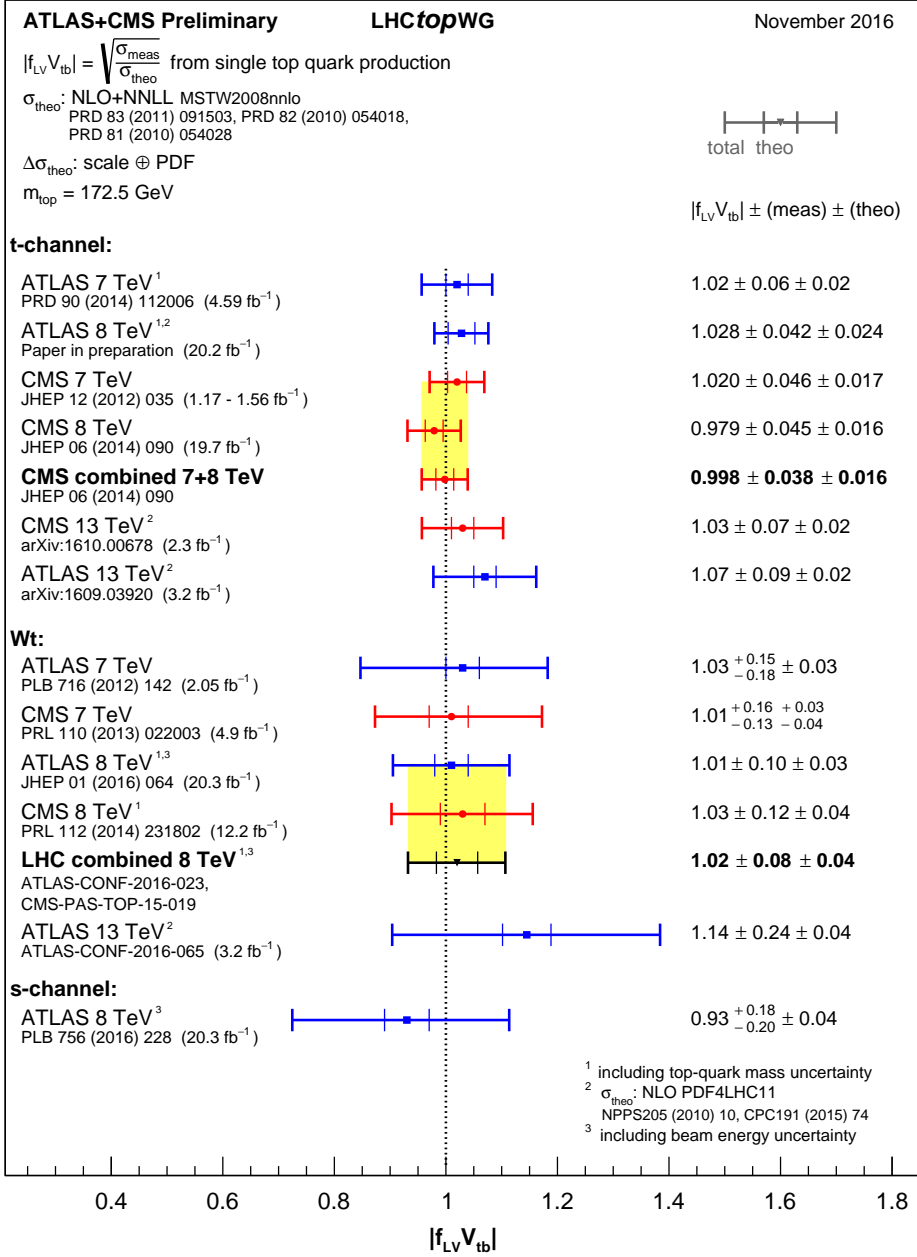


Figure 10: Compilation of LHC measurements of $|\mu_V^L V_{tb}|$ (denoted as $|f_{LV}V_{tb}|$ in the figure) [65].

physics. First direct limits on the tHq (and tHW) production cross section in Higgs-boson decays to $\gamma\gamma$, $b\bar{b}$, and multiple charged leptons using LHC data at $\sqrt{s} = 8$ TeV and $\sqrt{s} = 13$ TeV have been published in [255, 256]. Indirect limits on the Htq coupling were also obtained from the search for $t\bar{t}H$ production in the $H \rightarrow \gamma\gamma$ decay channel [217].

4.6. Summary

The production of top quarks in the SM is very well understood both experimentally and theoretically. Most kinematic distributions are well described by modern MC event generators. This provides a solid basis for studying the properties of the top quark as well as for searches for BSM physics in which top quarks are part of the signal and/or of the background. A possible new direction is measuring the fiducial cross section of the full process $pp \rightarrow W^+ b W^- \bar{b} + X$, which includes double-resonant ($t\bar{t}$), single-resonant (Wt), as well as non-resonant contributions.

5. Top-Quark Mass

The top-quark mass m_t is an important free parameter of the SM. Quantum corrections to certain SM observables lead to relations with other SM parameters, such as the masses of the W boson and the Higgs boson. Therefore precise measurements of m_t are an important ingredient of precision tests of the SM¹⁹. At hadron colliders the conventional way of measuring m_t relies on the kinematic reconstruction of the $t\bar{t}$ final state. Kinematic reconstruction is the most precise method to determine m_t to date, with innovations including the matrix-element method (MEM) and in-situ calibration of the jet energy scale to increase the m_t sensitivity, see Section 1.2. The different $t\bar{t}$ decay channels and different observables sensitive to m_t are subject to different systematic uncertainties. If measurements from different channels and with different observables are consistent, even higher precision is obtained by combining them.

As discussed in Section 2.4.2, m_t measurements based on the kinematic reconstruction of the $t\bar{t}$ final state suffer from ambiguities in the definition of m_t . Therefore alternative methods to determine the top-quark mass at

¹⁹The relation of m_t with the stability of universe, assuming that the SM is valid up to very high energy scales, has been an interesting point of discussion in recent years, see e. g. [257, 258].

hadron colliders have been proposed that are based either on different kinematic observables such as endpoints of distributions or on (differential) cross section measurements. These methods have not reached the precision of the kinematic reconstruction but provide valuable independent cross checks with complementary systematic uncertainties. The perspectives of precision m_t measurements, both at the LHC and its upgrades, and at future e^+e^- colliders, will be discussed in Section 7. Further details on measurements of the mass of the top quark can be found in a recent review article [16].

5.1. Kinematic Reconstruction

Mass Determination Methods. A straightforward way to determine the top-quark mass is to compare the m_t distribution²⁰ as reconstructed from the data with a set of MC-simulated m_t distributions (“templates”) with different values of the top-quark mass parameter in the simulation. Alternatively, each event can be assigned an m_t -dependent likelihood. This event-level likelihood is composed of process-level likelihoods that included the hard-scattering matrix elements of the signal and the most important background processes (MEM, see Section 3.4.3 [52, 53]). The ideogram method [259, 260] represents an alternative to the MEM that is less computing-intensive. In the ideogram method the likelihood for each process is assumed to factorize into an m_t -independent factor depending only on the event topology and an m_t -dependent factor depending on the event kinematics.

In-Situ Jet Energy Scale Calibration. A major limitation on the precision of kinematic methods is the limited resolution of m_t when reconstructed (partly) from jet energies. In addition, a miscalibrated jet-energy scale would lead to shifts in the reconstructed m_t similar to shifts caused by a different m_t value. This correlation between m_t and the JES can be exploited by reconstructing hadronic decays of other particles with known mass in the same dataset. Hadronically decaying W bosons, available in single-lepton and all-hadronic $t\bar{t}$ events, are the particles of choice: by reconstructing m_t and m_W simultaneously and constraining m_W to the known value the precision of m_t is significantly improved [261]. This method of calibrating the JES in-situ can be applied to template, MEM, and ideogram methods alike. Strictly speaking the in-situ JES calibration is only applicable to the

²⁰In this chapter m_t may stand for any kinematic observable from which the top-quark mass may be inferred, e.g. the invariant mass of the top-quark’s decay products.

Table 2: Summary of the most precise individual measurements of the top-quark mass m_t from the Tevatron and the LHC experiments as of November 2016, together with their statistical and systematic uncertainties as well as their total relative uncertainties.

Experiment	m_t (GeV)	stat (GeV)	syst (GeV)	total (%)	Ref.
CDF	172.85	0.71	0.85	0.65	[262]
D0	174.98	0.58	0.49	0.43	[54, 55]
ATLAS	172.99	0.41	0.74	0.49	[264]
CMS	172.35	0.16	0.48	0.29	[263]

same composition of light-flavor quark jets the W boson decays to. On the other hand, the b -jets from top-quark decays fragment differently from light-flavor jets and could need a separate calibration (“ b -JES”). This is either dealt with by assigning a systematic uncertainty to the residual difference between b -jets and light-flavor jets or by determining both JES and b -JES in situ.

Tevatron and LHC Results. The most precise measurements of the top-quark mass currently available from the Tevatron and LHC experiments are summarized in Table 2. The CDF result [262] is obtained using a template method, while D0 utilizes a MEM [54, 55]. The CMS result—the single most precise m_t measurement to date—employs the ideogram method [263]. All measurements presented above were performed in the single-lepton channel and used an in-situ calibration of the JES scale. The most precise ATLAS result [264] is based on a template method in the dilepton channel.

While kinematic m_t measurements in other $t\bar{t}$ decay channels are less precise, they still provide valuable cross-checks, as they are subject to different systematic uncertainties and may be influenced by BSM physics differently. The Tevatron experiments have provided a full suite of further measurements, mostly with the full Run-II dataset, in the single-lepton channel [54], the dilepton channel [265, 266, 267], for fully hadronic $t\bar{t}$ decays [268], and for events with jets and missing transverse momentum [269]. With the large LHC datasets and better understanding of systematic effects, also the precision of m_t measurements in these channels is improving, as seen from the LHC results in the single and dilepton channel [270, 271, 272, 263] and the fully hadronic channel [273, 274, 275, 263]. As shown in Fig. 11, all results are compatible with each other within uncertainties.

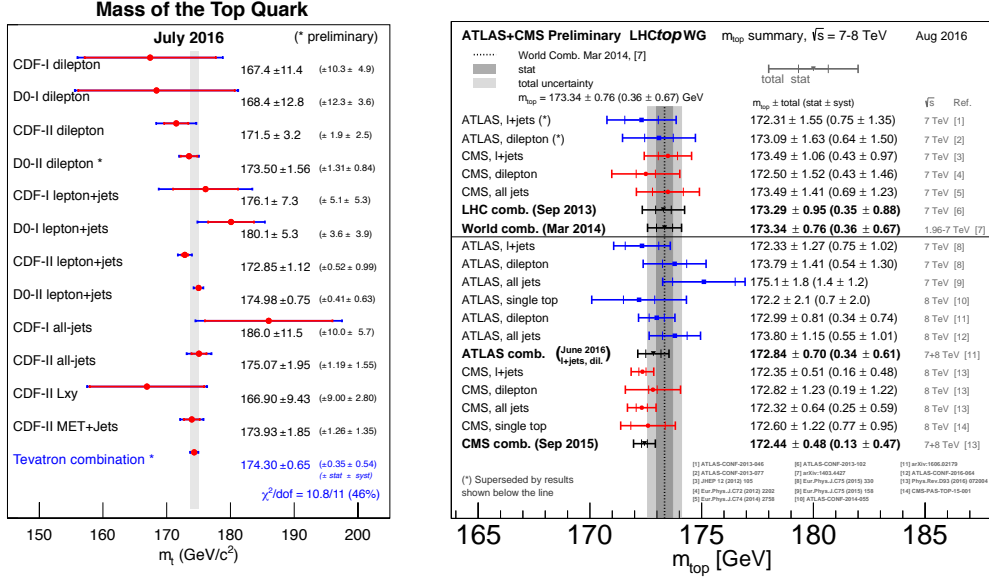


Figure 11: Compilation of recent top-quark mass measurements at the Tevatron [276] (left) and at the LHC [149] (right).

5.2. Alternative Methods to Extract The Top-Quark Mass

Various alternative methods to extract m_t from experimental data have been proposed. These methods may be separated into alternative kinematic methods with systematic uncertainties that are partly uncorrelated to those in standard methods and into methods that extract m_t from other physics observables such as cross sections and thus avoid the ambiguities in the definition of m_t .

5.2.1. Kinematic Methods

One class of alternative methods is designed to avoid calorimetric jet reconstruction and its limited resolution and scale uncertainties but rather to use purely track-based observables to determine m_t . The most important uncertainties when applying these methods are the modeling of the kinematic properties of the top quark and of the b -quark fragmentation.

Decay Length and Lepton Transverse Momentum. As virtually all top-quark decays involve a b -jet, the b -jet properties can be used to determine m_t . In a

method known as the “ L_{xy} method”²¹—pioneered at CDF—the correlation of m_t and the b hadron decay length is exploited [277, 278]. The decay length is determined from track information only, and the main systematic uncertainties of the method originate from the MC modeling of the track multiplicity in b hadron decays. Another measure of m_t exploited in [278] is the transverse momentum of the charged lepton (e or μ) from the leptonic decay of a W boson coming from the top quark. The combination of both leads to a 4% uncertainty on m_t , which is dominated by the limited size of the CDF Run-II dataset. The L_{xy} method has also been applied to the CMS dataset at $\sqrt{s} = 8$ TeV in a preliminary study [279], achieving a precision of 1.9% on m_t . The dominant systematic uncertainties for the L_{xy} and lepton transverse momentum methods come from the lepton moment scale and the MC modeling of signal, background, and the track multiplicity in b hadron decays. A further CMS analysis exploiting b -jets from top-quark decays extracts m_t from the peak position in the energy spectrum of b -jets in the laboratory frame—a method proposed in [280]—with a precision of 1.7% on the same dataset [281].

Invariant Mass of Final-State Particle Combinations. Another mass-dependent kinematic observable used to determine m_t that is based only on the momenta of charged particles is the invariant mass of the charged lepton from a leptonic W boson decay and the secondary vertex of a b hadron decay, both from a top-quark decay. In a CMS measurement, a precision of 0.9% has been achieved [282]. With the large LHC datasets also a more exclusive $t\bar{t}$ decay is accessible, in which the b hadron decays according to $B \rightarrow J/\psi + X \rightarrow \mu^+\mu^- + X$. As a proxy for m_t , the invariant mass of the charged lepton from a leptonic W boson decay and the J/ψ is employed [283]. A first result using this technique has been published recently based on the full CMS dataset at $\sqrt{s} = 8$ TeV [284]. The precision of the result is 1.8%, limited by the available statistics.

The reconstruction of m_t in the dilepton channel is kinematically under-constrained due to the two undetected neutrinos in the final state. In this case kinematic observables are explored whose shapes, peaks, edges, or endpoints are sensitive to m_t . One example is the invariant mass of the b -jet and

²¹The L_{xy} method is named after the two-dimensional projection of the distance between the primary vertex and the b hadron decay vertex in the transverse plane, usually denoted by L_{xy} .

the charged lepton from a top-quark decay, $m_{b\ell}$. Also observables initially developed for BSM physics searches with semi-invisible final states can be employed, such as “stransverse mass” m_{T2} [285, 286, 287]. A recent CMS measurement using $m_{b\ell}$ and m_{T2} reports a precision on m_t of 0.6% [288], becoming competitive with results from standard kinematic methods.

In the dilepton channel, m_t can also be determined from leptonic observables alone [289]. For example, the transverse momentum of the $\ell^+\ell^-$ pair, $p_T(\ell^+\ell^-)$ turns out to be sensitive to m_t and robust against modeling uncertainties. Sensitivities better than 2% are obtained from the shape of the $p_T(\ell^+\ell^-)$ distribution and its first and second moments [290].

Further kinematic methods to measure m_t are based on the ratio of the three-jet to the two-jet invariant mass, where one of the three jets is a b -jet [291]. In this method, the shape of the combinatorial background from wrong assignments of jets to the hadronic $t\bar{t}$ decay products, is determined by mixing jets from different events. A precision of 0.6% is achieved based on the full CMS dataset at $\sqrt{s} = 8$ TeV.

5.2.2. Top-Quark Mass from Single-Top Quark Events

While traditionally the top-quark mass has been extracted from $t\bar{t}$ events only, the large single top-quark datasets at the LHC also allow for m_t measurements based on the kinematic reconstruction of t -channel single top-quark events. The top-quark mass has been extracted from fits to the invariant mass distribution of the charged lepton, the neutrino, and the b -jet from the top-quark decay, $m_{\ell\nu b}$, with a precision of up to 0.7% [292, 293].

5.2.3. Cross-Section Methods

The inclusive $t\bar{t}$ production cross section predicted by perturbative QCD is a steeply falling function of m_t . In a given renormalization scheme, e. g. the on-shell scheme or the $\overline{\text{MS}}$ scheme, the m_t parameter in the $t\bar{t}$ cross section is defined unambiguously. The measured inclusive cross section also has a weak dependence on the m_t parameter used in the MC simulation: Because of the larger momenta transferred to the $t\bar{t}$ decay products with larger m_t , the acceptance for $t\bar{t}$ events increases slightly with m_t , hence the measured cross section decreases, see Eq. (20). The top-quark mass can be determined from the intersection of the curves describing the m_t dependence of the theoretical and the measured cross section, as illustrated in Fig. 12. This method has been pioneered by D0 [294] and has been applied both at the Tevatron and at the LHC. The results have reached a precision on the

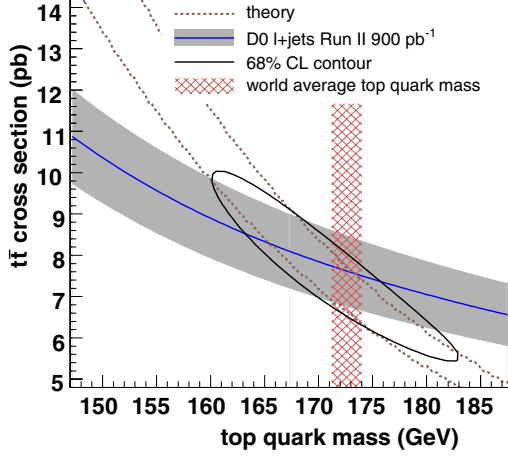


Figure 12: First determination of the top-quark mass from the $t\bar{t}$ production cross section. The cross section is obtained from the intersection of the measured and the theoretical $t\bar{t}$ cross section as a function of m_t [294].

pole mass of the top-quark below 2% at the Tevatron [152] and approximately 1% at the LHC [154, 155].

Also differential cross sections can be used to extract m_t . In $t\bar{t}$ events with one additional jet, the normalized differential cross section as a function of the observable $\rho_s = 2m_0/\sqrt{s_{t\bar{t}j}}$ is sensitive to the top-quark pole mass m_t^{pole} [295]:

$$\mathcal{R}(m_t^{\text{pole}}, \rho_s) = \frac{1}{\sigma_{t\bar{t}j}} \frac{d\sigma_{t\bar{t}j}(m_t^{\text{pole}}, \rho_s)}{d\rho_s}, \quad (23)$$

where $\sigma_{t\bar{t}j}$ is the inclusive or fiducial cross section for $t\bar{t}+1$ jet production, m_0 is a mass scale of the order of m_t and $\sqrt{s_{t\bar{t}j}}$ is the invariant mass of the $t\bar{t} + 1$ jet system in the final state. The LHC experiments have presented first m_t^{pole} measurements based on the observable \mathcal{R} [296, 297], which reach a precision of up to 1.3%.

5.3. Combinations of Top-Quark Mass Results

For an observable like m_t additional precision may be gained by combining measurements from different $t\bar{t}$ decay channels within the same experiment, and from different experiments, that are at least partially uncorrelated, see Sections 1.3 and 3.4.5. Combined results are also considered more robust if they contain channels with complementary systematic uncertainties. At

Table 3: Recent m_t combinations at the Tevatron and the LHC. Shown are the central values together with the statistical and systematic uncertainties and the total relative uncertainty of the combinations.

Experiment	m_t (GeV)	stat (GeV)	syst (GeV)	total (%)	Ref.
CDF + D0	174.30	0.27	0.71	0.44	[276]
ATLAS	172.84	0.34	0.61	0.40	[264]
CMS	172.44	0.13	0.47	0.28	[263]
CMS Alternative	172.58	0.21	0.72	0.43	[299]
World 2014	173.34	0.36	0.67	0.44	[298]

the Tevatron the most precise measurements of m_t from the full Run I and Run II datasets of CDF and D0 have recently been combined [276]. The LHC experiments have provided combinations of their results individually [264, 263]. Tevatron results on m_t have been combined with results from the LHC in the first (and so far only) m_t “world combination” in 2014 [298]. All CMS top-quark mass measurements using alternative methods have also been combined recently [299]. The value of m_t obtained in this combination is in excellent agreement with, but less precise than, the earlier CMS combination of high-precision kinematic m_t measurements [263].

The m_t combination results are summarized in Table 3. The central m_t values and the uncertainties are usually driven by the one or two most precise measurements, but show a moderate reduction of total uncertainty with respect to individual results.

5.4. Top Quark-Antiquark Mass Difference

A measurement of the mass difference between top quarks and antiquarks, Δm_t , is a test of the invariance of the SM under the simultaneous transformations of charge conjugation, parity, and time reversal (CPT). Such measurements have been conducted both at the Tevatron [300, 301] and at the LHC [302, 303, 304]. The analyses begin by performing a kinematic fit of the $t\bar{t}$ system in single-lepton events, where the top quark and antiquark are distinguished by the charge of the lepton²² and the fit does not assume m_t and $m_{\bar{t}}$ to be equal. In the next step methods similar to m_t measurements

²²The probability to misreconstruct the charge of a high- p_T electron is very small and negligible for the charge of a high- p_T muon.

are applied, e.g. the ideogram method in CMS and an unbinned ML fit to the reconstructed Δm_t distribution in ATLAS. All results obtained so far are consistent with the top quark and antiquark masses being the same, as required by CPT invariance. The uncertainty of the most precise measurement of Δm_t to date is 210 MeV [304].

5.5. Summary

From measurements of m_t at the Tevatron and the LHC, the top-quark mass has been determined with excellent precision, rendering the top-quark mass the most precisely known quark mass. The most precise methods are based on the kinematic reconstruction of the final state, with a current precision of approximately 500 MeV or 0.3%. Recently results obtained from a large number of alternative methods to extract the top-quark mass have become available, with complementary systematic uncertainties and reaching a precision up to 1 GeV or 0.6%. The prospects of these methods with increasing datasets at the LHC will be discussed in Section 7.1.

6. Top Quark Properties

In the SM the properties of the top quark are well defined, as outlined in Section 2.4. However, in BSM physics models, various deviations from the SM expectations are predicted. Therefore measurements of the properties of the top quark constitute tests of the SM and often provide constraints on BSM physics models at the same time. There is a wide range of top-quark properties to be tested: Basic properties include the electric charge, the mass (already discussed in Chapter 5), and the decay width of the top quark. Further insight into the production and decay properties of top quarks is gained by studying production asymmetries, spin observables, and the top quark's coupling structure in general.

In many BSM models, top quarks are preferred decay products of new heavy particles, leading to observable resonances in invariant mass spectra, or are produced in association with new particles, for example dark-matter candidates.

In kinematic regions where the SM predictions are known to describe experimental data well, top quarks may also be used as a powerful tool, for example to extract b -tagging efficiencies, parton distribution functions, or the strong coupling constant.

6.1. Basic Top-Quark Properties

6.1.1. Top-Quark Electric Charge

The electric charge of the top quark, which is $Q_t = 2/3$ in the SM, can be determined from its coupling strength to the photon or from the charge of its decay products.

The coupling strength of the $\gamma t\bar{t}$ vertex is related to the cross section for associated $t\bar{t}\gamma$ production, which has been studied both at the Tevatron [208] and the LHC [209], see Section 4.4. However, $t\bar{t}\gamma$ final states can not only be produced by photons coupling to top quarks, but also by photons coupling to other charged particles in the initial and final state of the process. The corresponding scattering amplitudes interfere, such that the interpretation as the top-quark charge would require more sophisticated techniques, such as an angular analysis of the final state, and therefore has not been attempted yet.

Charge conservation in the decay $t\bar{t} \rightarrow W^+W^-b\bar{b}$ allows exotic heavy quarks with $Q = -4/3$ decaying to W^-b instead of the top quark decaying to W^+b . From the combined charge of the decay products W boson and b quark, the charge of the mother particle can be inferred. In leptonic W -boson decays the W -boson charge sign can be determined with great confidence from the charge sign of the charged lepton. However the b quark is a colored particle whose charge information is diluted during hadronization. Experimentally the charge sign can only be determined on a statistical basis by constructing observables that infer the b quark charge from the charges of all particles in the corresponding b -jet after hadronization, such as the JetQ observable [305]:

$$\text{JetQ} = \frac{\sum_{\text{tracks}} (\vec{p}_{\text{track}} \cdot \vec{p}_{\text{jet}})^\kappa Q_{\text{track}}}{\sum_{\text{tracks}} (\vec{p}_{\text{track}} \cdot \vec{p}_{\text{jet}})^\kappa}, \quad (24)$$

where the charge of each particle in the b -jet, Q_{track} , is weighted with the particle's momentum \vec{p}_{track} derived from the track, projected on the jet momentum axis \vec{p}_{jet} . The exponent κ is a free parameter that has been optimized for $t\bar{t}$ events to be around $\kappa = 0.5$. The two charge hypotheses $Q = 2/3$ and $Q = -4/3$ can then be compared in a statistical hypothesis test, typically with the product of JetQ and the lepton charge as the test statistic. Measurements of the top-quark charge based on JetQ have been performed both at the Tevatron [306, 307] and at the LHC [308]. The hypothesis that all $W^+W^-b\bar{b}$ final states stem from exotic quarks with $Q = -4/3$ has been excluded with a significance of more than eight standard deviations [308]. In

the same publication, the charge of the top quark is determined as

$$Q_t = 0.64 \pm 0.02 \text{ (stat)} \pm 0.08 \text{ (syst)}, \quad (25)$$

compatible with the SM expectation of $Q_t = 2/3$.

6.1.2. Top-Quark Width and Lifetime

The total decay width of the top quark Γ_t , see Eq. (5), and its inverse, the top-quark lifetime $\tau_t = 1/\Gamma_t$ can be determined indirectly from a combination of two measurements: Γ_t is proportional to $|V_{tb}|^2 / \mathcal{B}(t \rightarrow Wb)$. The CKM matrix element factor $|V_{tb}|^2$ can be accessed by comparing the measured value of the cross section for single top-quark production in the t -channel, $\sigma_{t\text{-ch}}$, to the theory expectation $\sigma_{t\text{-ch}}^{\text{theo}}$, see Section 4.5. The ratio of branching fractions $\mathcal{R} = \mathcal{B}(t \rightarrow Wb) / \sum_q \mathcal{B}(t \rightarrow Wq)$, where the sum is over the down-type quarks, $q = d, s, b$, can be measured from the number of b -jets in $t\bar{t}$ events. Assuming $\sum_q \mathcal{B}(t \rightarrow Wq) = 1$, i. e. $\mathcal{R} = \mathcal{B}(t \rightarrow Wb)$, the top-quark width is given by

$$\Gamma_t = \frac{\sigma_{t\text{-ch}}}{\sigma_{t\text{-ch}}^{\text{SM}}} \cdot \frac{\Gamma(t \rightarrow Wb)^{\text{SM}}}{\mathcal{B}(t \rightarrow Wb)}, \quad (26)$$

where $\Gamma(t \rightarrow Wb)^{\text{SM}} \approx 1.35 \text{ GeV}$ is the SM expectation for the $t \rightarrow Wb$ partial decay width. Measurements of Γ_t based on Eq. (26) have been performed both at the Tevatron [309] and at the LHC [310]. The more precise LHC result is based on a profile likelihood ratio fit to the b -jet multiplicity in $t\bar{t}$ dilepton final states. The fits leaves Γ_t as a free parameter and treats the b -tagging and mistagging efficiencies as well as the uncertainties of $\sigma_{t\text{-ch}}$ and $\sigma_{t\text{-ch}}^{\text{SM}}$ as nuisance parameters. The resulting top-quark width of

$$\Gamma_t = (1.36 \pm 0.02 \text{ (stat)} {}^{+0.14}_{-0.11} \text{ (syst)}) \text{ GeV} \quad (27)$$

is in very good agreement with the SM expectation.

The width of the top-quark can also be determined directly from the kinematic reconstruction of its decay products, as performed by CDF [311] and CMS [312]. Similar to measurements of m_t , an observable sensitive to the top-quark width is built from reconstructed quantities. In the more recent CMS analysis, the observable is the invariant mass of charged lepton– b -jet pairs in dilepton $t\bar{t}$ events. In a series of binary hypothesis tests the SM value of Γ_t is probed against different non-SM width hypotheses to extract a 95% CL central confidence interval of $0.6 \text{ GeV} < \Gamma_t < 2.4 \text{ GeV}$ [312]. The sensitivity of this direct method is lower than the sensitivity of the indirect method described above.

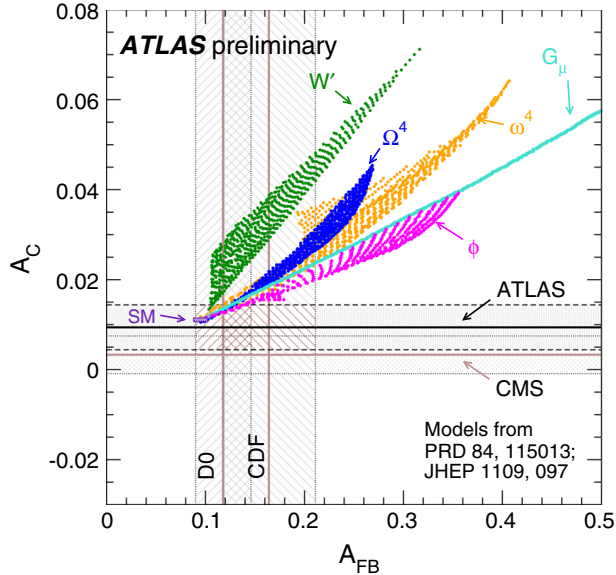


Figure 13: Measurements of A_{FB} at the Tevatron (vertical lines and bands) and A_C at the LHC (horizontal lines and bands) compared to the SM prediction as well as several classes of BSM models: heavy gauge boson (W'), heavy gluon with axial couplings (G_μ), scalar isodoublet (ϕ), color-triplet scalar (ω^4), and color-sextet scalar (Ω^4). The bands represent the 68% CL confidence intervals of the measurements [314].

6.2. $t\bar{t}$ Production Asymmetries

At LO in QCD perturbation theory, $t\bar{t}$ pair production is symmetric under the exchange of t and \bar{t} . While the production process $gg \rightarrow t\bar{t}$ remains symmetric also at NLO, the process $q\bar{q} \rightarrow t\bar{t}$ shows a small asymmetry [58]. The asymmetry is caused by the interference of tree-level and one-loop contributions to the squared amplitude for $t\bar{t}$ production, which is antisymmetric under the exchange of t and \bar{t} . Additional small asymmetries arise from electroweak corrections [313]. The observation of large $t\bar{t}$ production asymmetries would be a sign of BSM physics. The different initial states ($p\bar{p}$ vs. pp) and the different fractions of gg -initiated and $q\bar{q}$ -initiated $t\bar{t}$ production at the Tevatron and the LHC lead to different asymmetry observables, the forward-backward asymmetry A_{FB} at the Tevatron and the charge asymmetry A_C at the LHC, as defined below. Fig. 13 shows that BSM physics contributions would influence A_{FB} and A_C simultaneously but in different ways depending on the model.

The expected magnitude and sign of the asymmetries depend on the

kinematic region considered; therefore, with increasingly large datasets, differential asymmetries as a function of kinematic observables with increasingly fine binning are being reported in addition to inclusive asymmetries. Further details on the physics of $t\bar{t}$ production asymmetries can be found e.g. in a recent review article [17].

6.2.1. Forward-Backward Asymmetries at the Tevatron

At the Tevatron the $t\bar{t}$ production asymmetry manifests itself as a forward-backward asymmetry, generally defined as

$$A_{\text{FB}} = \frac{N_F - N_B}{N_F + N_B}, \quad (28)$$

where N_F is the number of forward events and N_B is the number of backward events. The forward-backward asymmetry in $t\bar{t}$ production is usually defined at parton level. The observable of choice is the rapidity difference of the top quark and antiquark, $\Delta y = y_t - y_{\bar{t}}$, which is invariant under Lorentz boosts in the beam direction. The kinematics of the top quark and antiquark are measured and then corrected back to the parton level using unfolding techniques. The uncertainties on A_{FB} are dominated by the limited size of the Tevatron datasets. The largest systematic uncertainties originate from the background estimation and the MC modeling of hadronization.

Early measurements of A_{FB} at the Tevatron showed discrepancies to NLO QCD predictions, in particular in events with large $t\bar{t}$ invariant masses [61]. However, the CDF and D0 results with the full Run-II dataset [315, 316, 317, 318] and the most recent SM predictions with QCD corrections up to NNLO [319] or approximate N³LO [320], both with NLO electroweak corrections, are compatible within less than 1.5 standard deviations, as shown in Table 4. Also the differential A_{FB} measurements show agreement with the SM prediction at the level of two standard deviations or better [316, 321].

A complementary approach to determine $t\bar{t}$ production asymmetries is to measure the charge asymmetry of leptons from $t\bar{t}$ decays. These may be defined as a function of the product of charge and pseudorapidity of the leptons, $Q_\ell \cdot \eta_\ell$, or as the pseudorapidity difference of the leptons in dilepton events, $\Delta\eta = \eta_{\ell^+} - \eta_{\ell^-}$. SM predictions for the lepton asymmetries are available with NLO QCD and electroweak corrections [322] and include cuts on the lepton acceptance, resulting in a very small model dependence. The experimental results from the full Tevatron Run-II dataset [323, 324, 325] are in good agreement with the SM predictions. A summary is given in

Table 4: Inclusive $t\bar{t}$ production asymmetry results from the Tevatron compared to the most recent SM predictions. The asymmetries are quoted together with their combined statistical and systematic uncertainties.

Source	A_{FB}	Ref.
CDF Combination	0.160 ± 0.045	[316]
D0 Combination	0.118 ± 0.028	[318]
NNLO QCD + NLO electroweak	0.095 ± 0.007	[319]
approx. N ³ LO QCD + NLO electroweak	0.100 ± 0.006	[320]

Fig. 14 (left). With a full set of measurements using the full Tevatron Run-II dataset and SM predictions including corrections beyond NLO, no strong hints of BSM physics in $t\bar{t}$ production asymmetries remain.

6.2.2. Charge Asymmetries at the LHC

The initial deviations from the SM expectation for A_{FB} observed during Tevatron Run II also triggered an extensive measurement program at the LHC. Due to the symmetric pp initial state at the LHC, $t\bar{t}$ production asymmetries do not manifest themselves as forward-backward asymmetries like in $p\bar{p}$ collisions. Instead a charge asymmetry A_C can be observed, where top antiquarks from the process $q\bar{q} \rightarrow t\bar{t}$ show a narrower rapidity distribution compared to the top quarks from the same process. The process $gg \rightarrow t\bar{t}$ remains charge-symmetric. The charge asymmetry A_C is defined in terms of the difference of absolute rapidity, $\Delta|y| = |y_t| - |y_{\bar{t}}|$:

$$A_C = \frac{N(\Delta|y| > 0) - N(\Delta|y| < 0)}{N(\Delta|y| > 0) + N(\Delta|y| < 0)}. \quad (29)$$

In the SM, the inclusive charge asymmetry is expected to be small; the expectation at NLO QCD with electroweak corrections at $\sqrt{s} = 8$ TeV amounts to $A_C = 0.0111 \pm 0.0004$ [322]. In many BSM physics models that predict larger A_{FB} compared to the SM, also significant deviations in A_C are expected [326, 327], see also Fig. 13.

Measurements of A_C have been presented both at $\sqrt{s} = 7$ TeV and at $\sqrt{s} = 8$ TeV. The sensitivities are similar, as the smaller expected A_C due to the larger fraction of gg -initiated $t\bar{t}$ events at $\sqrt{s} = 8$ TeV is compensated by the four-fold increase in dataset size. In the single-lepton channel, ATLAS and CMS have measured inclusive asymmetries and asymmetries differential

in the invariant mass and transverse momentum of the $t\bar{t}$ system at parton level [328, 329, 330, 314]. The inclusive A_C measurements using data taken by ATLAS and CMS at $\sqrt{s} = 7$ TeV have been combined in the context of the LHCtopWG [331].

As the charge asymmetry expected at the LHC is small, much care has been taken in unfolding the data, using a regularized matrix unfolding technique in CMS and fully Bayesian unfolding in ATLAS, see Section 3.4.4. This included detailed studies of the correlations between the bins of the unfolded differential asymmetries. Statistical uncertainties dominate the total uncertainty for the measurements at $\sqrt{s} = 7$ TeV while their size becomes similar to the size of the systematic uncertainties for $\sqrt{s} = 8$ TeV. The dominant systematic uncertainties stem from the incomplete knowledge of the jet energy scale and resolution as well as from MC signal modeling, in particular for differential asymmetries where migrations occur between bins of the differential distributions within the systematic uncertainties.

To increase the A_C sensitivity for invariant $t\bar{t}$ masses above 750 GeV, where the Tevatron A_{FB} measurements hinted at tensions with the SM, ATLAS has also applied boosted top-quark reconstruction techniques in an A_C measurement [332]. In addition to A_C measurements based on unfolding, CMS has applied a template method in an inclusive A_C analysis. The template method results in smaller statistical uncertainties compared to unfolding, at the expense of a larger model dependence [333].

As for the A_{FB} measurements from the Tevatron, leptonic asymmetries with reduced model dependence are accessible in $t\bar{t}$ dilepton events at the LHC [334, 335, 336, 337]. The uncertainties of these measurement are dominated by statistical uncertainties, followed by signal modeling uncertainties.

All inclusive, differential, and leptonic asymmetry measurements at the LHC agree well with SM predictions with NLO QCD and electroweak corrections [322]. This is illustrated in Fig. 14 (right). It remains to be seen if the even larger datasets, counteracted by the smaller expected A_C due to the larger fraction of gg initial states at $\sqrt{s} = 13$ TeV, will allow for more stringent tests of A_C at LHC Run 2.

6.3. Spin Observables in Events with Top-Quarks

As introduced in Sections 2.5 and 2.6, top quarks and antiquarks from $t\bar{t}$ production are expected to be essentially unpolarized in the SM, but the t and \bar{t} spins are correlated. On the other hand, single top quarks produced via a Wtb vertex are 100% polarized. Likewise W bosons from the decay

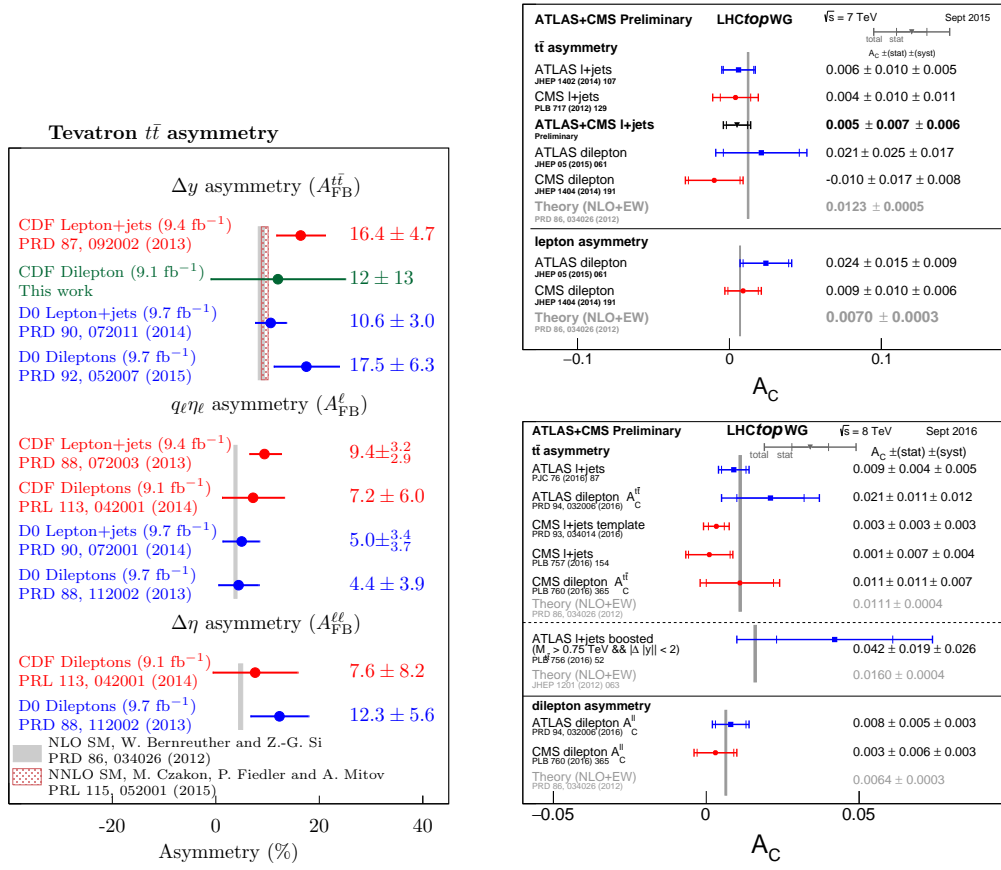


Figure 14: Compilation of inclusive $t\bar{t}$ forward-backward asymmetry results from the Tevatron [316] (left) and of charge asymmetry results from the LHC [149] (right) compared to SM predictions. Note the different A_C axis scales in the LHC summary plots for $\sqrt{s} = 7 \text{ TeV}$ (top right) and $\sqrt{s} = 8 \text{ TeV}$ (bottom right).

$t \rightarrow Wb$ are polarized. Measurements of polarization observables sensitive to the above effects are tests of SM predictions for the top-quark couplings and may reveal BSM physics contributions to top-quark production or decay, or both.

6.3.1. *W*-Boson Polarization in Top-Quark Decays

Observables. The polarization of W bosons stemming from top-quark decays is measured as a differential cross section in the observable $\cos \theta^*$. The angle θ^* is defined as the angle between the charged lepton or the down-type quark from the W -boson decay and the t or \bar{t} boost direction²³ in the W -boson rest frame. As the above definition of θ^* relies on parton-level information, a W -boson polarization measurement requires either folding the polarization effects into reconstructed observables or unfolding of the reconstructed observables. Usually the first step to compute $\cos \theta^*$ is to reconstruct both the t and the \bar{t} , from the b -jet and the W -boson decay products, either $\ell\nu$ or the jets from $q\bar{q}'$, employing a kinematic fit.

Assuming that the top quark and antiquark in a $t\bar{t}$ event are unpolarized, the polarization of each W boson is decoupled from the rest of the event and can be studied separately. The differential production cross section can then be expressed as a function of the fractions of left-handed polarization (F_L), longitudinal polarization (F_0), and right-handed polarization (F_R) of the W bosons introduced in Section 2.4:

$$\frac{1}{\sigma} \frac{d\sigma}{d \cos \theta^*} = \frac{3}{8} (1 - \cos \theta^*)^2 F_L + \frac{3}{4} (1 - \cos^2 \theta^*) F_0 + \frac{3}{8} (1 + \cos \theta^*)^2 F_R. \quad (30)$$

Measurements of the W -boson polarization fractions can be compared with the SM predictions directly and also be interpreted as limits on anomalous Wtb couplings, which will be discussed in Section 6.4.1. The W -boson polarization has been measured in $t\bar{t}$ events with single-lepton decays both at the Tevatron and the LHC in fits that determine F_L and F_0 simultaneously, taking into account the correlations between these polarization fractions, and derive F_R from the constraint $F_L + F_0 + F_R = 1$ ²⁴.

²³Most measurements consider both the t and the \bar{t} , regardless of their decay mode, to exploit the full polarization information from the two W bosons in each $t\bar{t}$ event.

²⁴In the publications the polarization fractions are also quoted for the case when one fraction is fixed to the SM expectation.

Tevatron Results. Using the first 2.7 fb^{-1} to 5.4 fb^{-1} of Tevatron Run II data, the W -boson polarization has been measured using the matrix-element method (MEM) and template-fit techniques. In the CDF MEM analysis, a likelihood ratio discriminant is constructed from the LO $t\bar{t}$ production matrix element parameterized as a function of the W -boson polarization fractions [338]. In the D0 template-fit analysis, independent templates for the three polarization states as a function of the reconstructed $\cos \theta^*$ distribution are constructed from simulated data and fitted to the data [339]. The results of these measurements have been combined [340] to arrive at a relative uncertainty on F_L and F_0 of 11%. From the full Run II CDF dataset a relative uncertainty of 13% is achieved, again employing a MEM [341]. Within their uncertainties the W -boson polarization results obtained at the Tevatron are compatible with the SM predictions.

LHC Results. The ATLAS and CMS collaborations have performed their first set of measurements of the W -boson polarization using LHC Run 1 data at $\sqrt{s} = 7 \text{ TeV}$. CMS has extracted the W -boson polarization from a template fit technique [342]. ATLAS has determined the W -boson polarization from a template fit and additionally from a complementary set of observables that is based on asymmetries in $\cos \theta^*$ [343]. An example of $\cos \theta^*$ templates is shown in Fig. 15 (left). The dominant systematic uncertainties on these measurements are due to the modeling of the $t\bar{t}$ signal and the determination of the dominant $W + \text{jets}$ background, which is a source of unpolarized W bosons. Based on the above individual ATLAS and CMS measurements, a combination was performed in the context of the LHCtopWG [344]. The relative uncertainties on F_L and F_0 obtained in the combination are around 10%. Improved measurements have been presented using the $\sqrt{s} = 8 \text{ TeV}$ dataset: the uncertainties on F_L and F_0 were further reduced to below 5% [345].

Also events with dilepton $t\bar{t}$ decays [346] as well as events with a single reconstructed top quark [347, 348] have been used to measure the W -boson polarization, albeit with larger uncertainties than using single-lepton $t\bar{t}$ events. The LHC results on the W -boson polarization are summarized in Fig. 16. They are compatible with the SM predictions within their uncertainties.

6.3.2. Top Quark Polarization and $t\bar{t}$ Spin Correlations

The top-quark polarization in $t\bar{t}$ events is predicted to be very small in the SM [113]; the exact value depends on the choice of the spin quantization axis, as discussed in Section 2.4.1. Because of the different initial states

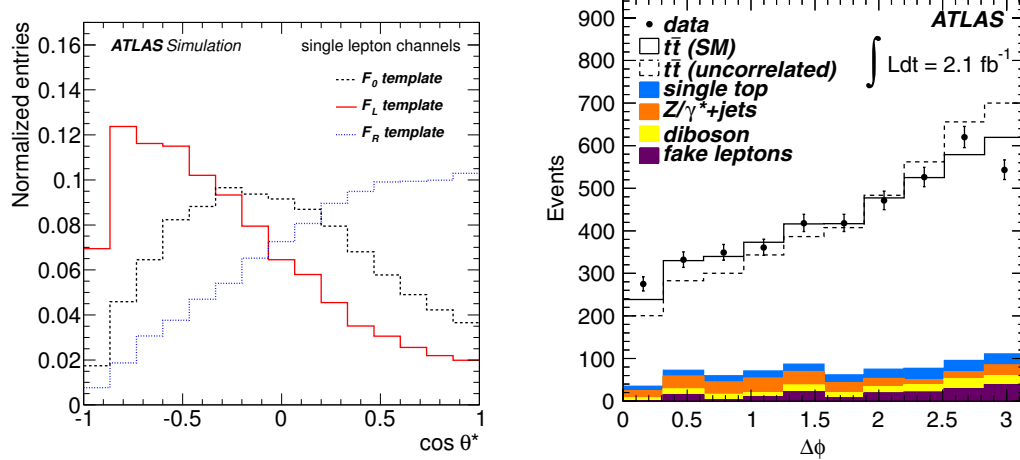


Figure 15: Simulated signal templates for longitudinal (F_0), left-handed (F_L), and right-handed (F_R) W boson polarization as a function of $\cos \theta^*$ [343] (left). Reconstructed distribution of the angle $\Delta\phi$ between the two charged leptons in $t\bar{t}$ dilepton decays in data compared to simulated $t\bar{t}$ and background distributions (right). The simulated $t\bar{t}$ distributions are shown for the case of spin correlations as expected in the SM (solid line) and for the case of no spin correlations (dashed line) [349].

at the Tevatron ($p\bar{p}$) and at the LHC (pp), different degrees of top-quark polarization are expected for a given set of quantization axes.

In the dilepton decay channel, a clean way to extract the polarization is to measure double-differential distributions of the polar angles θ^+ and θ^- for the positively and negatively charged lepton with respect to a given set of spin quantization axes:

$$\frac{1}{\sigma} \frac{d\sigma}{d \cos \theta_+ d \cos \theta_-} = \frac{1}{4} (1 + P_+ \kappa_+ \cos \theta_+ + P_- \kappa_- \cos \theta_- - C \cos \theta_+ \cos \theta_-). \quad (31)$$

Here P_{\pm} are the polarizations of the charged leptons and κ_{\pm} are their spin analyzing power, while C is the spin correlation coefficient. Instead of analyzing the full angular distribution, the more robust spin asymmetry observable A_s can be constructed. The spin asymmetry is related with the polarization and the spin analyzing power via $A_{s,\pm} = P_{\pm} \kappa_{\pm} / 2$.

Top-Quark Polarization. Top-quark polarization measurements from the Tevatron have been presented first simultaneously with the leptonic and inclusive forward-backward asymmetries [350, 318] with which the polarization is an-

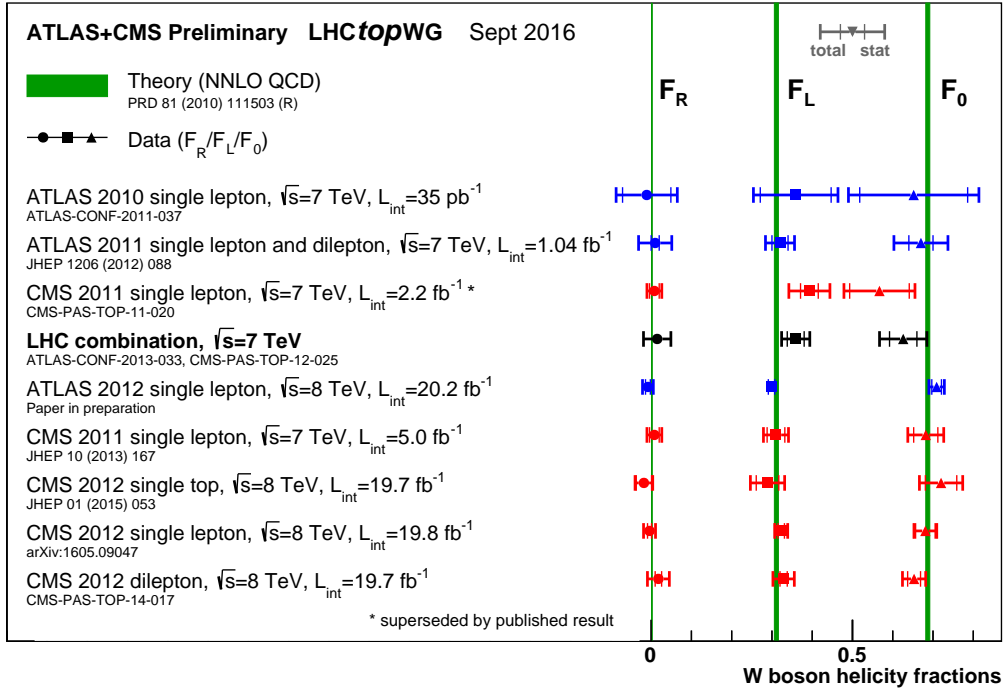


Figure 16: Compilation of LHC results on the W -boson polarization in top-quark decays, expressed as the polarization fractions F_R , F_L , and F_0 [149]. The experimental results are compared to SM predictions at NNLO [92].

ticorrelated. Also a dedicated D0 measurement of the top-quark polarization along several quantization axes, including its transverse polarization, is available [351]. Direct measurements of the top-quark polarization have also been presented by the LHC experiments [352, 353, 354]. These measurements start from the kinematic reconstruction of the $t\bar{t}$ event and proceed by unfolding distributions sensitive to the top-quark polarization to parton or particle level. Earlier measurements also used template fits to the reconstructed distributions. The most important uncertainties include those originating from the $t\bar{t}$ modeling; for some polarization observables also the JES uncertainty becomes relevant. Within the current uncertainties, all top-quark polarization observables in $t\bar{t}$ events are compatible with the SM expectation.

The top-quark polarization times spin analyzing power has also been determined in single-top quark events. The main observable is the angle θ_ℓ

between the top-quark spin quantization axis and the charged lepton from the top decay. Unfolding this observable to parton level, values of $P\kappa \approx 0.9$ are obtained [355, 348], compatible with the SM expectation.

Spin Correlations. The correlation between the spins of the $t\bar{t}$ pair predicted by the SM is another interesting spin observable to be tested. The different dominant $t\bar{t}$ production mechanisms at the Tevatron and the LHC make measurements of $t\bar{t}$ spin correlations at the two colliders complementary. Recent $t\bar{t}$ spin correlation measurements have also be interpreted as limits on top-squark pair production in supersymmetric models. The measurement is complementary to other top-squark searches in that it probes top-squark masses close to m_t .

A very good observable to measure $t\bar{t}$ spin correlations is the difference $\Delta\phi$ in azimuthal angle of the two leptons in the dilepton channel in the laboratory frame. From the $\Delta\phi$ distribution, the asymmetry in $\Delta\phi$ can be extracted as a measure of spin correlations. The spin correlations can be extracted either from a template fit to the reconstructed data or from the unfolded distribution. The hypotheses of fully correlated spins and uncorrelated spins are then tested against each other in a hypothesis test. The first spin correlation measurements have been presented at the Tevatron [356, 357, 358]; however, with significances for correlated spins below five standard deviations. The first observation of $t\bar{t}$ spin correlations with more than five standard deviations was reported by ATLAS [349], illustrated in Fig. 15 (right). More precise ATLAS and CMS measurements both at $\sqrt{s} = 7$ TeV [359, 360, 361] and $\sqrt{s} = 8$ TeV [362] with similar analysis strategies followed. A different approach is taken in [363], where the single-lepton $t\bar{t}$ decay channel is considered instead of the dilepton channel. A hypothesis test is constructed from a likelihood ratio test statistic, for which the LO $t\bar{t}$ matrix elements with and without spin correlations are compared. The data do not show a clear preference for either hypotheses, and from a template fit to the test statistic, the fraction of $t\bar{t}$ pairs with correlated spins is determined. Spin correlations have also been observed with more than five standard deviations significance in a recent top-quark polarization measurement [348].

6.4. Anomalous Top-Quark Couplings

Top-quark couplings can also be analyzed in a more general context: The Wtb vertex structure can be studied to constrain anomalous couplings, as they occur in BSM physics models. The most general Wtb coupling contains

CP-conserving as well as CP-violating contributions. Processes that change a quark's flavor without changing its charge, known as flavor-changing neutral current (FCNC) interactions, are forbidden in the SM at tree level and heavily suppressed at the level of quantum corrections. Strong enhancement of FCNC interactions in top-quark production or decay would be a clear sign of BSM physics. Due to the special role the top quark is expected to play in many BSM physics models, it is plausible to assume that hypothetical new particles with masses at the TeV scale have significant couplings to the top quark. Therefore top quarks are preferred decay products of heavy particles in many BSM models. The large Yukawa coupling of the top quark may also indicate a relation to dark matter (DM) that can be studied in the associated production of $t\bar{t}$ pairs with DM. In the absence of new heavy resonances accessible experimentally, the top-quark couplings may be studied in an effective field theory (EFT) approach, in which all heavy BSM particles are “integrated out” and their effect at energies accessible experimentally is parameterized in a comprehensive set of effective couplings.

6.4.1. Anomalous Wtb Couplings and CP Violation

In BSM physics models, the SM Wtb vertex may be modified. The Lagrangian density corresponding to the most general Wtb coupling structure extends Eq. (4) to read:

$$\begin{aligned} \mathcal{L}_{Wtb} = & -\frac{g}{\sqrt{2}} \bar{b} \gamma^\mu (f_V^L P_L + f_V^R P_R) t W_\mu^- \\ & -\frac{g}{\sqrt{2}} \bar{b} \frac{i\sigma^{\mu\nu} q_\nu}{m_W} (f_T^L P_L + f_T^R P_R) t W_\mu^- + \text{h.c.}, \end{aligned} \quad (32)$$

where $P_{L,R} = (1 \mp \gamma_5)/2$, $\sigma_{\mu\nu} = i[\gamma_\mu, \gamma_\nu]/2$, and q_ν is the four-momentum of the W boson. The Lagrangian contains left-handed and right-handed vector and tensor couplings, expressed through the complex coupling constants $f_V^{L,R}$ and $f_T^{L,R}$. In the SM at LO, the only non-vanishing constant is $f_V^L = V_{tb}$, giving rise to a purely left-handed $V-A$ coupling structure. Non-zero imaginary parts of the couplings could be either due to final-state interactions or to CP violation, see e.g. [364].

Limits on the coupling constants in Eq. (32) have been derived e.g. in [365]. There are also software tools available to extract the coupling constants from fits to data: The TOPFIT program code [366, 367] is specialized to the Wtb vertex, and EFTFITTER [368] is a more general software tool

to perform fits to arbitrary coupling structures, showcasing the above Wtb coupling model in the publication.

Anomalous Wtb couplings have been studied in t -channel single top-quark production, by interpreting measurements of the W -boson polarization in the framework of Eq. (32) [241, 347], by measuring the differential production cross section as a function of angular variables [369], and by constructing asymmetries in various angular distributions [370, 348]. Major systematic uncertainties arise from the JES calibration and the single top-quark signal modeling. When interpreting the results, it should be noted that the tightness of the constraints on the individual coupling constants depends on the assumptions on the other constants. For example, when fixing $f_V^L = 1$ and $f_V^R = 0$, the real part of f_T^R can be constrained to better than ± 0.08 , while the ratios of the real and imaginary part of f_T^R/f_V^L are much less constrained, of the order of 0.2 to 0.3 [369]. Within the current measurement precision, all results from LHC Run 1 agree with the SM predictions and limits on anomalous Wtb couplings have been set. The sensitivity of searches for anomalous Wtb couplings is expected to increase with the increased size of the data samples at 13 TeV in LHC Run 2 compared to Run 1.

CP-violating observables can be constructed from the $t\bar{t}$ decay products in a framework with CP-violating operators [371, 372, 373]. CP asymmetries in four of these observables have been studied for the first time at CMS [374]. No signs of CP violation in single top-quark production or $t\bar{t}$ decay have been found yet.

As b hadrons produced directly from $b\bar{b}$ pairs or in hadronic interactions, also those from top-quark decays undergo mixing and decay. In $t \rightarrow Wb$ decays, the b quark's charge sign at production time can be determined from the charge sign of the lepton from the W -boson decay. The charge sign at decay time can be obtained from the soft lepton in a semileptonic b hadron decay. Based on the measurements of these two charges, various charge asymmetries sensitive to CP violation can be constructed. These charge asymmetries are compatible with the SM expectation within current uncertainties [375].

6.4.2. Flavor-Changing Neutral Currents

FCNC top-quark interactions are interactions with a transition of a top quark into another up-type quark q ($q = u, c$) by coupling to a neutral gauge boson (γ , Z , or g) or the Higgs boson. In the SM, FCNC interactions are forbidden at tree level. They can occur via higher-order corrections, but are strongly suppressed due to destructive interference effects in loop

corrections, a variant of the GIM mechanism [26]. For example the SM prediction for the FCNC decay $t \rightarrow Zc$ is far below current detection limits, $\mathcal{B}(t \rightarrow Zc) \approx 10^{-14}$. On the other hand, in many BSM physics models the expected rates of FCNC processes are increased by several orders of magnitude, see [376] for a recent review.

Searches for FCNC interactions in the top-quark sector can be pursued by searching for either production or decay channels in addition to the channels predicted by the SM, governed by one of the above (effective) interactions.

FCNC Top-Quark Production. The LEP experiments have set first limits on anomalous single top-quark production in the process $e^+e^- \rightarrow tq$, with sensitivity to γtu and Ztu couplings [377, 378, 379, 380, 381]. While the cross section for SM single top-quark production at the ep collider HERA was too small to be detected, the HERA data were used to search for anomalous single top-quark production via the same γtu and Ztu vertices relevant at LEP [382, 383, 384, 385, 386]. A concise review of the HERA results on FCNC top-quark production can be found in [18].

Hadron-collider searches for FCNC processes mediated by gtq vertices are performed best as searches for anomalous single top-quark production, as the decay $t \rightarrow gq$ is overwhelmed by QCD multijet background. Similar to the Wtb vertex, the flavor-changing gtq vertex can be parameterized in the most general way as

$$\mathcal{L}_{gtq} = \frac{\kappa_{gtq}}{\Lambda} g_s \bar{q} \sigma^{\mu\nu} \frac{\lambda^a}{2} t G_{\mu\nu}^a, \quad (33)$$

where κ_{gtq} is the dimensionless coupling constant of the interaction, Λ is the expected BSM physics scale, $g_s = \sqrt{4\pi\alpha_S}$ is the QCD coupling, λ^a are the Gell-Mann matrices and $G_{\mu\nu}^a$ is the gluon field strength tensor.

FCNC searches via anomalous single top-quark production have been conducted both at the Tevatron [387, 388] and with LHC Run-1 data [389, 390, 391]. Similar to measurements of the SM single top-quark production cross section, these searches employ multivariate methods to separate signal from background; hence they share similar systematic uncertainties. However the searches are performed in kinematic regions different from those of single top-quark production and the multivariate methods are optimized for the separation of a possible FCNC signal from the SM background, including single top-quark production. The current best 95% CL limits on the branching fractions for $t \rightarrow gq$ are $\mathcal{B}(t \rightarrow gu) < 2 \times 10^{-5}$ [391] and $\mathcal{B}(t \rightarrow gc) < 2 \times 10^{-4}$ [390]. In the framework of Eq. (33) these limits can

also be expressed as limits on κ_{gtq}/Λ . In anomalous single top-quark production associated with a photon, also the γtq vertex can be probed [392].

FCNC Top-Quark Decays. Studying top-quark decays at the Tevatron and the LHC, the FCNC γtq , Ztq , and Htq couplings can be probed. The Tevatron experiments have searched for decays governed by these couplings, for example for the decay $t \rightarrow Zc$ in events with two or three charged leptons and jets. Template fits were performed to observables sensitive to the final state of the FCNC interaction. In the absence of a significant signal, limits on the FCNC branching fraction were derived. For $\mathcal{B}(t \rightarrow Zq)$, the Tevatron limits are of the order of a few percent [393, 394], where the sensitivity was limited by the dataset size and irreducible backgrounds, for example $Z + \text{jets}$ production.

The much larger datasets recorded at LHC Run 1 allow for more stringent FCNC limits [395, 396, 397, 398], while using analysis techniques very similar to the Tevatron experiments. For example, a limit of $\mathcal{B}(t \rightarrow Zq) < 5 \times 10^{-4}$ is obtained from the CMS data taken at $\sqrt{s} = 7 \text{ TeV}$ and $\sqrt{s} = 8 \text{ TeV}$ [398]. The main systematic limitations of these searches are uncertainties in the modeling of the SM $t\bar{t}$ background and from the JES calibration.

At the LHC also flavor-changing top-Higgs couplings (Htq) have been studied [399, 400]. A search in final states with two leptons with the same charge sign and with three leptons is sensitive to Higgs-boson decays into WW , ZZ , and $\tau^+\tau^-$ final states. In addition final states with a photon pair and with a charged lepton and a b -jet are studied, to cover the decays $H \rightarrow \gamma\gamma$ and $H \rightarrow b\bar{b}$. The current best 95% CL limit of $\mathcal{B}(t \rightarrow Hc) < 4.3 \times 10^{-3}$ is derived from a simultaneous fit to suitable kinematic observables in all decay channels [400]. A recent summary of limits on FCNC interactions is given in Fig. 17.

6.4.3. Heavy-Particle Decays to Top Quarks

Many BSM models predict heavy particles that have top quarks among their decay products. In order not to depend on a specific BSM model, heavy particles can be classified according to their generic decay signatures that in turn depend on their quantum numbers and couplings. Electrically neutral particles may decay into $t\bar{t}$ pairs, while charged particles may decay into a single top quark plus another particle. While the larger center-of-mass energy makes LHC searches for heavy particles generally more sensitive for masses above 1 TeV, the Tevatron experiments were often able to add com-

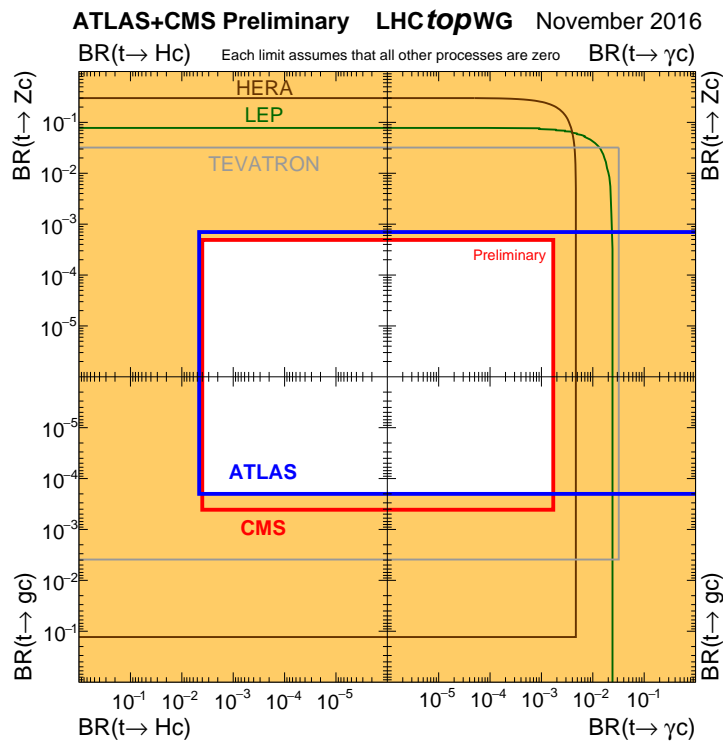


Figure 17: Summary of 95% CL limits on the branching fractions of FCNC processes $t \rightarrow Xc$, where $X = g, Z, \gamma, H$ [65].

plementary sensitivity to lower-mass particles. The large Lorentz boost of the decay products of heavy particle with masses well above 1 TeV makes heavy-particle searches a prime field to apply the boosted top-quark reconstruction techniques introduced in Section 3.3.3.

Neutral Heavy Particles. The signature of neutral heavy particle decays $X \rightarrow t\bar{t}$ is resonances in the invariant mass spectrum of the $t\bar{t}$ pair, $m_{t\bar{t}}$. As the “true” $m_{t\bar{t}}$ is only accessible at parton level, usually a proxy for $m_{t\bar{t}}$ is computed from the four-momenta of reconstructed objects. The decay width of a heavy resonance depends on the underlying BSM physics model, and narrow resonances lead to different experimental signatures than wide resonances. Narrow resonances feature decay widths of the order of a few percent of their mass, comparable with the detector resolution. They are often represented by a benchmark model with a “leptophobic” Z' boson, a heavy neutral gauge boson that only shows weak couplings to leptons (or else the resonance would have been discovered in searches for $Z' \rightarrow \ell^+ \ell^-$ decays already). Such Z' bosons occur for example in topcolor-assisted technicolor (TC2) models [401] and are often assumed to have a relative width of 1% or 1.2%. Wide resonances show a decay width of 10% of their mass or above. Representative of wide resonances are Kaluza-Klein (KK) gluons or gravitons, as they are predicted in Randall-Sundrum models of warped extra dimensions with SM particles propagating in the five-dimensional bulk (RS2) [402].

At the Tevatron, a CDF search excluded a narrow Z' resonance in the $m_{t\bar{t}}$ spectrum up to masses of 915 GeV at 95% CL [403], while D0 reports a slight excess around $m_{t\bar{t}} = 950$ GeV, leading to a weaker limit [404]. The LHC experiments have published $t\bar{t}$ resonance searches in both boosted and resolved decay channels with the full dataset at $\sqrt{s} = 7$ TeV [405, 406, 407, 408, 409] and $\sqrt{s} = 8$ TeV [410, 411]. The searches target single-lepton, dilepton, and fully hadronic $t\bar{t}$ final states. The object reconstruction is adapted to the $m_{t\bar{t}}$ range considered, for example with narrower fat jets and less isolated charged leptons at large $m_{t\bar{t}}$, well above 1 TeV. The dominant uncertainties are related to the modeling of the non-resonant $t\bar{t}$ background, the JES of fat jets, and the PDFs. As a result of the LHC searches for heavy resonances decaying into $t\bar{t}$ pairs, leptophobic Z' bosons were excluded up to masses of 2.4 TeV at 95% CL. If the data are interpreted in RS2 models [412], KK gluons up to masses of 2.8 TeV can be excluded at 95% CL. An example of a reconstructed $m_{t\bar{t}}$ spectrum and its interpretation in terms of KK gluons is shown in Fig. 18. At the time of writing this review results

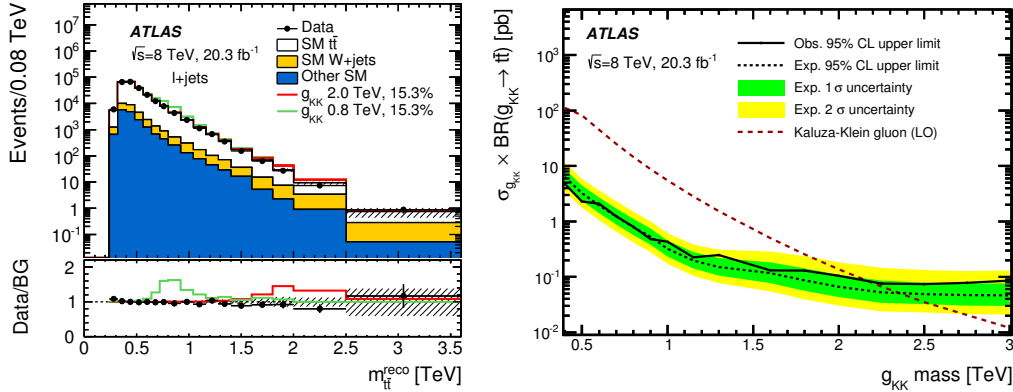


Figure 18: Reconstructed $m_{t\bar{t}}$ distribution for both boosted and resolved $t\bar{t}$ decay channels (left). The distribution is overlaid with the expected distributions of hypothetical KK gluons with masses of 0.8 TeV and 2.0 TeV and a relative width of 15.3%. Observed and expected 95% CL upper limits on the production cross section times branching fraction to $t\bar{t}$ final states of a KK gluon (right). The data exclude KK gluon masses between 0.4 TeV and 2.2 TeV. Taken from [410].

of $t\bar{t}$ resonance searches with the first LHC Run 2 from 2015 [413, 414, 415] arrived at sensitivities similar to Run 1. With more data at $\sqrt{s} = 13$ TeV improved sensitivities are expected.

In BSM models with an extended Higgs sector, such as two-Higgs doublet models, heavy scalar or pseudoscalar particles may decay to $t\bar{t}$ pairs. A search for a model in the single-lepton channel that takes into account the interference with the SM process $gg \rightarrow t\bar{t}$ for the first time, is presented in [416]. Due to the interference a peak-dip structure is expected instead of a simple resonance peak, leading to reduced sensitivity of “bump hunt”-style analyses. The sensitivity is restored if the interference effects are accounted for in the fit model.

Charged Heavy Particles. A charged heavy gauge boson (W') features a different set of decay channels than a Z' boson, e.g. with decays into tb ($t\bar{b}$ and $\bar{t}b$). In contrast to the SM W bosons, arbitrary combinations of left-handed and right-handed couplings to fermions are allowed for W' bosons. For example, in a CDF search [417] neural networks are trained to separate a hypothetical W' -boson signal from background due to QCD, $W/Z + \text{jets}$ and $t\bar{t}$ processes. The data are fitted to a combined neural-network discriminant to extract a limit on the W' -boson mass. The uncertainties are dominated

by the limited knowledge of W and Z boson production in association with heavy-flavor jets. In a scenario with purely right-handed W' couplings the Tevatron experiments have excluded W' masses up to 885 GeV [418, 417].

The LHC experiments also used multivariate methods to select $W' \rightarrow tb$ decays. The analyses arrived at 95%-CL limits of up to 2.15 TeV for the same W' model with only right-handed couplings using data from LHC Run 1 [419, 420, 421]. With the large center-of-mass energy available at LHC Run 2, a simpler approach was sufficient to supersede the Run-1 limits, a search for bumps in the invariant mass spectrum of the tb system, as reconstructed from a charged lepton, jets and missing transverse momentum (MET). No deviation from the SM prediction was observed and a 95%-CL limit of 2.38 TeV was derived [422].

Vector-Like Quarks. In addition to heavy bosons, heavy colored fermions are predicted in many BSM models. Heavier quarks with the same chiral couplings as the six SM quarks (“fourth-generation quarks”) have been searched for at the Tevatron [423, 424, 425, 426, 427]. However, a fourth quark generation has been excluded by the fact that Higgs boson production and decay rates are compatible with the SM prediction [428]²⁵. An attractive alternative are vector-like quarks (VLQs), colored fermions that have left-right symmetric couplings and do not have Yukawa couplings to acquire their mass, see [429] for a recent theory review. As an example searches for vector-like heavy T quarks with charge $Q = 2/3$ will be discussed below. Vector-like T quarks mix with the SM top quark and decay into Ht , Zt , and Wb final states. Other VLQs considered at the LHC are heavy B quarks with charge $Q = -1/3$, and heavy X quarks ($Q = 5/3$) and Y quarks ($Q = -4/3$).

At hadron colliders, VLQs can be produced either singly or in pairs, similar to top quarks. The LHC experiments have conducted searches for VLQs with Run-1 and in Run-2 data and in various final states. The searches in $T\bar{T}$ production [430, 431, 432, 433, 434, 435, 436, 437, 438, 439, 440, 441] generally aim at reconstructing an invariant mass spectrum sensitive to resonances due to VLQs. For low invariant masses regular resolved jets are used in the reconstruction, while for high invariant masses, boosted-jet techniques are employed that also allow for b -tagging in the dense environment of fat jets. No signs of significant resonance peaks were observed and lower lim-

²⁵Both the production channel $gg \rightarrow H$ and the decay channel $H \rightarrow \gamma\gamma$ are mediated by fermionic triangle diagrams which are dominated by heavy quarks.

Table 5: Summary of the most stringent 95% CL limits on the mass of heavy particles decaying into top quarks.

Heavy Particle	95%-CL Mass Limit (TeV)	Experiment	Reference
Leptophobic Z'	> 2.4	CMS 8 TeV	[421]
Kaluza-Klein gluon	> 2.8	CMS 8 TeV	[421]
Right-handed W'	> 2.38	CMS 8 TeV	[422]
VLQ $T \rightarrow Zt$	> 1.10	ATLAS 13 TeV	[435]

its on the T -quark mass m_T were derived, for example $m_T > 1.10$ TeV at 95% CL assuming $\mathcal{B}(T \rightarrow Zt) = 1.0$ [435]²⁶. In single T quark production, stronger exclusion limits can be obtained [442, 443, 444, 445, 446, 447], but these limits rely on assumptions on the WTb coupling. Searches for heavy B , X , and Y quarks have also been conducted at the LHC, see e.g. [434, 441].

Composite Top Quarks. A feature of BSM models with composite instead of fundamental top quarks is excited top quarks (t^*). In [448] a search for $t^* \bar{t}^* \rightarrow tg\bar{t}g$ is documented. The final state is reconstructed using a kinematic fit and the tg invariant mass distribution is scanned for resonances. With the analysis, excited t^* quarks with masses below 803 GeV are excluded at 95% CL in one specific Randall-Sundrum model [449].

Summary on Heavy Resonances. So far none of the searches for heavy particles decaying into top quarks has provided a significant excess in the data compared to the SM prediction. The current best lower limits on the masses of these heavy particles are summarized in Table 5. With additional Run-2 data from 2016 and beyond included in the analyses, these limits are expected to improve significantly. A comprehensive review of LHC searches for exotic new particles, including the ones mentioned above, can be found in [450].

6.4.4. Top Quarks and Dark Matter

In general, DM can be searched for either in direct-detection experiments, in which DM particles scatter off baryonic matter, or indirectly in SM sig-

²⁶Note that depending on the BSM model and the masses of the VLQs also other T decays may be kinematically allowed, including decays into other VLQs.

natures of pair annihilation of DM particles in the universe, or in pair production under laboratory conditions at colliders. DM searches at colliders have the distinct advantage that their interpretation is independent of astrophysical input. Classic DM searches require at least a single detectable SM object recoiling against the undetected DM particles; the most well-known signature is a single high- p_T jet (“monojet”) in association with a significant amount of MET. Events with a $t\bar{t}$ pair or a single top quark and large MET ($t\bar{t} + E_T^{\text{miss}}$, $t + E_T^{\text{miss}}$) are also among the attractive signatures studied in the quest for DM at colliders.

DM searches at the LHC have been interpreted first in EFT-based models [451, 452] and limits on the DM-nucleon cross section as a function of the DM mass were derived. As a consequence of a coordinated effort between the LHC experiments for Run 2 (“Dark Matter Forum”), the focus shifted to simplified models with defined benchmark points [453].

In simplified models the interaction between top quarks and a fermionic DM candidate is mediated by a scalar or pseudoscalar mediator particle. A recent comprehensive study of the collider phenomenology of topophilic DM is presented in [454]. The $t\bar{t} + E_T^{\text{miss}}$ signature is also employed in searches for pairs of top squarks in supersymmetric models. From such top-squark searches with LHC Run-2 data, the most sensitive limits on the mass of the DM and the mediator particles so far were derived [455, 456, 457, 458].

Monotop signatures occur in models in which a new scalar resonance decays into a top-quark and a colored “dark” fermion or in FCNC interactions producing a “dark” vector boson. The LHC experiments have searched for this signature with data taken at $\sqrt{s} = 8 \text{ TeV}$ [459, 460] and recently also in the $\sqrt{s} = 13 \text{ TeV}$ data and using boosted-top techniques [461]. All measurements agree with the SM expectation and lower limits on the masses of the scalar resonance and the “dark” vector boson have been placed, of the order of 3 TeV at 95% CL in a model in which the top quark and the DM particle originate from a heavy resonance.

6.4.5. Top Couplings in an Effective Field Theory Approach

In view of the null results of the searches for new heavy particles decaying into top quarks, a comprehensive effective field theory approach to study top-quark couplings becomes attractive. In such an approach the indirect effects of BSM physics on the top-quark couplings are treated in a consistent way, by constructing a full set of effective operators that mediate top-quark couplings

with mass-dimension six [462]:

$$\mathcal{L}_{\text{eff}} = \mathcal{L}_{\text{SM}} + \sum_i \frac{C_i^{(6)} O_i^{(6)}}{\Lambda^2} + \mathcal{O}(\Lambda^{-4}). \quad (34)$$

In the above equation, the effective Lagrangian density \mathcal{L}_{eff} is given by the SM Lagrangian \mathcal{L}_{SM} and a sum of dimension-six operators $O_i^{(6)}$, each weighted with a Wilson coefficient $C_i^{(6)}$, calculable in perturbation theory [463]. These interactions are suppressed by the square of the new-physics scale Λ . The operators relevant for top-quark interactions have been worked out e. g. in [464, 465].

Compared to the anomalous coupling approaches discussed before the EFT is the more comprehensive description of the top couplings in a gauge-invariant and renormalizable way that respects all SM symmetries. Confronting the EFT approach with data requires a global fit to Tevatron and LHC data on differential cross sections. A first global fit at LO has been performed with the TOPFITTER software tool [466, 467], where the complementarity between LHC and Tevatron measurements has been demonstrated [468] and boosted-top final states have been included [469]. To match the experimental precision, NLO corrections to the EFT are being worked out, with complications such as mixing of the operators in the renormalization group evolution. A first NLO analysis of FCNC interactions in the top-quark sector in an EFT framework has been presented in [470].

6.5. Top Quarks as a Tool

Given the excellent understanding of the properties of the top quark, the top quark is more and more considered a “standard candle” within the SM, similar to the role of the W and Z bosons at the Tevatron and the LHC so far. Events containing top quarks can be used as a calibration source or as a reference for other measurements. Top-quark production can also be used to better constrain proton parton distribution functions (PDFs) and to measure the strong coupling constant α_S .

B-Tagging Efficiency. One unique property of $t\bar{t}$ events is that they contain at least two b -flavored quarks in the partonic final state. This can be exploited in measurements of the b -tagging efficiency ϵ_b in a “busy” environment with several jets and charged leptons, similar to the signal region of many BSM physics searches. Often the observable of interest is not ϵ_b itself, but the

b-tagging scale factor SF_b , defined as the ratio of ϵ_b obtained in a given data sample and in an equivalent simulated data sample. One way of measuring SF_b is a profile likelihood ratio fit in $t\bar{t}$ dilepton candidate events, similar to what is used in cross section measurements presented in Chapter 4. The data sample is split into categories according to the number of jets and the number of *b*-jets in the event and SF_b is extracted from the event counts in these categories with a precision of up to 3% [471, 472]. Another method to extract SF_b is to apply a tag-and-probe technique to *b*-jets in $t\bar{t}$ events.

Strong Coupling Constant and Parton Distribution Functions. The strong coupling constant has been extracted from the $t\bar{t}$ production cross section together with the pole mass of the top quark [473]. While NNLO computations of QCD jet production at hadron colliders have only arrived in late 2016 [474], $t\bar{t}$ production is already known to NNLO precision since 2013. Therefore the extraction of α_S from $t\bar{t}$ production constitutes the first NNLO measurement of α_S at a hadron collider. The resulting value of α_S evaluated at the energy scale m_Z is

$$\alpha_S(m_Z) = 0.1151^{+0.0028}_{-0.0027}, \quad (35)$$

which tends to be lower than α_S values from other sources. The value is the only hadron collider result included into the most recent world average value of $\alpha_S(m_Z) = 0.1181 \pm 0.0011$ [91].

Precision measurements and NNLO calculations of the differential cross section for $t\bar{t}$ production, see Section 4.3, can be used to include $t\bar{t}$ data into proton PDF fits, together with other data, e.g. from the HERA ep collider. Including $t\bar{t}$ production improves the precision of the gluon PDF at large longitudinal momentum fractions x [107]. As mentioned in Section 4.5, also single top-quark production can be used to constrain PDFs. The ratio of single t to single \bar{t} production in the t -channel is a measure of the ratio of the u and d quark PDFs [239, 240, 242]; however, this method is not yet precise enough to contribute to PDF fits significantly.

Also more general properties of hadron collision events can be measured in $t\bar{t}$ production. The color flow in $t\bar{t}$ events has been studied by measuring the pull angle between pairs of jets, which is different for jet pairs coming from decays of color singlet and color octet states [475]. Another example is the underlying event, defined as any hadronic activity not attributed to the particles coming from the hard scattering [476, 477].

7. Future Top-Quark Physics

Top physics has come a long way from discovery and first measurements at the Tevatron in the 1990s to more and more sophisticated analyses using Tevatron Run II and LHC data. In the top-quark physics community the perspectives for the field are being evaluated, both for the high-luminosity upgrade of the LHC and for future lepton and hadron colliders. As it is notoriously difficult to predict future improvements and novel ideas, all of the projections presented below should be taken with a grain of salt: all studies are only valid in a context in which their underlying assumptions are valid as well.

7.1. Towards the High-Luminosity LHC

At the time of writing this review, Run 2 of the LHC is in full swing, with data-taking expected until 2018. Together with Run 3 (2021–2023) the LHC will have recorded data corresponding to about 0.3 ab^{-1} of integrated luminosity. After that the ATLAS and CMS detectors will undergo major upgrades, before the High-Luminosity LHC (HL-LHC) era will commence in 2026. At the end of data-taking at the HL-LHC in the late 2030s, integrated luminosities of the order of 3 ab^{-1} are expected.

The LHC experiments have carried out some studies of the top-quark physics potential at the HL-LHC with projections of key results, most prominently the expected uncertainty on the top-quark mass. In the absence of obvious BSM physics signals at the LHC so far, precision modeling of SM backgrounds, often including top quarks, is essential. The couplings of the top quark as well as rare processes such as FCNCs may reveal deviations from the SM. The large top-quark datasets at high center-of-mass energies will also allow investigation into new corners of the kinematic phase space, such as very high invariant $t\bar{t}$ masses, to search for particles that decay into top quarks.

A recent CMS projection of the expected uncertainty on the top-quark mass m_t is displayed in Fig. 19. The projection assumes that the upgraded CMS detector will maintain the same physics performance as the current detector, that the trigger efficiency may be reduced by up to a factor of three, and that the understanding of many systematic uncertainties can be improved. The study shows that kinematic methods to determine m_t will continue to be the most precise, with rather optimistic uncertainty estimates below 200 MeV, or 0.12%, using the full HL-LHC dataset. Methods based

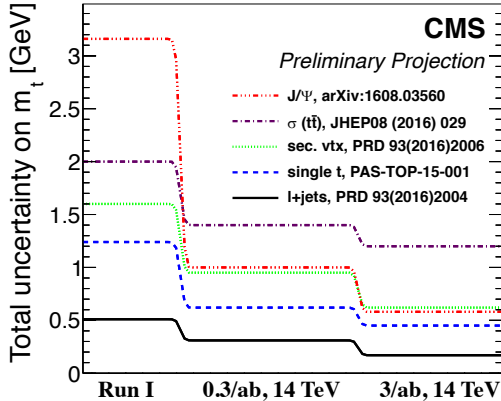


Figure 19: Total uncertainty on the mass of the top quark with different measurement methods comparing the uncertainty achieved in LHC Run 1 with projections for integrated luminosities of 0.3 ab^{-1} and 3 ab^{-1} at $\sqrt{s} = 14 \text{ TeV}$ [478].

on the reconstruction of exclusive final states, e.g. J/ψ from the hadronization of the b quark, profit most from the increased dataset sizes, arriving at uncertainties below 600 MeV [478].

Projections have also been performed for FCNC searches. As an example, depending on the assumptions on the systematic uncertainties, improvements by factors of two to six are expected for the limit on $\mathcal{B}(t \rightarrow Zq)$ [479].

The $t\bar{t}$ charge asymmetry, while reduced at 14 TeV compared to LHC Run 1 center-of-mass energies due to the larger fraction of gg -initiated $t\bar{t}$ events, will profit from new analysis ideas based the large number of events with boosted top quarks. It is expected that A_C can be measured very precisely also at the HL-LHC [376]. Also the precision with which the couplings of the top quarks can be determined in the future is expected to improve significantly with the large data samples at the HL-LHC. This includes knowledge about the Wtb vertex, as well as the electroweak couplings of the top-quarks. The expected precision on the SM γtt (Ztt) coupling with the full HL-LHC dataset is 1.4% (17%) [376], which at the same time increases the sensitivity for anomalous top-quark couplings. Also the sensitivity to the Yukawa couplings of the top-quark to the Higgs boson will be improved significantly. An uncertainty of 10% to 15% on the $t\bar{t}H$ signal strength is expected for the full HL-LHC dataset [480, 481].

The large HL-LHC datasets will also allow exploring $t\bar{t}$ production in final states with many jets, very high MET and large $t\bar{t}$ or $t + X$ invariant

masses. Such measurements will improve the modeling of SM processes with top quarks in extreme corners of phase space. This is a prerequisite for measurements of rare SM processes, such as $t\bar{t}H$ production, and of BSM searches, e. g. for supersymmetry, heavy resonances decaying into top quarks, and associated production of top quarks and DM. As an example, searches for heavy-resonance decays $Z' \rightarrow t\bar{t}$ and $W' \rightarrow tb$ are expected to improve, with sensitivities to Z' and W' masses up to 4 TeV [478].

7.2. Top-Quark Physics at Future Lepton and Hadron Colliders

Plans for future particle colliders include both lepton (e^+e^-) colliders and hadron (pp) colliders, which are at different stages of their planning. Lepton collider projects include the linear-collider projects International Linear Collider (ILC) [482], with Japan as the proposed host country, and Compact Linear Collider (CLIC) [483] at CERN, the circular collider projects Circular Electron Positron Collider (CEPS) [484, 485] in China, and the e^+e^- option of the CERN Future Circular Collider (FCC-ee). While the CEPS center-of-mass energy will be too small for $t\bar{t}$ pairs to be produced, the option of the ILC with $\sqrt{s} = 0.5$ TeV, all CLIC options, and the FCC-ee are intended to operate above the $t\bar{t}$ production threshold of approximately 350 GeV. Plans for future hadron colliders include the High-Energy LHC (HE-LHC), an upgraded version of the LHC with very high-field magnets and center-of-mass energies of up to 33 TeV, the Chinese Super Proton-Proton Collider (SppC) with up to $\sqrt{s} = 70$ TeV as part of the CEPS project, and the hadron collider option of the FCC (FCC-hh) with up to $\sqrt{s} = 100$ TeV, all of which are circular storage rings.

At future e^+e^- colliders, the exact knowledge of the initial state, in particular the center-of-mass energy, can be exploited to determine the top-quark mass via a scan of the $t\bar{t}$ production threshold at $\sqrt{s} = 2m_t$. The beam energies are varied such that \sqrt{s} is around $2m_t$ and the $t\bar{t}$ production cross section is measured as a function of \sqrt{s} . From the characteristic shape of the cross section turn-on, which has been computed including corrections up to either N³LO [486] or NNLL [487] accuracy, m_t can be determined with an expected total uncertainty of 100 MeV or below, without the ambiguities of the kinematic reconstruction. The top-quark mass can also be determined from the kinematics of the $t\bar{t}$ decay products. The excellent expected precision of future e^+e^- colliders will also allow for more precise studies of the QCD and electroweak couplings of the top quark in an EFT framework. The top-quark's Yukawa coupling is expected to be known to around 4%. A recent

summary of top-quark physics at future e^+e^- colliders can be found in [488].

At a hadron collider with $\sqrt{s} = 100$ TeV the cross section for $t\bar{t}$ production will increase by a factor of almost 40 compared to the current 13-TeV LHC. The mass reach of all searches for BSM physics with top quarks will be extended significantly. Also the role of the top quark will change: the top quark will become a “light” quark compared to the available collision energy. This will have an impact on $t\bar{t}$ production, which will prefer forward rapidity, similar to $b\bar{b}$ production at the LHC, and much higher boosts of the top quarks. In addition proton PDF sets will likely have to include top quark (and W and Z boson) PDFs. However at this point it seems very difficult to scale the LHC expectations for systematic uncertainties to very high luminosities at future hadron colliders. Reviews discussing the perspectives of SM and BSM physics at the FCC-hh can be found in [489, 490].

8. Conclusions

Studying the physics of the top quark, the heaviest particle of the standard model of particle physics, is an important, and very interesting, task. Since the discovery of the top quark, more than 20 years of research went into establishing its properties. With more and more sophisticated analysis methods, the top quark properties are remarkably well understood. In addition, the top-quark is considered a possible stepping stone to physics beyond the SM, both as part of a signal and as a major background. All SM measurements and searches for BSM physics so far are compatible with the expectations of the SM and contribute significantly to constraining possible BSM physics models. Top-quark physics will remain important after the upcoming upgrades of the LHC experiments, and experiments at future colliders may take the quest for the top to the next level.

Acknowledgment

It is my pleasure to thank Alison Lister for her valuable comments on this article.

Bibliography

References

- [1] M. Cristinziani and M. Mulders, preprint arXiv:1606.00327 [hep-ex], accepted at *J. Phys. G: Nucl. Part. Phys.*
- [2] E. Boos et al., *Usp. Fiz. Nauk* 185 (2015) 1241 (in Russian), *Phys. Usp.* 58 (2015) 1133 (in English)
- [3] K. Kröninger, A. B. Meyer and P. Uwer, in: T. Schörner-Sadenius (ed.), “The Large Hadron Collider – Harvest of Run 1”, Springer 2015
- [4] R. Chierici, *Riv. Nuovo Cim.* 37 (2014) 47
- [5] F. Déliot, N. Hadley, S. Parke and T. Schwarz, *Ann. Rev. Nucl. Part. Sci.* 64 (2014) 363.
- [6] C. E. Gerber and C. Vellidis, *Int. J. Mod. Phys. A* 30 (2015) 1541005
- [7] A. W. Jung, *Mod. Phys. Lett. A* 29 (2014) 1430014
- [8] S. Jabeen, *Int. J. Mod. Phys. A* 28 (2013) 1330038
- [9] E. Barberis, *Int. J. Mod. Phys. A* 28 (2013) 1330027
- [10] F. P. Schilling, *Int. J. Mod. Phys. A* 27 (2012) 1230016
- [11] V. del Duca and E. Laenen, *Int. J. Mod. Phys. A* 30 (2015) 1530063
- [12] W. Bernreuther, *J. Phys. G* 35 (2008) 083001
- [13] J. Wagner-Kuhr, *acta physica slovaca* 66 (2016) 1
- [14] A. Giammanco, *Rev. Phys.* 1 (2016) 1
- [15] E. Boos and L. Dudko, *Int. J. Mod. Phys. A* 27 (2012) 1230026
- [16] G. Cortiana, *Rev. Phys.* 1 (2016) 60
- [17] J. A. Aguilar-Saavedra, D. Amidei, A. Juste and M. Perez-Victoria, *Rev. Mod. Phys.* 87 (2015) 421
- [18] O. Behnke, A. Geiser and M. Lisovyi, *Prog. Part. Nucl. Phys.* 84 (2015) 1
- [19] F. Abe et al. (CDF Collaboration), *Phys. Rev. Lett.* 74 (1995) 2626
- [20] S. Abachi et al. (D0 Collaboration), *Phys. Rev. Lett.* 74 (1995) 2632
- [21] M. Gell-Mann, *Phys. Lett.* 8 (1964) 214
- [22] G. Zweig, CERN-TH-401, CERN-TH-412.
- [23] M. Gell-Mann, *Phys. Rev.* 125 (1962) 1067
- [24] Y. Ne’eman, *Nucl. Phys.* 26 (1961) 222
- [25] N. Cabibbo, *Phys. Rev. Lett.* 10 (1963) 531
- [26] S. L. Glashow, J. Iliopoulos and L. Maiani, *Phys. Rev. D* 2 (1970) 1285
- [27] J. J. Aubert et al. (E598 Collaboration), *Phys. Rev. Lett.* 33 (1974) 1404
- [28] J. E. Augustin et al. (SLAC-SP-017 Collaboration), *Phys. Rev. Lett.* 33 (1974) 1406
- [29] J. H. Christenson, J. W. Cronin, V. L. Fitch and R. Turlay, *Phys. Rev. Lett.* 13 (1964) 138
- [30] M. Kobayashi and T. Maskawa, *Prog. Theor. Phys.* 49 (1973) 652
- [31] M. L. Perl et al., *Phys. Rev. Lett.* 35 (1975) 1489
- [32] S. W. Herb et al., *Phys. Rev. Lett.* 39 (1977) 252

- [33] C. Berger et al. (Pluto Collaboration), *Phys. Lett.* B 76 (1978) 243
- [34] W. Bartel et al. (JADE Collaboration), *Phys. Lett.* B 146 (1984) 437
- [35] G. Arnison *et al.* (UA1 Collaboration), *Phys. Lett.* B 147 (1984) 493
- [36] H. Albrecht et al. (ARGUS Collaboration), *Phys. Lett.* B 192 (1987) 245
- [37] C. Albajar et al. (UA1 Collaboration), *Phys. Lett.* B 186 (1987) 247, Erratum: *Phys. Lett.* B 197 (1987) 565
- [38] D. Abbaneo (ALEPH, DELPHI, L3, OPAL Collaborations, LEP Electroweak Working Group), preprint CERN-PPE-94-187, C94-07-20.
- [39] ALEPH, DELPHI, L3, OPAL, SLD Collaborations, LEP Electroweak Working Group, SLD Electroweak and Heavy Flavour Groups, *Phys. Rept.* 427 (2006) 257
- [40] F. Abe et al. (CDF Collaboration), *Phys. Rev.* D 50 (1994) 2966
- [41] F. Abe et al. (CDF Collaboration), *Phys. Rev. Lett.* 68 (1992) 447
- [42] S. Abachi et al. (D0 Collaboration), *Phys. Rev.* D 52 (1995) 4877, preliminary results in preprint arXiv:hep-ex/9409006
- [43] T. M. Liss and P. L. Tipton, *Sci. Am.* 277, Vol. 3 (1997) 54
- [44] T. Affolder et al. (CDF Collaboration), *Phys. Rev.* D 64 (2001) 032002, Erratum: *Phys. Rev.* D 67 (2003) 119901
- [45] V. M. Abazov et al. (D0 Collaboration), *Phys. Rev.* D 67 (2003) 012004
- [46] P. Azzi et al. (CDF and D0 and Tevatron Electroweak Working Group Collaborations), preprint arXiv:hep-ex/0404010
- [47] T. Affolder et al. (CDF Collaboration), *Phys. Rev. Lett.* 84 (2000) 216
- [48] V. M. Abazov et al. (D0 Collaboration), *Phys. Lett.* B 617 (2005) 1
- [49] T. Affolder et al. (CDF Collaboration), *Phys. Rev. Lett.* 85 (2000) 2062
- [50] T. Affolder et al. (CDF Collaboration), *Phys. Rev.* D 62 (2000) 012004
- [51] V. M. Abazov et al. (D0 Collaboration), *Phys. Rev. Lett.* 88 (2002) 151803
- [52] K. Kondo, *J. Phys. Soc. Jap.* 4126 (1988) 57
- [53] V. M. Abazov et al. (D0 Collaboration), *Nature* 429 (2004) 638
- [54] V. M. Abazov et al. (D0 Collaboration), *Phys. Rev. Lett.* 113 (2014) 032002
- [55] V. M. Abazov et al. (D0 Collaboration), *Phys. Rev.* D 91 (2015) 112003
- [56] V. M. Abazov et al. (D0 Collaboration), *Phys. Rev. Lett.* 103 (2009) 092001
- [57] T. Aaltonen et al. (CDF Collaboration), *Phys. Rev. Lett.* 103 (2009) 092002
- [58] J. H. Kühn and G. Rodrigo, *Phys. Rev. Lett.* 81 (1998) 49
- [59] V. M. Abazov et al. (D0 Collaboration), *Phys. Rev. Lett.* 100 (2008) 142002
- [60] T. Aaltonen et al. (CDF Collaboration), *Phys. Rev. Lett.* 101 (2008) 202001
- [61] T. Aaltonen et al. (CDF Collaboration), *Phys. Rev.* D 83 (2011) 112003
- [62] V. Khachatryan et al. [CMS Collaboration], *Phys. Lett.* B 695 (2011) 424
- [63] G. Aad et al. (ATLAS Collaboration), *Eur. Phys. J.* C 71 (2011) 1577
- [64] Tevatron Electroweak Working Group, Top Subgroup,
<http://tevewwg.fnal.gov/top/> (retrieved: 11 July 2016)
- [65] LHC Top Physics Working Group,
<https://twiki.cern.ch/twiki/bin/view/LHCPhysics/LHCTopWG>

(retrieved: 24 Nov 2016)

- [66] R. D. Ball et al. (NNPDF Collaboration), *J. High Energy Phys.* 1504 (2015) 040
- [67] S. Dulat et al., *Phys. Rev. D* 93 (2016) 033006
- [68] L. A. Harland-Lang et al., *Eur. Phys. J. C* 75 (2015) 204
- [69] H. Abramowicz et al. (H1 and ZEUS Collaborations), *Eur. Phys. J. C* 75 (2015) 580
- [70] S. Alekhin et al., preprint arXiv:1609.03327 [hep-ph]
- [71] A. Buckley et al., *Eur. Phys. J. C* 75 (2015) 132
- [72] B. Andersson, G. Gustafson, G. Ingelman and T. Sjöstrand, *Phys. Rept.* 97 (1983) 31.
- [73] B. R. Webber, *Nucl. Phys. B* 238 (1984) 492
- [74] P. Nason, *J. High Energy Phys.* 0411 (2004) 040
- [75] S. Frixione, P. Nason and C. Oleari, *J. High Energy Phys.* 0711 (2007) 070
- [76] S. Alioli et al., *J. High Energy Phys.* 1006 (2010) 043
- [77] T. Ježo et al., *Eur. Phys. J. C* 76 (2016) 691
- [78] S. Frixione and B. R. Webber, *J. High Energy Phys.* 0206 (2002) 029
- [79] J. Alwall et al., *J. High Energy Phys.* 1407 (2014) 079
- [80] T. Sjöstrand, S. Mrenna and P. Z. Skands, *J. High Energy Phys.* 0605 (2006) 026
- [81] T. Sjöstrand et al., *Comput. Phys. Commun.* 191 (2015) 159
- [82] J. Bellm et al., *Eur. Phys. J. C* 76 (2016) 196
- [83] M. L. Mangano et al., *J. High Energy Phys.* 0307 (2003) 001
- [84] T. Gleisberg et al., *J. High Energy Phys.* 0902 (2009) 007
- [85] S. Höche et al., *Phys. Lett. B* 748 (2015) 74
- [86] M. Czakon, P. Fiedler and A. Mitov, *Phys. Rev. Lett.* 110 (2013) 252004
- [87] M. Brucherseifer, F. Caola and K. Melnikov, *Phys. Lett. B* 736 (2014) 58
- [88] E. L. Berger et al., *Phys. Rev. D* 94 (2016) 075101
- [89] J. Gao, C. S. Li and H. X. Zhu, *Phys. Rev. Lett.* 110 (2013) 042001
- [90] M. Brucherseifer, F. Caola and K. Melnikov, *J. High Energy Phys.* 1304 (2013) 059
- [91] C. Patrignani et al., *Chin. Phys. C* 40 (2016) 100001
- [92] A. Czarnecki, J. G. Körner and J. H. Piclum, *Phys. Rev. D* 81 (2010) 111503
- [93] P. W. Higgs, *Phys. Rev. Lett.* 13 (1964) 508
- [94] P. W. Higgs, *Phys. Lett.* 12 (1964) 132
- [95] F. Englert and R. Brout, *Phys. Rev. Lett.* 13 (1964) 321
- [96] Y. Nambu and G. Jona-Lasinio, *Phys. Rev.* 122 (1961) 345
- [97] G. S. Guralnik, C. R. Hagen and T. W. B. Kibble, *Phys. Rev. Lett.* 13 (1964) 585
- [98] P. Marquard et al., *Phys. Rev. Lett.* 114 (2015) 142002
- [99] P. Marquard et al., *Phys. Rev. D* 94 (2016) 074025
- [100] M. Beneke et al., preprint arXiv:1605.03609 [hep-ph].
- [101] M. Butenschoen et al., *Phys. Rev. Lett.* 117 (2016) 232001

- [102] D. Binosi and L. Theussl, *Comput. Phys. Commun.* 161 (2004) 76
- [103] P. Nason, S. Dawson and R. K. Ellis, *Nucl. Phys. B* 303 (1988) 607
- [104] W. Beenakker et al., *Phys. Rev. D* 40 (1989) 54
- [105] M. Czakon and A. Mitov, *Comput. Phys. Commun.* 185 (2014) 2930
- [106] M. Aliev et al., *Comput. Phys. Commun.* 182 (2011) 1034
- [107] M. Guzzi, K. Lipka and S. O. Moch, *J. High Energy Phys.* 1501 (2015) 082
- [108] W. Beenakker et al. *Nucl. Phys. B* 411 (1994) 343
- [109] W. Bernreuther, M. Fücker and Z. G. Si, *Phys. Rev. D* 74 (2006) 113005
- [110] J. H. Kühn, A. Scharf and P. Uwer, *Eur. Phys. J. C* 51 (2007) 37
- [111] A. Denner et al., *Phys. Rev. Lett.* 106 (2011) 052001
- [112] F. Cascioli et al., *Eur. Phys. J. C* 74 (2014) 2783
- [113] W. Bernreuther, D. Heisler and Z. G. Si, *J. High Energy Phys.* 1512 (2015) 026
- [114] N. Kidonakis, *Phys. Rev. D* 83 (2011) 091503
- [115] N. Kidonakis, *Phys. Rev. D* 81 (2010) 054028
- [116] N. Kidonakis, *Phys. Rev. D* 82 (2010) 054018
- [117] J. M. Campbell and R. K. Ellis, *Nucl. Phys. Proc. Suppl.* 205-206 (2010) 10
- [118] P. Kant et al., *Comput. Phys. Commun.* 191 (2015) 74
- [119] S. Chatrchyan et al. (CMS Collaboration), *JINST* 7 (2012) P10002
- [120] M. Cacciari, G. P. Salam and G. Soyez, *J. High Energy Phys.* 0804 (2008) 063
- [121] G. Aad et al. (ATLAS Collaboration), *Eur. Phys. J. C* 75 (2015) 17
- [122] S. Chatrchyan et al. (CMS Collaboration), *JINST* 6 (2011) P11002
- [123] CMS Collaboration, preprint CMS-PAS-PFT-10-002
- [124] L. Sonnenschein, *Phys. Rev. D* 73 (2006) 054015, Erratum: *Phys. Rev. D* 78 (2008) 079902
- [125] J. Thaler and K. Van Tilburg, *J. High Energy Phys.* 1103 (2011) 015
- [126] G. P. Salam, *Eur. Phys. J. C* 67 (2010) 637
- [127] A. Altheimer et al., *J. Phys. G* 39 (2012) 063001
- [128] D. Adams et al., *Eur. Phys. J. C* 75 (2015) 409
- [129] R. Brun and F. Rademakers, *Nucl. Instrum. Meth. A* 389 (1997) 81
- [130] G. Cowan, “Statistical data analysis,” Clarendon Press, Oxford (1998)
- [131] K. S. Cranmer, *Comput. Phys. Commun.* 136 (2001) 198
- [132] W. Verkerke and D. P. Kirkby, *eConf C* 0303241 (2003) MOLT007
- [133] L. Moneta et al., *PoS ACAT* (2010) 057
- [134] T. Müller, J. Ott and J. Wagner-Kuhr, <http://www.theta-framework.org> (retrieved: 4 July 2016)
- [135] T. Hastie, R. Tibshirani and J. Friedman, “The Elements of Statistical Learning”, 2nd edition, Springer (2009)
- [136] A. Höcker et al., *PoS ACAT* (2007) 040
- [137] F. Pedregosa et al., *J. Machine Learning Res.* 12 (2011) 2825
- [138] M. Feindt and U. Kerzel, *Nucl. Instrum. Meth. A* 559 (2006) 190
- [139] J. Alwall, A. Freitas and O. Mattelaer, *Phys. Rev. D* 83 (2011) 074010

- [140] J. M. Campbell, W. T. Giele and C. Williams, *J. High Energy Phys.* 1211 (2012) 043
- [141] T. Martini and P. Uwer, *J. High Energy Phys.* 1509 (2015) 083
- [142] F. Fiedler et al., *Nucl. Instrum. Meth. A* 624 (2010) 203
- [143] S. Schmitt, *JINST* 7 (2012) T10003
- [144] A. Höcker and V. Kartvelishvili, *Nucl. Instrum. Meth. A* 372 (1996) 469
- [145] G. Choudalakis, preprint arXiv:1201.4612 [physics.data-an]
- [146] L. Lyons, D. Gibaut and P. Clifford, *Nucl. Instrum. Meth. A* 270 (1988) 110
- [147] A. Buckley et al., *Comput. Phys. Commun.* 184 (2013) 2803
- [148] CMS Collaboration, preprint CMS-PAS-TOP-16-015, June 2016
- [149] LHC Top Working Group Summary Plots, <https://twiki.cern.ch/twiki/bin/view/LHCPhysics/LHCTopWGSummaryPlots>, (retrieved: 22 Sep 2016)
- [150] T. Aaltonen et al. (CDF and D0 Collaborations), *Phys. Rev. D* 89 (2014) 072001
- [151] T. Aaltonen et al. (CDF Collaboration), *Phys. Rev. Lett.* 105 (2010) 012001
- [152] V. M. Abazov et al. (D0 Collaboration), *Phys. Rev. D* 94 (092004) 2016
- [153] T. Aaltonen et al. (CDF Collaboration), *Phys. Rev. D* 88 (2013) 091103
- [154] G. Aad et al. (ATLAS Collaboration), *Eur. Phys. J. C* 74 (2014) 3109
- [155] V. Khachatryan et al. (CMS Collaboration), *J. High Energy Phys.* 1608 (2016) 029
- [156] ATLAS and CMS Collaborations, preprint ATLAS-CONF-2014-054, CMS-PAS-TOP-14-016, September 2014
- [157] M. Aaboud et al. (ATLAS Collaboration), *Phys. Lett. B* 761 (2016) 136
- [158] CMS Collaboration (CMS Collaboration), preprint CMS-PAS-TOP-16-006, July 2016
- [159] V. M. Abazov et al. (D0 Collaboration), *Phys. Rev. D* 82 (2010) 071102
- [160] T. Aaltonen et al. (CDF Collaboration), *Phys. Rev. Lett.* 109 (2012) 192001
- [161] T. Aaltonen et al. (CDF Collaboration), *Phys. Rev. D* 89 (2014) 091101
- [162] G. Aad et al. (ATLAS Collaboration), *Phys. Lett. B* 717 (2012) 89
- [163] S. Chatrchyan et al. (CMS Collaboration), *Phys. Rev. D* 85 (2012) 112007
- [164] G. Aad et al. (ATLAS Collaboration), *Eur. Phys. J. C* 73 (2013) 2328
- [165] V. M. Abazov et al. (D0 Collaboration), *Phys. Rev. D* 82 (2010) 032002
- [166] T. Aaltonen et al. (CDF Collaboration), *Phys. Rev. D* 81 (2010) 052001
- [167] S. Chatrchyan et al. (CMS Collaboration), *J. High Energy Phys.* 1305 (2013) 065
- [168] V. Khachatryan et al. (CMS Collaboration), *Eur. Phys. J. C* 76 (2016) 128
- [169] CMS Collaboration, preprint CMS-PAS-TOP-16-013, June 2016
- [170] R. Aaij et al. (LHCb Collaboration), *Phys. Lett. B* 767 (2017) 110
- [171] M. Cacciari and G. P. Salam, *Phys. Lett. B* 659 (2008) 119
- [172] G. Aad et al. (ATLAS Collaboration), *J. High Energy Phys.* 1506 (2015) 100
- [173] CMS Collaboration, preprint CMS-PAS-TOP-15-011, December 2015

- [174] V. Ahrens et al., *J. High Energy Phys.* 1009 (2010) 097
- [175] A. Broggio, A. S. Papanastasiou and A. Signer, *J. High Energy Phys.* 1410 (2014) 98
- [176] N. Kidonakis, *Phys. Rev. D* 91 (2015) 031501
- [177] M. Czakon, D. Heymes and A. Mitov, *Phys. Rev. Lett.* 116 (2016) 082003
- [178] M. Czakon, D. Heymes and A. Mitov, submitted to *J. High Energy Phys.*, preprint arXiv:1606.03350 [hep-ph]
- [179] T. Aaltonen et al. (CDF Collaboration), *Phys. Rev. Lett.* 102 (2009) 222003
- [180] V. M. Abazov et al. (D0 Collaboration), *Phys. Rev. D* 90 (2014) 092006
- [181] G. Aad et al. (ATLAS Collaboration), *Eur. Phys. J. C* 73 (2013) 2261
- [182] G. Aad et al. (ATLAS Collaboration), *Phys. Rev. Lett.* 90 (2014) 072004
- [183] S. Chatrchyan et al. (CMS Collaboration), *Eur. Phys. J. C* 73 (2013) 2339
- [184] G. Aad et al. (ATLAS Collaboration), *Eur. Phys. J. C* 76 (2016) 538
- [185] M. Aaboud et al. (ATLAS Collaboration), *Phys. Rev. D* 94 (2016) 092003
- [186] V. Khachatryan et al. (CMS Collaboration), *Eur. Phys. J. C* 75 (2015) 542
- [187] ATLAS Collaboration, preprint ATLAS-CONF-2016-040, August 2016
- [188] CMS Collaboration, preprint CMS-PAS-TOP-16-011, March 2016
- [189] CMS Collaboration, preprint CMS-PAS-TOP-16-007, August 2016
- [190] V. Khachatryan et al. (CMS Collaboration), preprint arXiv:1610.04191 [hep-ex], accepted by *Phys. Rev. D*
- [191] CMS Collaboration, preprint CMS-PAS-TOP-14-013, July 2016
- [192] G. Aad et al. (ATLAS Collaboration), *Phys. Rev. D* 93 (2016) 032009
- [193] V. Khachatryan et al. (CMS Collaboration), *Phys. Rev. D* 94 (2016) 072002
- [194] ATLAS Collaboration, preprint ATLAS-CONF-2016-100, September 2016
- [195] CMS Collaboration, preprint CMS-PAS-TOP-15-015, September 2016
- [196] G. Aad et al. (ATLAS Collaboration), *J. High Energy Phys.* 1501 (2015) 020
- [197] M. Aaboud et al. (ATLAS Collaboration), *J. High Energy Phys.* 1609 (2016) 074
- [198] ATLAS Collaboration, preprint ATLAS-CONF-2015-065, December 2015
- [199] M. Aaboud et al. (ATLAS Collaboration), preprint arXiv:1610.09978 [hep-ex], submitted to *Eur. Phys. J. C*
- [200] S. Chatrchyan et al. (CMS Collaboration), *Eur. Phys. J. C* 74 (2015) 3014, Erratum: *Eur. Phys. J. C* 75 (2015) 216
- [201] V. Khachatryan et al. (CMS Collaboration), *Eur. Phys. J. C* 76 (2016) 379
- [202] CMS Collaboration, preprint CMS-PAS-TOP-15-006, July 2016
- [203] V. Khachatryan et al. (CMS Collaboration), *Phys. Lett. B* 746 (2015) 132
- [204] G. Aad et al. (ATLAS Collaboration), *Eur. Phys. J. C* 76 (2016) 11
- [205] CMS Collaboration, preprint CMS-PAS-TOP-16-010, July 2016
- [206] V. Khachatryan et al. (CMS Collaboration), *Phys. Rev. D* 94 (2016) 052006
- [207] CMS Collaboration, preprint CMS-PAS-TOP-15-013, November 2015
- [208] T. Aaltonen et al. (CDF Collaboration), *Phys. Rev. D* 84 (2011) 031104
- [209] G. Aad et al. (ATLAS Collaboration), *Phys. Rev. D* 91 (2015) 072007
- [210] CMS Collaboration, preprint CMS-PAS-TOP-14-008, September 2016

- [211] G. Aad et al. (ATLAS Collaboration), *J. High Energy Phys.* 1511 (2015) 172
- [212] V. Khachatryan et al. (CMS Collaboration), *J. High Energy Phys.* 1601 (2016) 096
- [213] M. Aaboud et al. (ATLAS Collaboration), preprint arXiv:1609.01599 [hep-ex], submitted to *Eur. Phys. J. C*
- [214] CMS Collaboration, preprint CMS-PAS-TOP-16-009, March 2016
- [215] CMS Collaboration, preprint CMS-PAS-TOP-16-017, August 2016
- [216] LHC Higgs Cross Section Working Group, <https://twiki.cern.ch/twiki/bin/view/LHCPhysics/LHCHXSWG> (retrieved: 9 Oct 2016)
- [217] G. Aad *et al.* [ATLAS Collaboration], *Phys. Lett. B* 740 (2015) 222
- [218] G. Aad et al. (ATLAS Collaboration), *Phys. Lett. B* 749 (2015) 519
- [219] G. Aad et al. (ATLAS Collaboration), *J. High Energy Phys.* 1605 (2016) 160
- [220] V. Khachatryan et al. (CMS Collaboration), *J. High Energy Phys.* 1409 (2014) 087, Erratum: *J. High Energy Phys.* 1410 (2014) 106
- [221] V. Khachatryan et al. (CMS Collaboration), *Eur. Phys. J. C* 75 (2015) 251
- [222] G. Aad et al. (ATLAS and CMS Collaborations), *J. High Energy Phys.* 1608 (2016) 045
- [223] CMS Collaboration, preprint CMS-PAS-HIG-16-004, March 2016
- [224] CMS Collaboration, preprint CMS-PAS-HIG-15-008, March 2016
- [225] CMS Collaboration, preprint CMS-PAS-HIG-16-022, August 2016
- [226] CMS Collaboration, preprint CMS-PAS-HIG-16-020, August 2016
- [227] CMS Collaboration, preprint CMS-PAS-HIG-16-038, November 2016
- [228] ATLAS Collaboration, preprint ATLAS-CONF-2016-080, August 2016
- [229] ATLAS Collaboration, preprint ATLAS-CONF-2016-067, August 2016
- [230] ATLAS Collaboration, preprint ATLAS-CONF-2016-058, August 2016
- [231] ATLAS Collaboration, preprint ATLAS-CONF-2016-068, August 2016
- [232] S. Chatrchyan et al. (CMS Collaboration), *Phys. Rev. Lett.* 107 (2011) 091802
- [233] G. Aad et al. (ATLAS Collaboration), *Phys. Lett. B* 717 (2012) 330
- [234] V. M. Abazov et al. (D0 Collaboration), *Phys. Lett. B* 726 (2013) 656
- [235] T. Aaltonen *et al.* [CDF Collaboration], *Phys. Rev. D* 93 (2016) 032011
- [236] T. Aaltonen et al. (CDF and D0 Collaborations), *Phys. Rev. Lett.* 115 (2015) 152003
- [237] T. Aaltonen et al. (CDF and D0 Collaborations), *Phys. Rev. Lett.* 112 (2014) 231803
- [238] S. Chatrchyan et al. (CMS Collaboration), *J. High Energy Phys.* 1212 (2012) 035
- [239] G. Aad et al. (ATLAS Collaboration), *Phys. Rev. D* 90 (2014) 112006
- [240] V. Khachatryan et al. (CMS Collaboration), *J. High Energy Phys.* 1406 (2014) 090
- [241] ATLAS Collaboration, preprint ATLAS-CONF-2014-007, March 2014

- [242] A. M. Sirunyan et al. (CMS Collaboration), preprint arXiv:1610.00678 [hep-ex], submitted to *Phys. Lett. B*
- [243] M. Aaboud et al. (ATLAS Collaboration), preprint arXiv:1609.03920 [hep-ex], submitted to *J. High Energy Phys.*
- [244] CMS Collaboration, preprint CMS-PAS-TOP-15-007, September 2015
- [245] CMS Collaboration, preprint CMS-PAS-TOP-14-004, October 2014
- [246] CMS Collaboration, preprint CMS-PAS-TOP-16-004, May 2016
- [247] S. Chatrchyan et al. (CMS Collaboration), *Phys. Rev. Lett.* 110 (2013) 022003
- [248] G. Aad et al. (ATLAS Collaboration), *Phys. Lett. B* 716 (2012) 142
- [249] S. Chatrchyan et al. (CMS Collaboration), *Phys. Rev. Lett.* 112 (2014) 231802
- [250] G. Aad et al. (ATLAS Collaboration), *J. High Energy Phys.* 1601 (2016) 064
- [251] ATLAS Collaboration, preprint ATLAS-CONF-2016-065, August 2016
- [252] ATLAS and CMS Collaborations, preprint ATLAS-CONF-2016-023, CMS-PAS-TOP-15-019, May 2016
- [253] G. Aad et al. (ATLAS Collaboration), *Phys. Lett. B* 756 (2016) 228
- [254] V. Khachatryan et al. (CMS Collaboration), *J. High Energy Phys.* 1609 (2016) 027
- [255] V. Khachatryan et al. (CMS Collaboration), *J. High Energy Phys.* 1606 (2016) 177
- [256] CMS Collaboration, preprint CMS-PAS-HIG-16-019, August 2016
- [257] G. Degrassi et al., *J. High Energy Phys.* 1208 (2012) 098
- [258] S. Alekhin, A. Djouadi and S. Moch, *Phys. Lett. B* 716 (2012) 214
- [259] M. P. Mulders, Ph.D. Thesis, Universiteit van Amsterdam, 2001, CERN-DELPHI-THESIS-237
- [260] V. M. Abazov et al. (D0 Collaboration), *Phys. Rev. D* 75 (2007) 092001
- [261] J. F. Arguin, Ph.D. Thesis, University of Toronto, 2005, FERMILAB-THESIS-2005-63, UMI-NR-15918
- [262] T. Aaltonen et al. (CDF Collaboration), *Phys. Rev. Lett.* 109 (2012) 152003
- [263] V. Khachatryan et al. (CMS Collaboration), *Phys. Rev. D* 93 (2016) 072004
- [264] M. Aaboud et al. (ATLAS Collaboration), *Phys. Lett. B* 761 (2016) 350
- [265] T. Aaltonen et al. (CDF Collaboration), *Phys. Rev. D* 92 (2015) 032003
- [266] V. M. Abazov et al. (D0 Collaboration), *Phys. Rev. B* 752 (2016) 18
- [267] V. M. Abazov et al. (D0 Collaboration), *Phys. Rev. D* 94 (2016) 032004
- [268] T. Aaltonen et al. (CDF Collaboration), *Phys. Rev. D* 90 (2014) 091101
- [269] T. Aaltonen et al. (CDF Collaboration), *Phys. Rev. D* 88 (2013) 011101
- [270] G. Aad et al. (ATLAS Collaboration), *Eur. Phys. J. C* 75 (2015) 330
- [271] S. Chatrchyan et al. (CMS Collaboration), *J. High Energy Phys.* 1212 (2012) 105
- [272] S. Chatrchyan et al. (CMS Collaboration), *Eur. Phys. J. C* 72 (2012) 2202
- [273] G. Aad et al. (ATLAS Collaboration), *Eur. Phys. J. C* 75 (2015) 158

- [274] ATLAS Collaboration, preprint ATLAS-CONF-2016-064, August 2016
- [275] S. Chatrchyan et al. (CMS Collaboration), *Eur. Phys. J. C* 74 (2014) 2758
- [276] Tevatron Electroweak Working Group, preprint arXiv:1608.01881 [hep-ex]
- [277] C. S. Hill, J. R. Incandela and J. M. Lamb, *Phys. Rev. D* 71 (2005) 054029
- [278] T. Aaltonen et al. (CDF Collaboration), *Phys. Rev. D* 81 (2010) 032002
- [279] CMS Collaboration, preprint CMS-PAS-TOP-12-030, July 2013
- [280] K. Agashe, R. Franceschini and D. Kim, *Phys. Rev. D* 88 (2013) 057701
- [281] CMS Collaboration, preprint CMS-PAS-TOP-15-002, September 2016
- [282] V. Khachatryan et al. (CMS Collaboration), *Phys. Rev. D* 93 (2016) 092006
- [283] A. Kharchilava, *Phys. Lett. B* 476 (2000) 73
- [284] V. Khachatryan et al. (CMS Collaboration), *J. High Energy Phys.* 1612 (2016) 123
- [285] C. G. Lester and D. J. Summers, *Phys. Lett. B* 463 (1999) 99
- [286] T. Aaltonen et al. CDF Collaboration, *Phys. Rev. D* 81 (2010) 031102
- [287] ATLAS Collaboration, preprint ATLAS-CONF-2012-082, June 2012
- [288] CMS Collaboration, preprint CMS-PAS-TOP-15-008, August 2016
- [289] S. Frixione and A. Mitov, *J. High Energy Phys.* 1409 (2014) 012
- [290] CMS Collaboration, preprint CMS-PAS-TOP-16-002, March 2016
- [291] CMS Collaboration, preprint CMS-PAS-TOP-14-011, November 2015
- [292] ATLAS Collaboration, preprint ATLAS-CONF-2014-055, September 2014
- [293] CMS Collaboration, preprint CMS-PAS-TOP-15-001, March 2016
- [294] V. M. Abazov et al. (D0 Collaboration), *Phys. Rev. Lett.* 100 (2008) 192004
- [295] S. Alioli et al., *Eur. Phys. J. C* 73 (2013) 2438
- [296] G. Aad et al. (ATLAS Collaboration), *J. High Energy Phys.* 1510 (2015) 121
- [297] CMS Collaboration, preprint CMS-PAS-TOP-13-006, May 2016
- [298] ATLAS and CDF and CMS and D0 Collaborations, preprint arXiv:1403.4427 [hep-ex]
- [299] CMS Collaboration, preprint CMS-PAS-TOP-15-012, November 2016
- [300] V. M. Abazov et al. (D0 Collaboration), *Phys. Rev. D* 84 (2011) 052005
- [301] T. Aaltonen et al. (CDF Collaboration), *Phys. Rev. D* 87 (2013) 052013
- [302] S. Chatrchyan et al. (CMS Collaboration), *J. High Energy Phys.* 1206 (2012) 109
- [303] G. Aad et al. (ATLAS Collaboration), *Phys. Lett. B* 728 (2014) 363
- [304] S. Chatrchyan et al. (CMS Collaboration), preprint arXiv:1610.09551 [hep-ex], submitted to *Phys. Lett. B*
- [305] R. D. Field and R. P. Feynman, *Nucl. Phys. B* 136 (1978) 1
- [306] T. Aaltonen et al. (CDF Collaboration), *Phys. Rev. D* 88 (2013) 032003
- [307] V. M. Abazov et al. (D0 Collaboration), *Phys. Rev. D* 90 (2014) 051101, Erratum: *Phys. Rev. D* 90 (2014) 079904,
- [308] G. Aad et al., (ATLAS Collaboration), *J. High Energy Phys.* 1311 (2013) 031
- [309] V. M. Abazov et al., (D0 Collaboration), *Phys. Rev. D* 85 (2012) 091104
- [310] V. Khachatryan et al., (CMS Collaboration), *Phys. Lett. B* 736 (2014) 33

- [311] T. Aaltonen et al. (CDF Collaboration), *Phys. Rev. Lett.* 111 (2013) 202001
- [312] CMS Collaboration, preprint CMS-PAS-TOP-16-019, September 2016
- [313] W. Hollik and D. Pagani, *Phys. Rev. D* 84 (2011) 093003
- [314] G. Aad et al. (ATLAS Collaboration), *Eur. Phys. J. C* 76 (2016) 87
- [315] T. Aaltonen et al. (CDF Collaboration), *Phys. Rev. D* 87 (2013) 092002
- [316] T. Aaltonen et al. (CDF Collaboration), *Phys. Rev. D* 93 (2016) 112005
- [317] V. M. Abazov et al. (D0 Collaboration), *Phys. Rev. D* 90 (2014) 072011
- [318] V. M. Abazov et al. (D0 Collaboration), *Phys. Rev. D* 92 (2015) 052007
- [319] M. Czakon, P. Fiedler and A. Mitov, *Phys. Rev. Lett.* 115 (2015) 052001
- [320] N. Kidonakis, *Phys. Rev. D* 91 (2015) 071502
- [321] M. Czakon, P. Fiedler, D. Heymes and A. Mitov, *J. High Energy Phys.* 1605 (2016) 034
- [322] W. Bernreuther and Z. G. Si, *Phys. Rev. D* 86 (2012) 034026
- [323] V. M. Abazov et al. (D0 Collaboration), *Phys. Rev. D* 88 (2013) 112002
- [324] V. M. Abazov et al. (D0 Collaboration), *Phys. Rev. D* 90 (2014) 072001
- [325] T. Aaltonen et al. (CDF Collaboration), *Phys. Rev. Lett.* 113 (2014) 042001, Erratum: *Phys. Rev. Lett.* 117 (2016) 199901
- [326] J. A. Aguilar-Saavedra and M. Perez-Victoria, *Phys. Rev. D* 84 (2011) 115013
- [327] J. A. Aguilar-Saavedra and M. Perez-Victoria, *J. High Energy Phys.* 1109 (2011) 097
- [328] S. Chatrchyan et al. (CMS Collaboration), *Phys. Lett. B* 717 (2012) 129
- [329] V. Khachatryan et al. (CMS Collaboration), *Phys. Lett. B* 757 (2016) 154
- [330] G. Aad et al. (ATLAS Collaboration), *J. High Energy Phys.* 1402 (2014) 107
- [331] ATLAS and CMS Collaborations, preprint ATLAS-CONF-2014-012, CMS-PAS-TOP-14-006, March 2014
- [332] G. Aad et al. (ATLAS Collaboration), *Phys. Lett. B* 756 (2016) 52
- [333] V. Khachatryan et al. (CMS Collaboration), *Phys. Rev. D* 93 (2016) 034014
- [334] S. Chatrchyan et al. (CMS Collaboration), *J. High Energy Phys.* 1404 (2014) 191 d
- [335] V. Khachatryan et al. (CMS Collaboration), *Phys. Lett. B* 760 (2016) 365
- [336] G. Aad et al. (ATLAS Collaboration), *J. High Energy Phys.* 1505 (2015) 061
- [337] G. Aad et al. (ATLAS Collaboration), *Phys. Rev. D* 94 (2016) 032006
- [338] T. Aaltonen et al. (CDF Collaboration), *Phys. Rev. Lett.* 105 (2010) 042002
- [339] V. M. Abazov et al. (D0 Collaboration), *Phys. Rev. D* 83 (2011) 032009
- [340] T. Aaltonen et al. (CDF and D0 Collaborations), *Phys. Rev. D* 85 (2012) 071106
- [341] T. Aaltonen et al. (CDF Collaboration), *Phys. Rev. D* 87 (2013) 031104
- [342] S. Chatrchyan et al. (CMS Collaboration), *J. High Energy Phys.* 1310 (2013) 167
- [343] G. Aad et al. (ATLAS Collaboration), *J. High Energy Phys.* 1206 (2012) 088
- [344] ATLAS and CMS Collaborations, preprint ATLAS-CONF-2013-033, CMS-PAS-TOP-12-025, March 2013.

- [345] V. Khachatryan et al. (CMS Collaboration), *Phys. Lett. B* 762 (2016) 512
- [346] CMS Collaboration, preprint CMS-PAS-TOP-14-017, July 2015
- [347] V. Khachatryan et al. (CMS Collaboration), *J. High Energy Phys.* 1501 (2015) 053
- [348] ATLAS Collaboration, preprint ATLAS-CONF-2016-097, September 2016
- [349] G. Aad et al. (ATLAS Collaboration), *Phys. Rev. Lett.* 108 (2012) 212001
- [350] V. M. Abazov et al. (D0 Collaboration), *Phys. Rev. D* 87 (2013) 011103
- [351] V. M. Abazov et al. (D0 Collaboration), *Phys. Rev. D* 95 (2017) 011101
- [352] G. Aad et al. (ATLAS Collaboration), *Phys. Rev. Lett.* 111 (2013) 232002
- [353] V. Khachatryan et al. (CMS Collaboration), *Phys. Rev. D* 93 (2016) 052007
- [354] ATLAS Collaboration, preprint ATLAS-CONF-2016-099, September 2016
- [355] V. Khachatryan et al. (CMS Collaboration), *J. High Energy Phys.* 1604 (2016) 073
- [356] T. Aaltonen et al. (CDF Collaboration), *Phys. Rev. D* 83 (2011) 031104
- [357] V. M. Abazov et al. (D0 Collaboration), *Phys. Rev. Lett.* 108 (2012) 032004
- [358] V. M. Abazov et al. (D0 Collaboration), *Phys. Lett. B* 757 (2016) 199
- [359] G. Aad et al. (ATLAS Collaboration), *Phys. Rev. D* 90 (2014) 112016
- [360] G. Aad et al. (ATLAS Collaboration), *Phys. Rev. D* 93 (2016) 012002
- [361] S. Chatrchyan et al. (CMS Collaboration), *Phys. Rev. Lett.* 112 (2014) 182001
- [362] G. Aad et al. (ATLAS Collaboration), *Phys. Rev. Lett.* 114 (2015) 142001
- [363] V. Khachatryan et al. (CMS Collaboration), *Phys. Lett. B* 758 (2016) 321
- [364] W. Bernreuther, P. Gonzalez and M. Wiebusch, *Eur. Phys. J. C* 60 (2009) 197
- [365] M. Fabbrichesi, M. Pinamonti and A. Tonero, *Eur. Phys. J. C* 74 (2014) 3193
- [366] J. A. Aguilar-Saavedra and J. Bernabeu, *Nucl. Phys. B* 840 (2010) 349
- [367] J. A. Aguilar-Saavedra, <http://jaguar.web.cern.ch/jaguar/topfit/> (retrieved: 26 Oct 2016)
- [368] N. Castro et al., *Eur. Phys. J. C* 76 (2016) 432
- [369] G. Aad et al. (ATLAS Collaboration), *J. High Energy Phys.* 1604 (2016) 023
- [370] ATLAS Collaboration, preprint ATLAS-CONF-2013-032, March 2013
- [371] D. Atwood et al., *Phys. Rept.* 347 (2001) 1
- [372] S. K. Gupta, A. S. Mete and G. Valencia, *Phys. Rev. D* 80 (2009) 034013
- [373] S. K. Gupta and G. Valencia, *Phys. Rev. D* 81 (2010) 034013
- [374] V. Khachatryan et al. (CMS Collaboration), *J. High Energy Phys.* 03 (2017) 101
- [375] M. Aaboud et al. (ATLAS Collaboration), *J. High Energy Phys.* 02 (2017) 071
- [376] K. Agashe et al. (Snowmass Top Quark Working Group), preprint arXiv:1311.2028 [hep-ph], November 2013
- [377] A. Heister et al. (ALEPH Collaboration), *Phys. Rev. B* 543 (2002) 173

- [378] J. Abdallah et al. (DELPHI Collaboration), *Phys. Lett.* B 590 (2004) 21
- [379] J. Abdallah et al. (DELPHI Collaboration), *Eur. Phys. J.* C 71 (2011) 1555
- [380] P. Achard et al. (L3 Collaboration), *Phys. Lett.* B 549 (2002) 290
- [381] G. Abbiendi et al. (OPAL Collaboration), *Phys. Lett.* B 521 (2001) 181
- [382] S. Chekanov et al. (ZEUS Collaboration), *Phys. Lett.* B 672 (2009) 106
- [383] F. D. Aaron et al. (H1 Collaboration), *Eur. Phys. J.* C 64 (2009) 251
- [384] F. D. Aaron et al. (H1 and ZEUS Collaborations), *J. High Energy Phys.* 1003 (2010) 035
- [385] F. D. Aaron et al. (H1 Collaboration), *Phys. Lett.* B 678 (2009) 450
- [386] H. Abramowicz et al. (ZEUS Collaboration), *Phys. Lett.* B 708 (2012) 27
- [387] T. Aaltonen et al. (CDF Collaboration), *Phys. Rev. Lett.* 102 (2009) 151801
- [388] V. M. Abazov et al. (D0 Collaboration), *Phys. Lett.* B 693 (2010) 81
- [389] G. Aad et al. (ATLAS Collaboration), *Phys. Lett.* B 712 (2012) 351
- [390] G. Aad et al. (ATLAS Collaboration), *Eur. Phys. J.* C 76 (2016) 55
- [391] V. Khachatryan et al. (CMS Collaboration), *J. High Energy Phys.* 02 (2017) 079
- [392] V. Khachatryan et al. (CMS Collaboration), *J. High Energy Phys.* 1604 (2016) 035
- [393] T. Aaltonen et al. (CDF Collaboration), *Phys. Rev. Lett.* 101 (2008) 192002
- [394] V. M. Abazov et al. (D0 Collaboration), *Phys. Lett.* B 701 (211) 313
- [395] G. Aad et al. (ATLAS Collaboration), *J. High Energy Phys.* 1209 (2012) 139
- [396] S. Chatrchyan et al. (CMS Collaboration), *Phys. Lett.* B 718 (2013) 1252
- [397] G. Aad et al. (ATLAS Collaboration), *Eur. Phys. J.* C 76 (2016) 12
- [398] S. Chatrchyan et al. (CMS Collaboration), *Phys. Rev. Lett.* 112 (2014) 171802
- [399] G. Aad et al. (ATLAS Collaboration), *J. High Energy Phys.* 1512 (2015) 061
- [400] V. Khachatryan et al. (CMS Collaboration), preprint arXiv:1610.04857 [hep-ex], submitted to *J. High Energy Phys.*
- [401] C. T. Hill, *Phys. Lett.* B 345 (1995) 483
- [402] L. Randall and R. Sundrum, *Phys. Rev. Lett.* 83 (1999) 3370
- [403] T. Aaltonen et al. (CDF Collaboration), *Phys. Rev. Lett.* 110 (2013) 121802
- [404] V. M. Abazov et al. (D0 Collaboration), *Phys. Rev.* D 85 (2012) 051101
- [405] G. Aad et al (ATLAS Collaboration), *Phys. Rev.* D 88 (2013) 012004
- [406] G. Aad et al. (ATLAS Collaboration), *J. High Energy Phys.* 1301 (2013) 116
- [407] G. Aad et al. (ATLAS Collaboration), *J. High Energy Phys.* 1209 (2012) 041
- [408] S. Chatrchyan et al. (CMS Collaboration), *J. High Energy Phys.* 1212 (2012) 015
- [409] S. Chatrchyan et al. (CMS Collaboration), *Phys. Rev.* D 87 (2013) 072002
- [410] G. Aad et al. (ATLAS Collaboration), *J. High Energy Phys.* 1508 (2015) 148
- [411] V. Khachatryan et al. (CMS Collaboration), *Phys. Rev.* D 93 (2016) 012001
- [412] K. Agashe et al., *Phys. Rev.* D 77 (2008) 015003
- [413] ATLAS Collaboration, preprint ATLAS-CONF-2016-014, March 2016
- [414] CMS Collaboration, preprint CMS-PAS-B2G-15-002, March 2016

- [415] CMS Collaboration, preprint CMS-PAS-B2G-15-003, June 2016
- [416] ATLAS Collaboration, preprint ATLAS-CONF-2016-073, August 2016
- [417] T. Aaltonen et al. (CDF Collaboration), *Phys. Rev. Lett.* 115 (2015) 061801
- [418] V. M. Abazov et al. (D0 Collaboration), *Phys. Lett. B* 699 (2011) 145
- [419] G. Aad et al. (ATLAS Collaboration), *Phys. Lett. B* 743 (2015) 235
- [420] S. Chatrchyan et al. (CMS Collaboration), *J. High Energy Phys.* 1405 (2014) 108
- [421] V. Khachatryan et al. (CMS Collaboration), *J. High Energy Phys.* 1602 (2016) 122
- [422] CMS Collaboration, preprint CMS-PAS-B2G-15-004, December 2015
- [423] T. Aaltonen et al (CDF Collaboration), *Phys. Rev. Lett.* 106 (2011) 141803
- [424] T. Aaltonen et al. (CDF Collaboration), *Phys. Rev. Lett.* 106 (2011) 191801
- [425] T. Aaltonen et al. (CDF Collaboration), *Phys. Rev. Lett.* 107 (2011) 191803
- [426] T. Aaltonen et al. (CDF Collaboration), *Phys. Rev. Lett.* 107 (2011) 261801
- [427] V. M. Abazov et al. (D0 Collaboration), *Phys. Rev. Lett.* 107 (2011) 082001
- [428] A. Djouadi and A. Lenz, *Phys. Lett. B* 715 (2012) 310
- [429] J. A. Aguilar-Saavedra et al., *Phys. Rev. D* 88 (2010) 094010
- [430] G. Aad et al. (ATLAS Collaboration), *J. High Energy Phys.* 1411 (2014) 104
- [431] G. Aad et al. (ATLAS Collaboration), *J. High Energy Phys.* 1508 (2015) 105
- [432] G. Aad et al. (ATLAS Collaboration), *J. High Energy Phys.* 1510 (2015) 150
- [433] ATLAS Collaboration, preprint ATLAS-CONF-2016-013, March 2016
- [434] ATLAS Collaboration, preprint ATLAS-CONF-2016-032, June 2016
- [435] ATLAS Collaboration, preprint ATLAS-CONF-2016-101, September 2016
- [436] ATLAS Collaboration, preprint ATLAS-CONF-2016-102, September 2016
- [437] ATLAS Collaboration, preprint ATLAS-CONF-2016-104, September 2016
- [438] S. Chatrchyan et al. (CMS Collaboration), *Phys. Rev. B* 729 (2014) 149
- [439] V. Khachatryan et al. (CMS Collaboration), *J. High Energy Phys.* 1506 (2015) 080
- [440] V. Khachatryan et al. (CMS Collaboration), *Phys. Rev. D* 93 (2016) 012003
- [441] CMS Collaboration, preprint CMS-PAS-B2G-16-002, March 2016
- [442] G. Aad et al. (ATLAS Collaboration), *Eur. Phys. J. C* 76 (2016) 442
- [443] ATLAS Collaboration, preprint ATLAS-CONF-2016-072, August 2016
- [444] CMS Collaboration, preprint CMS-PAS-B2G-15-008, April 2016
- [445] A. M. Sirunyan et al. (CMS Collaboration), preprint arXiv:1612.05336 [hep-ex], submitted to *J. High Energy Phys.*
- [446] CMS Collaboration, preprint CMS-PAS-B2G-16-001, July 2016
- [447] CMS Collaboration, preprint CMS-PAS-B2G-16-006, August 2016
- [448] S. Chatrchyan et al. (CMS Collaboration), *J. High Energy Phys.* 1406 (2014) 125
- [449] B. Hassanain, J. March-Russell and J. G. Rosa, *JHEP* 0907 (2009) 077
- [450] T. Golling, *Prog. Part. Nucl. Phys.* 90 (2016) 156
- [451] G. Aad et al. (ATLAS Collaboration), *Eur. Phys. J. C* 75 (2015) 92
- [452] V. Khachatryan et al (CMS Collaboration), *J. High Energy Phys.* 1506

- (2015) 121
- [453] D. Abercrombie et al., preprint arXiv:1507.00966 [hep-ex]
 - [454] C. Arina et al., *J. High Energy Phys.* 1611 (2016) 111
 - [455] ATLAS Collaboration, preprint ATLAS-CONF-2016-050, August 2016
 - [456] ATLAS Collaboration, preprint ATLAS-CONF-2016-076, August 2016
 - [457] ATLAS Collaboration, preprint ATLAS-CONF-2016-077, August 2016
 - [458] CMS Collaboration, preprint CMS-PAS-EXO-16-005, August 2016
 - [459] G. Aad et al. (ATLAS Collaboration), *Eur. Phys. J. C* 75 (2015) 79
 - [460] CMS Collaboration, preprint CMS-PAS-B2G-15-001, April 2016
 - [461] CMS Collaboration, preprint CMS-PAS-EXO-16-040, August 2016
 - [462] W. Buchmüller and D. Wyler, *Nucl. Phys. B* 268 (1986) 621
 - [463] B. Grzadkowski et al., *J. High Energy Phys.* 1010 (2010) 085
 - [464] J. A. Aguilar-Saavedra, *Nucl. Phys. B* 812 (2009) 181
 - [465] C. Zhang and S. Willenbrock, *Phys. Rev. D* 83 (2011) 034006
 - [466] A. Buckley et al., *Phys. Rev. D* 92 (2015) 091501
 - [467] A. Buckley et al., *J. High Energy Phys.* 1604 (2016) 015
 - [468] M. P. Rosello and M. Vos, *Eur. Phys. J. C* 76 (2016) 200
 - [469] C. Englert et al., *Phys. Lett. B* 763 (2016) 9
 - [470] G. Durieux, F. Maltoni and C. Zhang, *Phys. Rev. D* 91 (2015) 074017
 - [471] S. Chatrchyan et al. (CMS Collaboration), *JINST* 8 (2013) P04013
 - [472] G. Aad et al. (ATLAS Collaboration), *JINST* 11 (2016) P04008
 - [473] S. Chatrchyan et al. (CMS Collaboration), *Phys. Lett. B* 728 (2014) 496, Erratum: *Phys. Lett. B* 738 (2014) 526
 - [474] J. Currie, E. W. N. Glover and J. Pires, *Phys. Rev. Lett.* 118 (2017) 072002
 - [475] G. Aad et al. (ATLAS Collaboration), *Phys. Lett. B* 750 (2015) 475
 - [476] CMS Collaboration, preprint CMS-PAS-TOP-13-007, September 2013
 - [477] CMS Collaboration, preprint CMS-PAS-TOP-15-017, December 2015
 - [478] CMS Collaboration, preprint CMS-DP-2016-064, October 2016
 - [479] ATLAS Collaboration, preprint ATL-PHYS-PUB-2016-019, August 2016
 - [480] CMS Collaboration, preprint arXiv:1307.7135
 - [481] ATLAS Collaboration, preprint ATL-PHYS-PUB-2014-016, October 2014
 - [482] T. Behnke et al., preprint arXiv:1306.6327 [physics.acc-ph]
 - [483] M. Aicheler et al., CERN-2012-007
 - [484] CEPC-SPPC Study Group, preprint IHEP-CEPC-DR-2015-01, IHEP-TH-2015-01, HEP-EP-2015-01, May 2015
 - [485] CEPC-SPPC Study Group, preprint IHEP-CEPC-DR-2015-01, IHEP-AC-2015-01, October 2015
 - [486] M. Beneke et al., *Phys. Rev. Lett.* 115 (2015) 192001
 - [487] A. H. Hoang and M. Stahlhofen, *J. High Energy Phys.* 1405 (2014) 121
 - [488] M. Vos et al., preprint arXiv:1604.08122 [hep-ex]
 - [489] M. L. Mangano et al., preprint arXiv:1607.01831 [hep-ph]
 - [490] T. Golling et al., preprint arXiv:1606.00947 [hep-ph], submitted to *Phys. Rep.*